



REVIEW ARTICLE

Recent developments of membranes and electrocatalysts for the hydrogen production by anion exchange membrane water electrolyzers: A review



Kishore Chand *, Ombretta Paladino *

Department of Civil, Chemical and Environmental Engineering (DICCA), University of Genoa, Via Opera Pia 15, 16145 Genoa, Italy

Received 22 July 2022; accepted 20 November 2022

Available online 25 November 2022

KEYWORDS

Hydrogen generation;
AEM water electrolysis;
Oxygen evolution reaction;
Hydrogen evolution reaction;
Membrane electrode assembly;
Ion conductivity

Abstract Hydrogen production using anion exchange membrane water electrolysis (AEMWE) offers hope to the energy crisis faced by humanity. AEM electrolysis can be coupled with intermittent and renewable energy sources as well as with the use of low-cost electrocatalysts and other low-cost stack components. In AEM water electrolysis, one of the biggest advantages is the use of low-cost transition metal catalysts instead of traditional noble metal electrocatalysts. AEMWE is still in its infancy despite irregular research on catalysts and membranes. In order to generate commercially viable hydrogen, AEM water electrolysis technology must be further developed, including energy efficiency, membrane stability, stack feasibility, robustness, ion conductivity, and cost reduction.

An overview of studies that have been conducted on electrocatalysts, membranes, and ionomers used in the AEMWE is here reported, with the aim that AEMWE research may be made more practical by this review report, by bridging technological gaps and providing practical research recommendations, leading to the production of scalable hydrogen.

© 2022 The Authors. Published by Elsevier B.V. on behalf of King Saud University. This is an open access article under the CC BY-NC-ND license (<http://creativecommons.org/licenses/by-nc-nd/4.0/>).

1. Introduction

The development of de-fossilization and renewable energy infrastructure is accelerating as people become more conscious of the negative effects of climate change. In the twenty-first century, hydrogen is arguably the most important energy carrier, referred to as the “ultimate energy carrier” (Li and Baek 2021). Steam reforming of partial oxidation of methane, natural gas, and coal gasification make up the majority of commercially available hydrogen. These methods emit contaminants into the atmosphere in addition to producing greenhouse gases (Shiva Kumar and Himabindu 2019). In order to realize

* Corresponding authors.

E-mail addresses: kishore.chand@edu.unige.it (K. Chand), paladino@unige.it (O. Paladino).

Peer review under responsibility of King Saud University.



Production and hosting by Elsevier

the ambitious target of reducing and ultimately eliminating CO₂ emissions within this timeframe, different scenarios for hydrogen production have been considered.

The production of hydrogen from water includes water splitting and electrolysis. Chemical conversion of biomass, thermal processes, photocatalytic water splitting are all ways to split water. With a series of successive chemical reactions, oxygen and hydrogen are produced when water is broken down. The thermal conversion occurs between 800 and 2000 °C (E. Funk 2001). Solar or nuclear power plants can convert water into hydrogen and oxygen to generate energy (Xiao et al., 2012). Thermal methods are advantageous due to the fact that they can be used to avoid the problems associated with the stages of component separation, but they are economically advantageous only coupled to plants where high surplus of thermal energy is available.

Hydrogen and oxygen can be made from water using water electrolysis at low temperatures (Steinfeld 2005, Wei et al., 2007, Senftle et al., 2010, Millet and Grigoriev 2013). Water electrolysis is the principal method for manufacturing huge volumes of hydrogen, which is the only carrier and storage medium for renewable electricity. Depending on the electrolyte used, electrolysis can be differentiated: proton exchange membrane water electrolysis (PEMWE) and Alkaline electrolysis (AEL) are the two major techniques in use for water electrolysis to produce hydrogen (Zeng and Zhang 2010, Marini et al., 2012, Manabe et al., 2013, Rashid et al., 2015).

To make hydrogen economically and environmentally competitive with fossil fuels, scientists are researching new efficient and cost-effective methods to produce it via water electrolysis. Hydrogen produced through traditional water electrolysis is inefficient, energy-intensive, has high overpotential, and can corrode easily. Polyelectrolyte membrane electrolyzed water provides several advantages over standard porous membrane electrolyzed water, including a longer electrolytic cell life, higher efficiency, lower hydrogen generation costs, and lower maintenance costs (Schmidt et al., 2017, Hadikhani et al., 2021). A water electrolyzer based on PEMWE has recently been investigated, and it performs exceptionally well in ultrapure/ distilled water due to its high efficiency up to 75 % (Ayers et al., 2010, Ul Hassan et al., 2020, Al Munsur et al., 2021). Unfortunately, a PEM-based water electrolysis device is expensive, due to the employment of expensive noble metal catalysts (IrO₂ and Pt) and defluorination membranes (Abbasi et al., 2019, Henkensmeier et al., 2020, Lindquist et al., 2020, Oh et al., 2021). PEM electrolyzers can function properly and are robust, but it has proven a difficult task to deploy them at the required industrial scale due to a paucity of platinum group metals (PGMs) used as electrocatalysts. Contrary to this, conventional AELs do not offer the flexibility to accommodate multi-megawatt installations at low cost (Carmo et al., 2013, Paoli et al., 2015). An alternative solution is a water electrolyzer based on anion-exchange membranes, which can use inexpensive PGM-free electrocatalysts (such as nickel, iron, or cobalt), in order to reduce cost of an electrolyzer and to efficiently produce pressurized hydrogen (Li et al., 2021).

Anion exchange membranes (AEMs) still perform poorly, which limits the progress of AEMWE. In order to prevent oxygen and hydrogen products from mixing while enabling transport of OH⁻, the AEM is used between the cathode and anode as a solid-state electrolyte (Zhang et al., 2018). Due to the lower mobility of OH⁻ ions than protons, AEM has a lower ionic conductivity than PEM (Park et al., 2018, Yan et al., 2020). Additionally, most AEMWEs degrade tremendously under alkaline conditions, reducing their performance over time (Mustain et al., 2020). The development of highly conductive and alkali stabilized AEMs is therefore imperative.

As public interest in MEA has grown, a number of studies have explored how commercial AEMs can be used to create high-performance AEMWEs, especially within MEA components. In the past few years, several commercial AEMs have been developed and commercialized. These include Fumapem® (Fumatech Co., Germany), A201® (Tokuyama Co., Japan), Sustainion® (Dioxide Materials Co., USA), Aemion™ (Ionomr Innovation Co., Canada), and Orion TM1™ (Orion Polymer, USA). As part of the early development of

the A201® and for the discontinued product, at 1.9 V_{cell} the low performance was observed for AEMWE (350–550 mAcm⁻²) (Pavel et al., 2014, Cho et al., 2017, Vincent et al., 2017). As a result of incorporating Fumapem® membranes in AEMWE, Park et al. (Park et al., 2019) achieved 1500 mA cm⁻² performance at 1.9 V_{cell} when analyzing method of fabrication, MEA parameters, operating conditions. A201® and Fumapem®, however, are known to have poor durability when used as AEM. Liu et al. (Liu et al., 2017) published a report on the performance and durability of Sustainion® membranes developed by Dioxide Materials Co.; by using FASE50® (Fumatech, Germany), they doubled the AEMWE performance. At 180 h, FASE50® showed a significant change in voltage, but it continued to perform at 1950 h. AEMWE with Aemion™ membrane was proposed by Fortin et al. (Fortin et al., 2020) and demonstrated 2000 mAcm⁻² performance at 1.82 V_{cell} and 60 °C. In addition, the degradation rate at 50 °C was 3.21 mV h⁻¹. Most AEMs have been checked with AEMWE except Orion TM1™.

Electrolyzers that use anion exchange membranes have shown increasing interest that combine the advantages of AEL and PEM (Wang et al., 2019). Vincent et al. (Vincent et al., 2017, Vincent and Bessarabov 2018) investigated different AEMs by adding different supporting electrolytes. (KHCO₃, K₂CO₃ and KOH). Using Tokuyama A201 membranes, Ni/(CeO₂-La₂O₃)/C and CuCoOx as cathode and anode catalysts, respectively, the best performance was achieved in 1 % K₂CO₃ electrolyte at 500 mAcm⁻² and 1.95 V at 60 °C. While using NH₃/H₂-treated and subsequently anodized Fe-NiMo as the anode catalyst, Chen et al. (Chen and Hu 2020) demonstrated the ability to obtain 1.0 A cm⁻² at 1.57 V and 80 °C in an AEM electrolyzer. According to Fabry et al. (Fabbri et al., 2017) the flame sprayed Ba_{0.5}Sr_{0.5}Co_{0.8}Fe_{0.2}O₃ δ anode catalyst increased the cell performance when deionized water was substituted for commercial IrO₂. Li et al. (Li et al., 2020) reported high current density at 85 °C (2.7 A cm⁻² at 1.8 V) when an electrode binder was used with quaternized polystyrene electrode and platinum as cathode catalyst, but the durability of these cells remains a challenge. It is important to have both flexibility and hydrophilicity of the side chains when creating AEMs with good alkaline stability and high ionic conductivity. A flexible linkage of a -(CH₂)₆- group is designed in the side chain to increase the density of local ionic groups. In addition, there is a long flexible spacer in the side chain (hexyleneoxy groups) linking the first QA group to the backbone, which would weaken the electron-withdrawing effect of QA groups. Furthermore, the ether-containing spacer can be made electronegative, which enhances cationic mobility and ionic interaction, ultimately facilitating the fabrication of microphase segregation morphology in AEMs (Gong et al., 2017).

2. Hydrogen production techniques

Since hydrogen has only one proton and one electron, it is considered a low-polluting and highly efficient fuel (Merle et al., 2011). Normally, hydrogen doesn't occur in nature. Methanol, gasoline, and propane are some of the fuels which contain it. Hydrogen is therefore produced by a number of processes. A variety of carbon-free methods such as reverse electro-dialysis, photo-assisted electrolysis, photo-thermal, electro-thermal, and thermochemical water splitting are being explored as potential sources of diverse energy (Dincer and Balta 2011, Dincer and Zamfirescu 2012, Acar et al., 2015, Tufa et al., 2016, Wang et al., 2017).

One of the technologies that is gaining popularity is water electrolysis to produce hydrogen, due to its high purity and a range of niche applications, including the production of power-to-gas. Alkaline electrolysis and PEM electrolysis are the two conventional types of electrolysis. Hydrogen can be produced by electrolysis using sources of renewable energy like

solar (Manabe et al., 2013). Solid polymer electrolytes like Nafion (often PEM) are used in PEM electrolysis (Carmo et al., 2013). PEM electrolyzers can operate at a current density of 2000 mA cm^{-2} at an operating voltage of 2.1 V at 90°C . In addition, platinum group metals are limited as electrocatalysts due to the acidic nature of the atmosphere (Millet et al., 2011). Compared to platinum group metal electrolysis, AEL uses less expensive catalysts and separators, such as diaphragms. Due to its high corrosion potential, the 30 % KOH electrolyte in contact with the ambient air leads to a formation of K_2CO_3 that reduces the efficacy of the alkaline electrolyser (Zeng and Zhang 2010). For electrolysis to become cheaper and more efficient, non-PGM catalysts and low-cost membrane systems are required. Electrolysis using AEMs based on polymer materials and non-platinum catalysts have recently been introduced (Vincent and Bessarabov 2018). The electrolysis technique called AEM could be considered as a combination between PEMWE and alkaline electrolysis. The anode and cathode of an AEM water electrolysis system usually contain non-noble metal electrocatalysts. Ionic conductivity is provided by 1 % dilute K_2CO_3 . At 1.9 V, the maximum current density is 500 mA cm^{-2} . An AEM electrolyser's performance is mainly determined by the AEM. In an electrochemical reaction, the AEMs serve as barriers for gases and electrons produced by the electrochemical reactions as well as carriers of hydroxyl ions (Manabe et al., 2013, Vincent and Bessarabov 2018).

2.1. Typical/Conventional electrolysis

2.1.1. Alkaline electrolysis

As with alkaline electrolysis mainly non noble metal are used but specially nickel-based oxide anodes and cobalt-based oxide cathodes are the most frequently used anodes and cathodes, respectively, and liquid electrolytes are usually 30 to 40 % KOH (Ganley 2009). Alkalinity is provided by the electrolyte circulated across the electrodes. Cathode and anode chambers are separated by porous diaphragms, though they do not conduct hydrogen and oxygen (Zeng and Zhang 2010). Among the many materials used for diaphragms are polyphenylene, polysulfide polypropylene, asbestos, and potassium titanate (Wendt and Hofmann 1989, Kjartansdóttir et al., 2013). Cell voltage is between 1.85 and 2.2 V and efficiency is around 60–80 % in an alkaline electrolysis cell operating at a current density of 400 mA cm^{-2} . In addition to being relatively safe due to the low temperatures, an advantage of alkaline electrolysis is that a noble metal catalyst is not required to produce hydrogen (Ferrero et al., 2013, Vincent and Bessarabov 2018).

2.1.2. Proton exchange membrane electrolysis

PEM electrolysis typically uses Pt black and IrO_2 as a cathode and anode catalysts, respectively (Millet et al., 2010). In place of a liquid electrolyte, a solid acidic membrane (Nafion, DuPont) is used (as the hydrogen is produced by the reaction, the ions travel from the anode to the cathode and are separated out as hydrogen and oxygen). At 90°C , PEM electrolyzers are capable of operating at 2.1 V and a current density of 2000 mA cm^{-2} . In PEM electrolysis, hydrogen and oxygen are produced more rapidly than in alkaline electrolysis due to the acidic nature of the electrolyte and the metal surface of the electrodes. PEM electrolysis is safe because it does not use a caustic electrolyte. In PEM electrolysis, high pressures are used

for the cathode, but atmospheric pressure is permitted for the anode (Rossmeisl et al., 2007).

2.1.3. Anion exchange membrane water electrolysis

The technology is still being developed. Research about AEMWE has generated a lot of interest among universities and research organizations, especially because of its low cost and possible high performance. The AEM electrolysis research community has published few articles compared to that of the other traditional electrolysis technologies. Further research is needed on the following aspects of AEM electrolysis, specifically: stability of membranes and catalysts, power efficiency, reduced cell costs, and ease of use (Leng et al., 2012, Pavel et al., 2014). Contribute to the development of a hydrogen economy, significant improvements still need to be made to AEM-based electrolyzers. Various parameters, including electrolysis performance of AEM, membranes, electrocatalysts, ionomers, and the MEA in general, should be thoroughly reviewed.

3. Polymeric anion exchange membranes

For electrochemical systems, polymeric AEMs have been developed since the past few years. In alkaline water electrolysis, a conventional diaphragm can be replaced with an AEM and, in addition to being adopted for electrolysis, these membranes are also useful for fuel cells. Electrolysis has not been accomplished at industrial scale with AEMs yet (Piana et al., 2008, Piana et al., 2010, Faraj et al., 2011, Varcoe et al., 2014), even if there are several potential benefits in using AEMs.

1. The platinum group metal (PGM) is replaced by a transition metal catalyst in this process [Economical Friendly].
2. Electrolytes can be substituted and instead of concentrated KOH, DI water or a small amount of alkaline solution is adopted.
3. In AEM electrolysis, a membrane containing quaternary ammonium ion exchange groups is less expensive than a membrane based on Nafion.
4. CO_2 and AEMs interact very little despite the fact that metal ions are absent from AEMs.

In this technology, there is no corrosive liquid electrolyte, which reduces weight and size, prevents leakage, provides volumetric stability, and facilitates handling. For hydrogen production, AEM technology is highly reliable and low-cost (Pavel et al., 2014).

3.1. Basic principle of polymeric AEM electrolysis

As an alternative to water electrolysis, the AEM method combines the merits of alkaline and PEM electrolysis into a single cell. AEM and its components are shown in Fig. 1. In order to provide DC current to the cathode and anode, power is supplied from a separate external source. The reaction is composed of two half-cell reactions, namely, the HER and OER. Water is passed through the anode and two electrons are added to produce hydrogen and hydroxyl ions. Thus, the hydroxyl ions diffuse to the anode portion of the AEM through positive attraction, whereas electrons move through

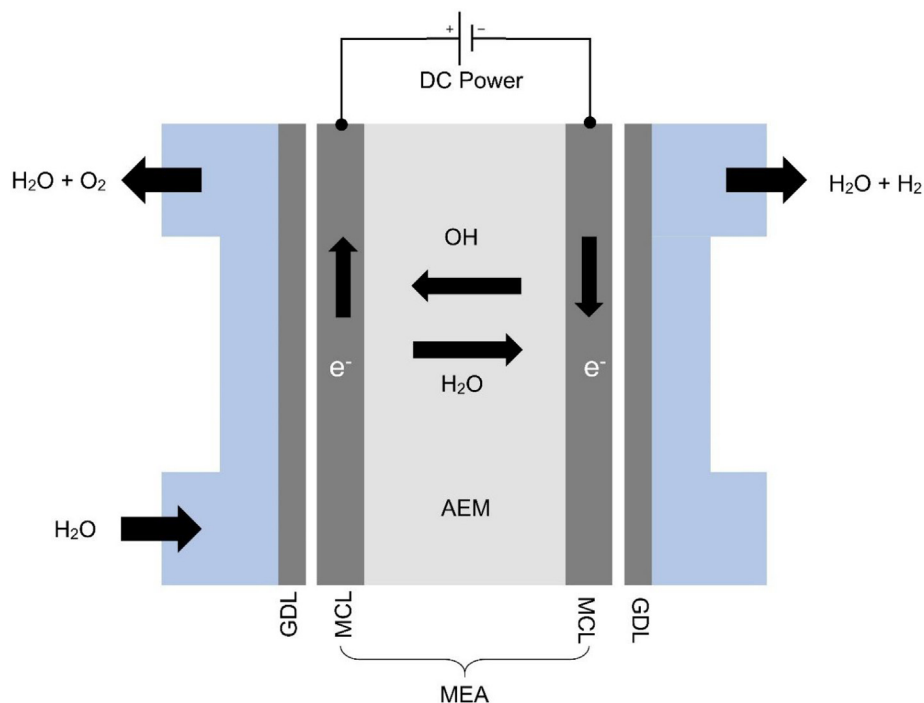
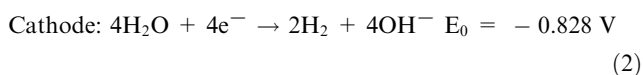


Fig. 1 Schematic diagram of an AEMWE. ACL: anode catalyst layer, MEA: membrane electrode assembly, GDL: gas diffusion layer and CCL: cathode catalyst layer, Elsevier 2018 granted a copyright license to reproduce the Figure (Vincent and Bessarabov 2018).

the external circuit to the anode portion. In the anode chamber, the hydroxyl ions are recombined with oxygen and water through the loss of electrons. By forming bubbles on the anode's surface, oxygen is released. During both half-cell reactions, the electrode surfaces must be actively catalyzed in order to generate and release the corresponding gases. Half-cell reactions are presented in Eqs. (1)–(3) (Rossmeis et al., 2007):



It takes 1.23 V of theoretical thermodynamic cell voltage to split water into hydrogen and oxygen at 25 °C. For efficient hydrogen production, however, the cell voltage must be higher than 1.23 V. Electrolyte and electrolyzer components must have additional voltage in order to overcome the ohmic and kinetic resistances. PEM electrolysis is typically performed at 1.75 V and alkaline electrolysis at 1.85–2.05 V, respectively, at 70–90 °C (Vincent and Bessarabov 2018).

4. Overview of the membranes, ionomers in the AEMWEs

Electrolysis makes up 4 % of global energy storage and transportation. Different electrode materials and diaphragm separators are being tested in the cathodic/anodic compartments to improve overall system efficiency. The Membranes and ionomers developed for AEMWE could also be used in reverse systems as AEMFC electrolytic membrane assembly, coupling options, and storage media all continue to improve in order to improve efficiencies.

The external circuit that supplies DC power is made up of the electrolysis reactor, cathode, and anode. AEMs separate the internal and external circuits in alkaline electrolytes. In the external circuit, OH is transferred from the anode side to the external circuit, where it combines with water at the anode side. As a result of this reaction, OH and oxygen are produced. Hydrogen gas is created by splitting the hydrogen network bond on the cathode side, which produces hydrogen ions when combined with electron transfer (Leng et al., 2012). The Gibbs free energy is greater than the theoretical potential when half-reactions occur. Due to ohmic resistance and electrolyte kinetics, the minimum applied potential is normally higher than 1.85 V, which is due to the minimum applied potential exceeding the theoretical potential (Dincer and Acar 2015).

The studies about AEMs are also carried out for the development of reverse systems, producing energy from hydrogen, as anion exchange membrane fuel cells (AEMWE). Recent AEMFC studies have concentrated on the mechanisms of oxidation of hydrogen and reduction of oxygen in alkaline media, as well as the development of new materials, including anion exchange membranes, ionomers, and electrocatalysts (Roche et al., 2007, Xu et al., 2007, Yanagi and Fukuta 2008, Li et al., 2009, Liang et al., 2009, Zhu et al., 2009, Kostowskyj et al., 2010, Yang et al., 2014). The schematic diagram of AEMWE is shown in the Fig. 2.

AEM materials with polymer backbones have previously been explored by the researchers, including (phenylene)s (Hibbs et al., 2009), poly(olefin)s (Noonan et al., 2012), poly(ether imide)s (Wang et al., 2009), poly(sulfone)s (Gu et al., 2009, Wang et al., 2009, Pan et al., 2010, Yan and Hickory 2010, Mohanty et al., 2014), poly(phenylene oxide)s (Li et al., 2012, Li et al., 2013), poly(arylene ether)s (Wang et al., 2010, Gu et al., 2011) and poly(styrene)s (Luo et al.,

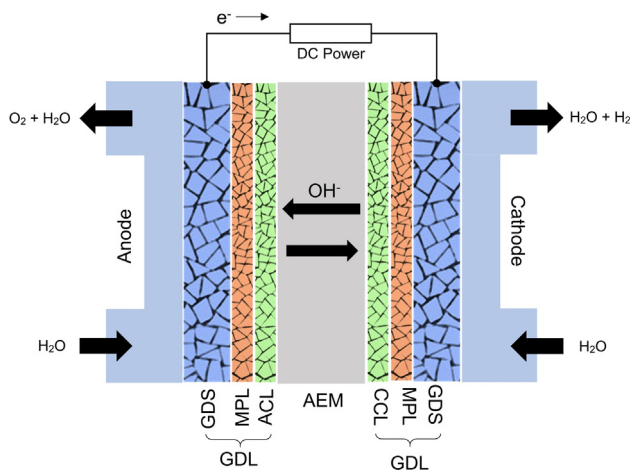


Fig. 2 Diagram of an AEMWE, figure modified and reproduced with the copyright permission from Elsevier 2018 (Truong et al., 2018).

2010, Zeng et al., 2010). AEM membrane candidates have also included quaternary ammonium (QA) functionalized polymer electrolyte membranes. The researchers also investigated polymers with tethered QA such as poly (aryl ether sulfones) (Rao et al., 2013, Jasti and Shahi 2014, Wang et al., 2015), poly (aryl ether ketones) (Xu et al., 2012, Chen and Hickner 2013, Jasti and Shahi 2014, Wu et al., 2014), radiation grafted poly(vinylidene fluorides) (Danks et al., 2003), poly(styrene)s (Ran et al., 2012, Ran et al., 2013), poly(olefins) (Ran et al., 2012, Nasef 2014) and poly(phenylene oxides) (Schauer et al., 2015). Due to the lower mobility of the hydroxyl ions within these alkaline exchange membranes, their conductivity is lower than acidic exchange membranes. Researchers have explored the following two strategies to address this issue: (1) researching the physics of organic cations with hydroxide conductivity, such as guanidinium (Zhang et al., 2010, Kim et al., 2011), phosphonium (Noonan et al., 2012), imidazolium (Yan et al., 2014); and (2) Besides controlling polymer architectures to produce phase-separated morphologies, block copolymers are also used (Price et al., 2013, Rao et al., 2013), the preparation of combs (Li et al., 2013), crosslinking, and adding spacer chain pendants, these methods have all led to the development of AEMs that provide sufficient hydroxide conductivity (higher than 10^{-2} S cm^{-1}).

Furthermore, AEMs are not chemically stable when exposed to alkaline environments, one of the major challenges they face in practical applications is their implementation in alkaline environments. It is possible for QA cations to degrade under certain conditions (at 60 °C and higher pH) in the following ways. The reactions include (i) nitrogen ylide formation (Chempath et al., 2008), (ii) Hofmann reaction elimination of β -hydrogen (E_2) (Cope and Trumbull), (iii) direct nucleophilic substitution of a carbon atom (SN_2) (Chempath et al., 2010), and direct nucleophilic substitution of arylene(SAr) (Choe et al., 2014). As a result of these degradation pathways, IEC and hydroxide conductivity are rapidly affected. AEMs functionalized with imidazolium are among the most exciting non-QA AEMs for increasing alkaline stability. Although imidazolium cations have five-membered heterocyclic rings and π -conjugated structures, they should still be stable in alkaline

conditions. The π -conjugated structure helps to delocalize positive charges by preventing nucleophilic attack by OH^- groups using SN_2 or Hofmann elimination of positive charges (Li et al., 2011, Ye and Elabd 2011). In the previous literature, there are numerous varying results and contradictory conclusions about imidazolium cations. The goal of Kim et al. was to improve the stability(cation) of the membrane using the commercial polymer parmax 1200 as a starting material. When immersed in 1.0 M KOH at 60 °C for seven days, parmax exhibited greater stability than quaternary ammonium functionalized polymers. A conjugate imidazole-ringed alkaline parmax polymer (Hossain et al., 2015) that is relatively resistant to the nucleophilic attacks of hydroxyl ions so that its limitations would not be experienced. AEMs functionalized with 1,2 dimethylimidazolium at 80 °C in 1 M KOH were prepared by Sun et al. and compared to 1-methyl-3-(4-vinylbenzyl) imidazolium chloride at same condition (1 M KOH & 80 °C). In comparison with the unsubstituted C2 imidazolium in alkaline environment, 1,2 dimethylimidazolium shows significant advantages (Yang et al., 2015). Zhang et al. found a 6.8 % mass and a 23.3 % conductivity for the imidazolium cation attached to polysulfone after 24 h in 3 M NaOH under 60 °C (Zhang et al., 2011). Also, Guo et al. reported that poly (styrene-*co*-butyl methacrylate)s containing imidazolium functionalized polymers were stable under 60 °C in 6 M NaOH for 120 h (Guo et al., 2010). Furthermore, a study was done by Lin and co-authors, investigating the alkaline stability of imidazolium cations that are substituted with methyl on a poly(phenylene oxide) backbone. Even after 9 days of ageing in the aqueous 2 M KOH solution, the IEC remained unchanged even after immersion at 25 °C. As the temperature was raised to 60 °C, IEC dropped suddenly to 40 % and 50 % for 7 and 9 days, respectively (Lin et al., 2013).

As compared to the conventional method EPTMAC is more straightforward, according to Xiu Qin Wang et al. who synthesized AEMs bearing pendent QA groups based on poly (ether sulfone) s by nucleophilic substitution polycondensation, functionalization and demethylation under mild conditions. The highest ionic conductivity measured at 80 °C was 46.8 mS cm^{-1} , as reported by Xiu Qin wang et al. According to the $^1\text{H NMR}$ analysis of the PES-80-IL membrane after immersion in a 2 M aqueous KOH, the membrane loses nearly 50 % of its QA groups as shown in the Fig. 3 (Wang et al., 2017).

An important aspect of AEMs is their ionic conductivity. For a hydroxide conductivity measure to be useful, it must be $>10 \text{ mS cm}^{-1}$ (Li et al., 2012). Membranes' conductivity to hydroxide can be observed in Fig. 4 (a). The temperature distribution is nearly linear between 30 and 80 °C. The hydroxide conductivity increased as the temperature increased due to the higher mobility of the flexible pendent QA group. In contrast to membranes with lower ion conductivity, such as the PES-*x*-IL membrane ($x = 40, 60, 80$), membranes with higher IEC have a higher conductivity. Due to its distinct microphase separated morphology and the presence of well-developed ion-conductive channels, the PES-100-IL membrane may also be highly conductive.

Comparing the conductivity of AEMs at 30 °C to PES-*x*-IL membranes can be seen in Fig. 4 (b). Despite its higher conductivity, the PES-*x*-IL membrane performs better at 30 °C than other PES-based AEMs, with values ranging from 4.5 to 24 mS cm^{-1} (Hu et al., 2012, Li et al., 2012, Di Vona et al.,

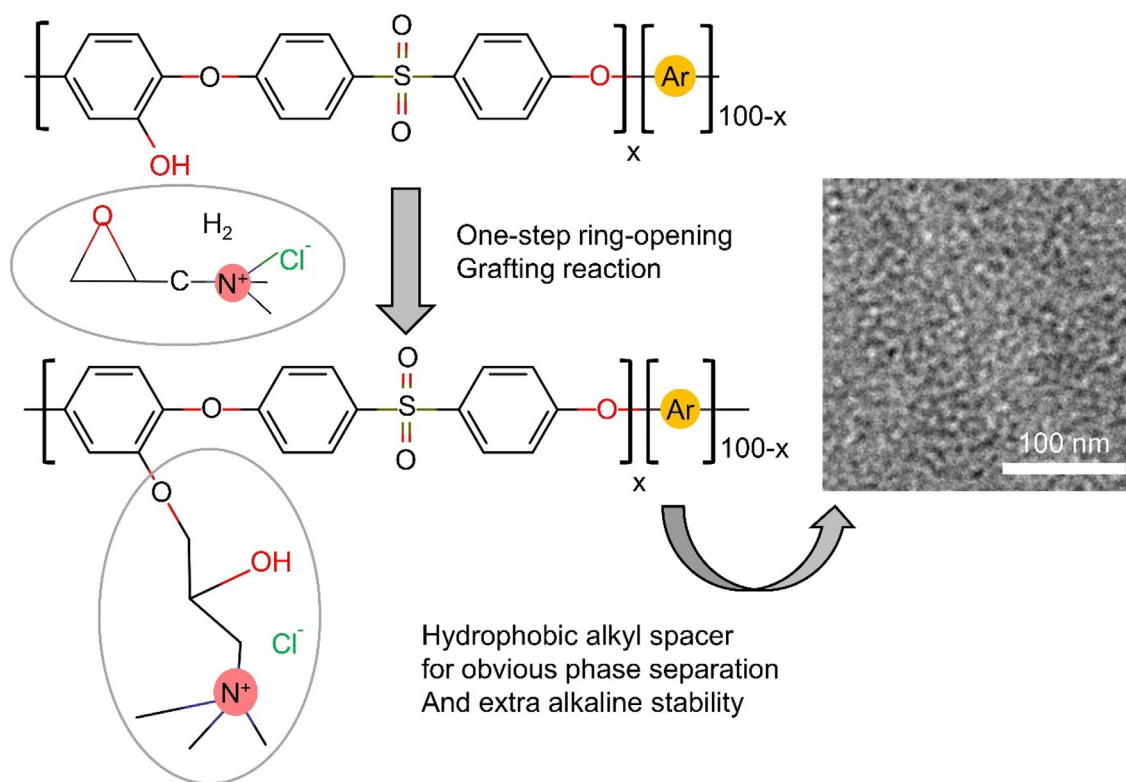


Fig. 3 Synthesis process of membrane (PES-80-IL). The Image was reproduced with the copyright permission of Elsevier 2017(Wang et al., 2017).

2014, Song et al., 2016), and even better than the Tokuyama AHA membrane. A key component to fabricating efficient ion conductive channels appears to be the formation of hydrophobic and hydrophilic phase separations in the membranes. The ionic conductivity of AEMs with sidechains is acceptable and makes them good candidates for fuel cell testing. But there is still room to improve ionic conductivity. The Arrhenius law relating hydroxide conductivity to temperature is shown in the logarithmic graph of Fig. 4(c). The activation energy (E_a 10.85 to 12.10 kJmol⁻¹) of PES-x-IL membranes is generally like that of reported AEMs (10 to 23 kJmol⁻¹) (Liu et al., 2016). From these experiments, it appears that PES-x-IL membranes exhibit similar ion conductivity in aqueous hydroxide solutions. The lower activation energy indicates fewer energy requirements for ionic conduction.

The activation energy of PES-100-IL is lower than that of PES-40-IL. Increasing the number of QA groups in the membrane reduces the activation energy. Higher IEC may result from the fact that more ionic groups can conduct ions, and therefore, higher IEC lowers activation energy. For testing the stability of the PES-x-IL membrane, the PES-80-IL membrane was treated. The ¹H NMR was used to examine the post-alkaline structure changes in the PES-80-IL membrane after being incubated at 60 °C in a 2 M aqueous KOH solution for 600 h. The degradation rate was computed based on the decrease in the integral ratio of QA band peaks (H_{12}) to the aromatic proton peaks (H_2). The ratio of H_{12}/H_2 is 1.15 in the alkaline stability test, which is about 56 % of the original value. Additionally, an abrupt decrease in the signal between 4.0 and 4.8 ppm was caused by nucleophilic substitution of

QA groups: Hofmann elimination of hydrogen b by attack of hydroxide ions. Testing was performed to determine if the membranes had alkaline stability by observing the IEC and hydroxide conductivity during the test. This can be seen in Fig. 4(d). Within 600 h, the PES-80-IL membrane conductivity reaches 26.6 mS cm⁻¹, which is 70 % of its initial value (38.6 mS cm⁻¹). In addition, the IEC for the PES-80-IL membrane decreases from 1.56 meq g⁻¹ to 0.92 meq g⁻¹, which is approximately 58 % of the initial value. Conductivity has a higher retention rate than IEC. Conductivity is explained by the fact that there may be basic tertiary amines, essentially degradation products left behind in copolymers.

As described in Shujan chao et al., (Zhao et al., 2021) one-pot ethylene glycol-assisted solvothermal method was used to prepare three-dimensional hierarchical flowers like layered hydroxide and QCS/PVA matrix blended together for improved mechanical strength (Fig. 5). The maximum hydroxide ion conductivity of the synthesized membrane is 25.7 mScm⁻¹, which is higher than the conductivity of pristine membrane. Furthermore, the membranes showed ionic conductivity of up to 92 % in 2 M KOH for 100 h. Due to the decreased methanol permeability and increased conductivity, the pristine membrane produced a peak power density of only 40mW cm⁻² in comparison with the composite membrane containing 6 % LDHs.

The radiation grafted anion exchange membrane (RG-AEM) developed by Wang et al. (Wang et al., 2019) has excellent performance characteristics when fully hydrated. An AEMFC peak power density of 850 mW cm⁻² was achieved using a PtRu/C, H₂/air and Pt/C (CO₂ free) H₂ anode and

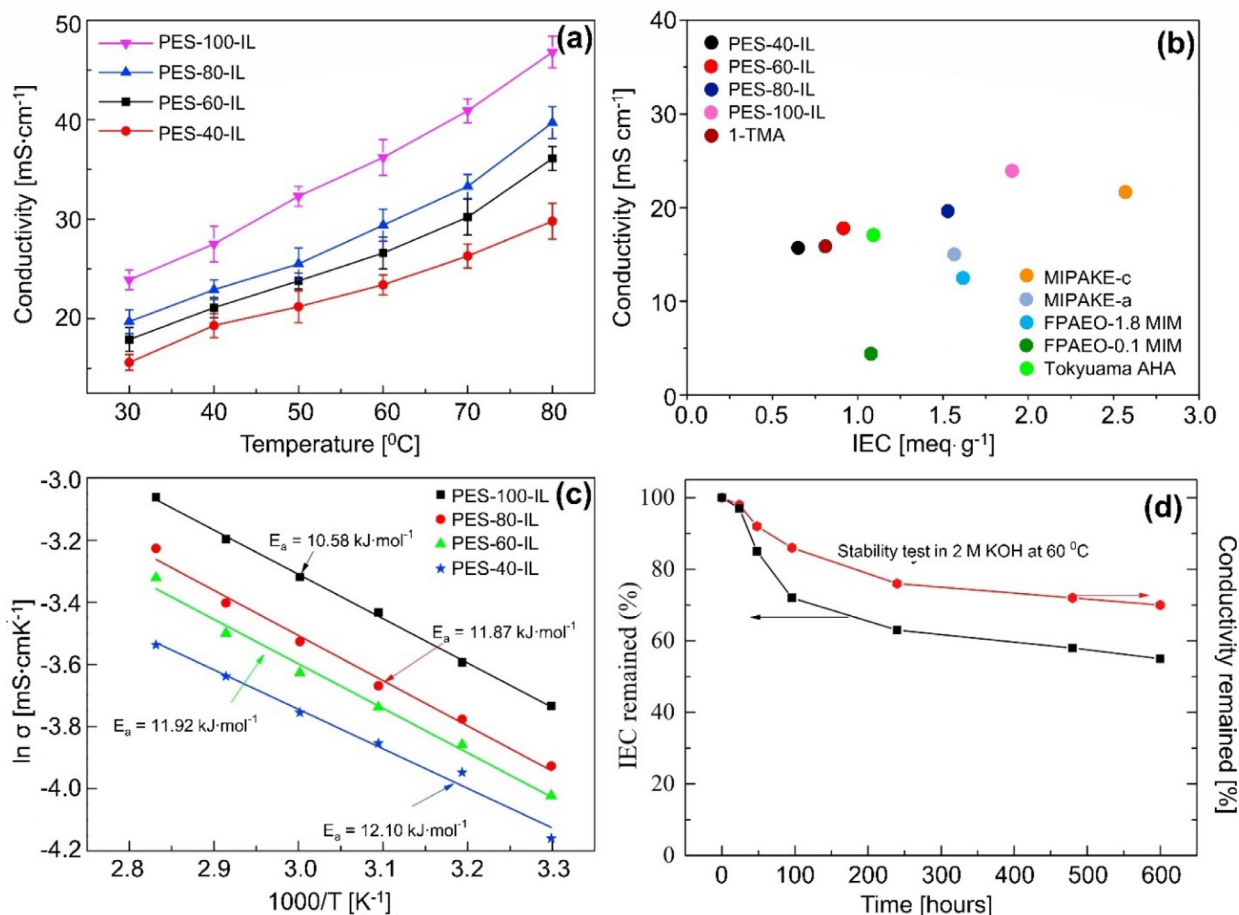


Fig. 4 Hydroxide conductivity of AEMs varies with temperature (a), IEC conductivity of various AEMs at 30°C (b), PES-x-IL membrane Arrhenius plots ($X = 40, 60, 80,$ and 100) (c), PEC-80-IL conductivity and (d) IEC is assessed at 60°C in a 2 M KOH solution, figures were reproduced with the copyright permission Elsevier 2017 (Wang et al., 2017).

Ag/C cathode oxide electrocatalyst in this membrane, 100 % relative humidity environment at 80°C with OH⁻ anion conductivity of $200\text{ mS}\cdot\text{cm}^{-1}$. The RG-AEM shows less than 7 % degradation at 80°C after 500 h when it is hydrated to 1/4 RH with 100 % N₂ (CO₂-free) atmospheres as mentioned in Fig. 6.

The membranes Q-POLY (1–3) were prepared by Koorosh Firouz Tadayani (Firouz Tadayani et al., 2019) as shown in Fig. 7 for the purpose of anion exchange as shown in Fig. 7 different cations were present, with varying degrees of basicity. They found that the membranes they synthesized were highly anion conductive, with conductivity between 83 and $117\text{ mS}\cdot\text{cm}^{-1}$ at 80°C . In addition to changing the OH⁻ conductivity, the crosslinking was also altered to alter mechanical properties and chemical stability. Among its physical properties, Q-poly-3 exhibits a power density of $89\text{ mW}\cdot\text{cm}^{-2}$, an OH⁻ conductivity close to or equal to $10\text{ mS}\cdot\text{cm}^{-1}$, a fuel crossover > 10 % of Nafion, and a tensile strain of 40.39 % and a tensile strength of 51.25 Mpa. The porous nature of the membrane along with its good mechanical properties leads to a high-water absorption value of 91 % at room temperature but due to cross linking it exhibits an 18 % swelling ratio. A synthesis procedure is given in Fig. 8 or the Q-Poly-3 monomer. The membrane's ionic conductivity remained within

7 % of that of its monomer after 14 days of storage in alkaline solution.

Fig. 8(a & b) reports the results of water uptake and swelling ratio measurements at 30, 50, and 70°C for all membranes. According to these results, water uptake of Q-poly-2 (115 % at 30°C) increased with increasing IEC value compared with Q-Poly-1 (14 % at 30°C) and Q-Poly-3 (91 % at 30°C). Furthermore, membrane performance improves with increasing temperature, indicating that membranes are capable of working effectively under cell conditions (70°C). Q-Poly-3 displayed a higher water uptake than Q-Poly 1, due to its higher porosity while Q-Poly-1 and Q-Poly-3 had similar IEC values. Increasing WU reduces mechanical properties and improves SR. Although both Q-Poly-3 and Q-Poly-2 membranes exhibited high WU, both membranes had a high level of mechanical strength. A titration was used to determine the IEC for all membranes in Fig. 8 (c and d), with Q-Poly-2, IEC increased in comparison to Q-Poly-1 because imidazole was added. The IEC values of Q-poly-3 were nearly identical to those of Q-poly-1.

In comparison to Q-Poly-1, Q-Poly-3 has shown higher anion conductivity, which can be attributed to its porous morphology that facilitates the transfer of ions through hydrophilic channels. In comparison with Q-Poly-2, the imidazole ratio

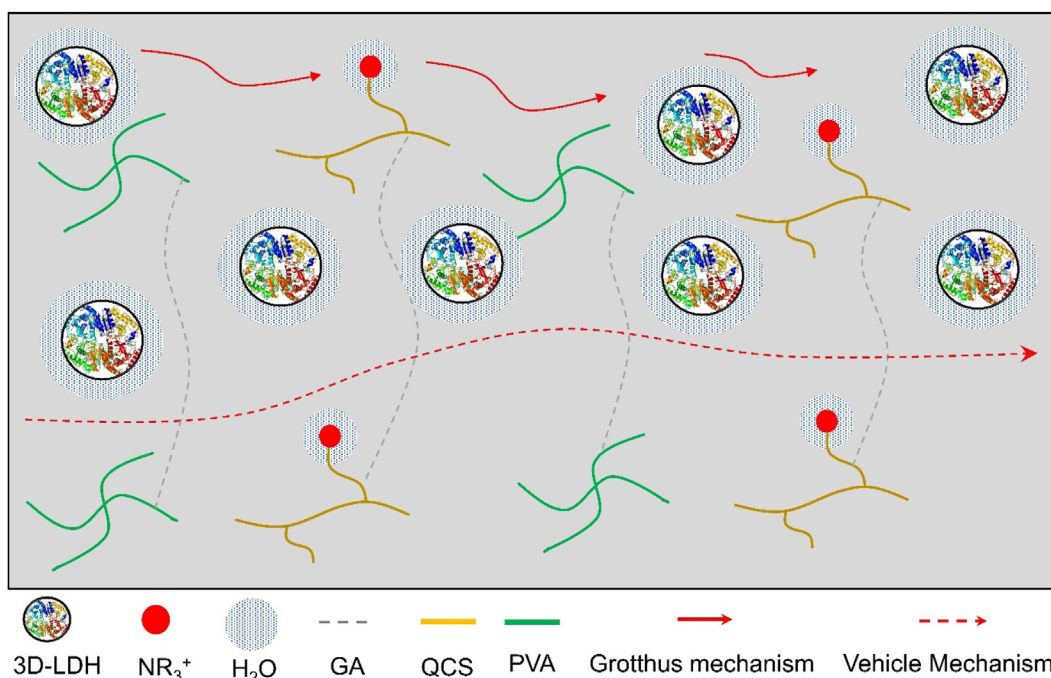


Fig. 5 An integration of 3D-LDH into QCS/PVA blend matrix and the fabrication of flower-like 3D-LDH. Images reproduced with permission from Elsevier 2021 (Zhao et al., 2021).

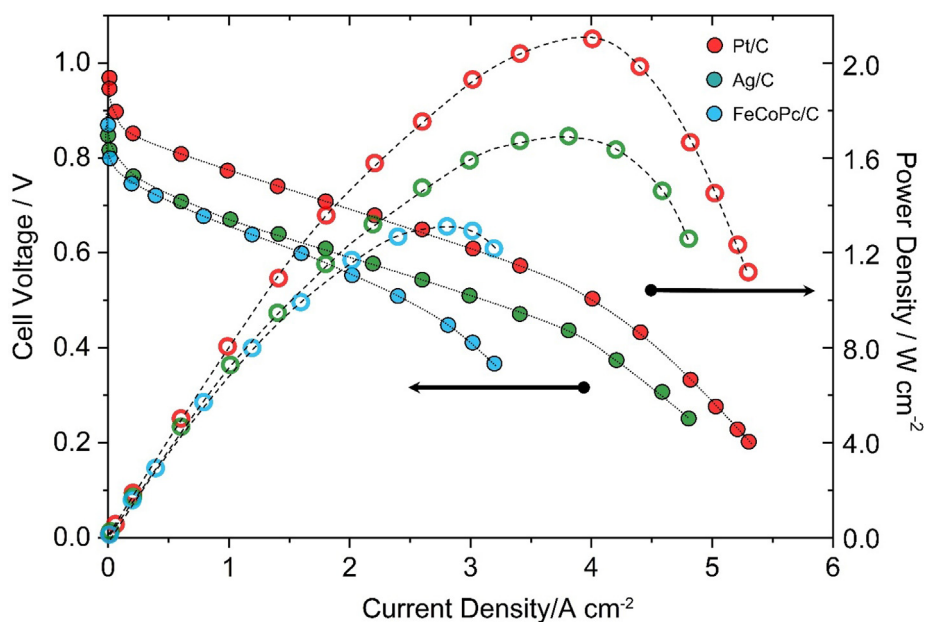


Fig. 6 LDPE15-AEM at 80 °C with different cathode electrocatalysts for H₂/O₂ AEMFCs. The Image reproduced with the copyright permission by RSC advances 2019 (Wang et al., 2019).

was reduced by adding vinyl benzene segments. Under various conditions, the prepared membranes were measured for hydroxide conductivity. Temperature and concentration of NaOH affect hydroxide conductivity as shown in Fig. 8(c and d). Q-Poly 2 exhibited the highest hydroxide conductivity in 2 M NaOH solution at 80 °C (117 mS cm⁻¹). Fig. 8 (d) demonstrates how NaOH concentration affects hydroxide conductivity at room temperature, and as NaOH concentration

was increased, hydroxide conductivity increased. Despite the importance of high anion conductivity in the preparation of membranes, maintaining ion conductivity for an extended period of time is a more important issue. The literature indicates that many membranes exhibit high ion conductivity. Although hydroxide conductivity was reduced by 50 % over time (200–500 h) (Lin et al., 2013, Dai et al., 2016, Feng et al., 2017, Lu et al., 2017). At 80 °C and 2 M NaOH solution, the mem-

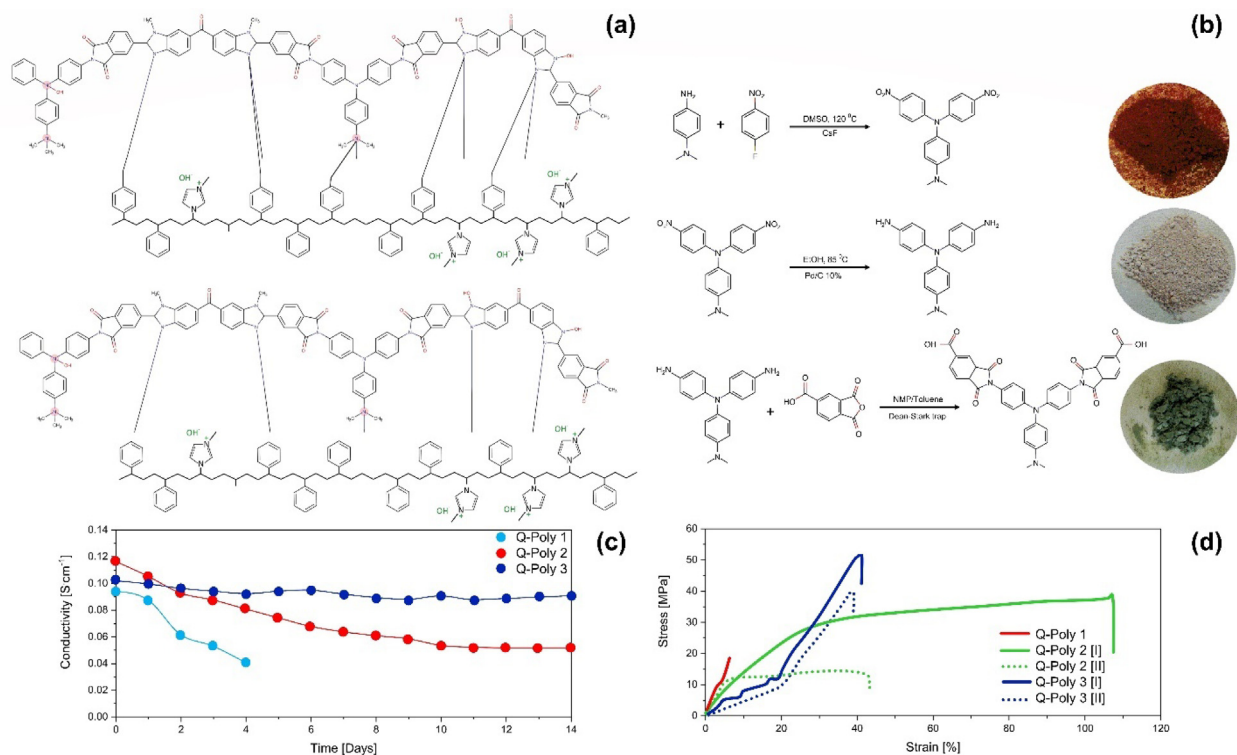


Fig. 7 Anion conductivity of membranes synthesized with various cations exhibits long-term chemical stability and simple monomer synthesis procedure (a-d). Elsevier 2019 provided permission to reproduce images (Firouz Tadavani et al., 2019).

brane conductivity was measured for 14 days with the membranes synthesized in this work (see Fig. 8 (e)). After 4 days, Q-Poly-1 degradation was high. Additionally, although Q-Poly-2 initially had the best ion conductivity, its ionic conductivity gradually declined (about 75 %) over time. During its stability study, Q-Poly-3's ion conductivity dropped by less than 7 %. According to the relationship between crosslinking and chemical stability (Lin et al., 2013, Firouz Tadavani et al., 2019), Q-Poly 3 is more stable because of its higher crosslinking.

AEM with four structures based on side chain type polysulfone was synthesized and studied by Chao wang et al (Wang et al., 2021) as shown in Fig. 9. Rather than using hazardous chemicals like chloromethyl ether, they selected chromethylate polysulfone. The Menshutkin reaction was used to synthesize cations and four side chains with different numbers. They claimed that it was possible to achieve high IEC values with four grafted side chains having two or three cations in the lower grafting degree thus alleviating the OH^- attack on the benzyl in the main chain. According to them, the synthesized AEM (CM-TQ6Q6Q⁻¹, 1.38 mmol. g⁻¹), 13.7 mScm⁻¹ OH⁻ conductivity, 8.9 % swelling ratio and 2.48 Ω cm² resistance is measured. Furthermore, 96 % of the original IEC reversion was observed. With an alkaline concentration time of ~ 1.8 , the CM-RQ6Q6Q⁻¹ AEM showed high performance (90.0 % efficiency and 8.47 kWh.kg⁻¹ energy consumption) while retaining 96.4 % of its original IEC, which is comparable to typical commercial AEM (Neosepta AHA). In addition, CMTQ6Q6Q⁻² was found to exhibit higher alkaline stability and OH⁻ conductivity than any other form of AEM with the same IEC (1.9 mmol. g⁻¹). The results were compared with

those from the commercially available form of Anion exchange membrane (Neosepta). The obtained outcomes indicate that, the synthesized CMTQ6Q6Q⁻¹ exhibits five times greater NaOH enrichment than Neosepta. AHA, as shown in Fig. 9 (a-d).

As we move forward in research, the main challenge is to improve alkaline stability. Tests showing hydride stability revealed that the majority of cationic groups adhered to the polymer chains, such as ruthenocene (Zha et al., 2012), phosphonium (Gu et al., 2009), sulfonium (Zhang et al., 2012) or trimethyl ammonium, (Zhang et al., 2010) guanidinium cations, are rapidly degraded in alkaline environments at elevated temperatures (Marino and Kreuer 2015). Moreover, most polymers are derived from polyether sulfones or ketones, and polymers can degrade under alkaline conditions (Arges and Ramani 2013). In addition to the polymer membrane, there are also polybenzimidazoles (Henkensmeier et al., 2011, Thomas et al., 2011, Lee et al., 2013, Henkensmeier et al., 2014, Wright et al., 2016) that help keep the polymer backbone stable. Hydroxide ion attack on imidazolium moiety C2 causes degradation (Henkensmeier et al., 2011).

According to Angela Marinkas et al., (Marinkas et al., 2018) (2,6-dimethyl-1,4-phenylene oxide) brominated backbones of polystyrene and methylated N atoms of the 2-mesitylbenzimidazole groups under the operating conditions 0.5 M KOH and 50 °C, are alkaline stable but are unstable at 80 °C for 1 M KOH. Under these conditions severe weight loss was observed. IEC values for the prepared materials are 1.6 to 2.9 mmol OH⁻ g⁻¹. A self-supporting membrane could only be reliably formed with materials that had an IEC value of 1.9 (PPO24-BIM). As IEC grows from 1.6 to 3 mmol

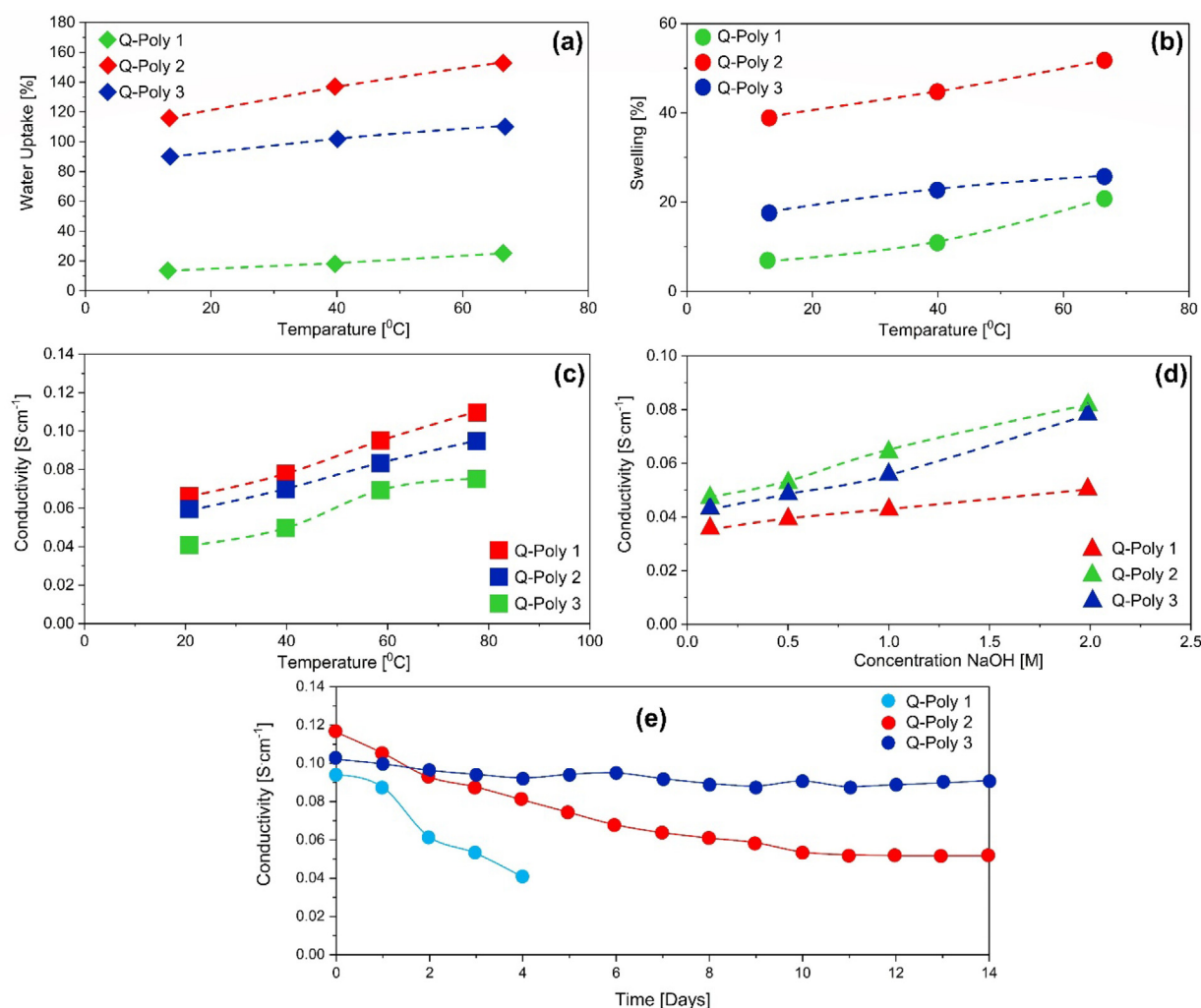


Fig. 8 WU and SR for Q-poly (1, 2 & 3) at various temperatures (a & b), conductivity of hydroxide at different temperatures and NaOH concentrations (c and d), and conductivity of hydroxide over 14 days at 80 °C and 2 M NaOH (e). The Elsevier 2019 has given permission to reproduce the figures (Firouz Tadavani et al., 2019).

$\text{OH}^- \text{ g}^{-1}$, there is a decrease in crystallinity, which decreased from 14 to 3 %. Self-supporting membranes can be formed using materials that have IEC values of 1.6 and 2.2, but not reproducibly. At room temperature PPO24-BIM had conductivity of 8 mS cm^{-1} , had a thermal stability above 200 °C, and had mechanical properties comparable to those of the commercially available membranes (FAA3-30). During water electrolysis 300 mAcm^{-2} were obtained at 1.8 V as shown in Fig. 10. Consequently, there is a need for further research on the stability of polymer backbones without ether groups.

Siarung Changkhamchom et al., (Changkhamchom et al., 2021) created a new type of membrane and they used it for a glucose fuel cell. The DMAOP and GO were combined with quaternized polybenzimidazole (3-PBI), which was quaternized with 3-bromopropyl trimethylammonium bromid, by using a composite AEM containing 0.5 % (V/V) Q-Go/Q-PBI. They states that highest hydroxide conductivity was highest at 27 °C, the ion exchange capacity was highest at $1.79 \pm 0.03 \text{ mmol g}^{-1}$, the water uptake was best at $66.61 \pm 0.57 \%$, and glucose permeability was highest $1.79 \pm 0.83 \times 10^{-8} \text{ cm}^2 \cdot \text{s}^{-1}$. The experimental data also showed

that this synthesized AEM has higher hydroxide conductivity and glucose permeability was lesser than that of commercially available membranes (FAB-PK-130-Fumasep®).

AEM application has been consistently pursued with different types of polymers, including poly (arylene ether sulfone), poly (phenylene oxide), poly (fluorenyl ether ketone sulfone), and poly (vinyl alcohol) (Pan et al., 2018, Zakaria and Kamarudin 2020). Various researchers states that the engineered plastic PBI containing the benzimidazole group is very chemically and thermally stable. For the improvement of anion stability, different researchers have used different processes, such as the methylation reaction (Henkensmeier et al., 2011), the quaternization reaction (Hou et al., 2011), and the alkaline doping procedure (Hou et al., 2008). Each technique has its own advantages and disadvantages, but the quaternization technique has also been shown to improve membrane durability and ionic conductivity. There are several advantages to Q-PBI (Shin et al., 2020) including the high hydroxide conductivity and chemical stability. However, some quaternized pendent groups within the leading polymer chain are unstable in alkaline aqueous solutions, creating an issue in AEMFC

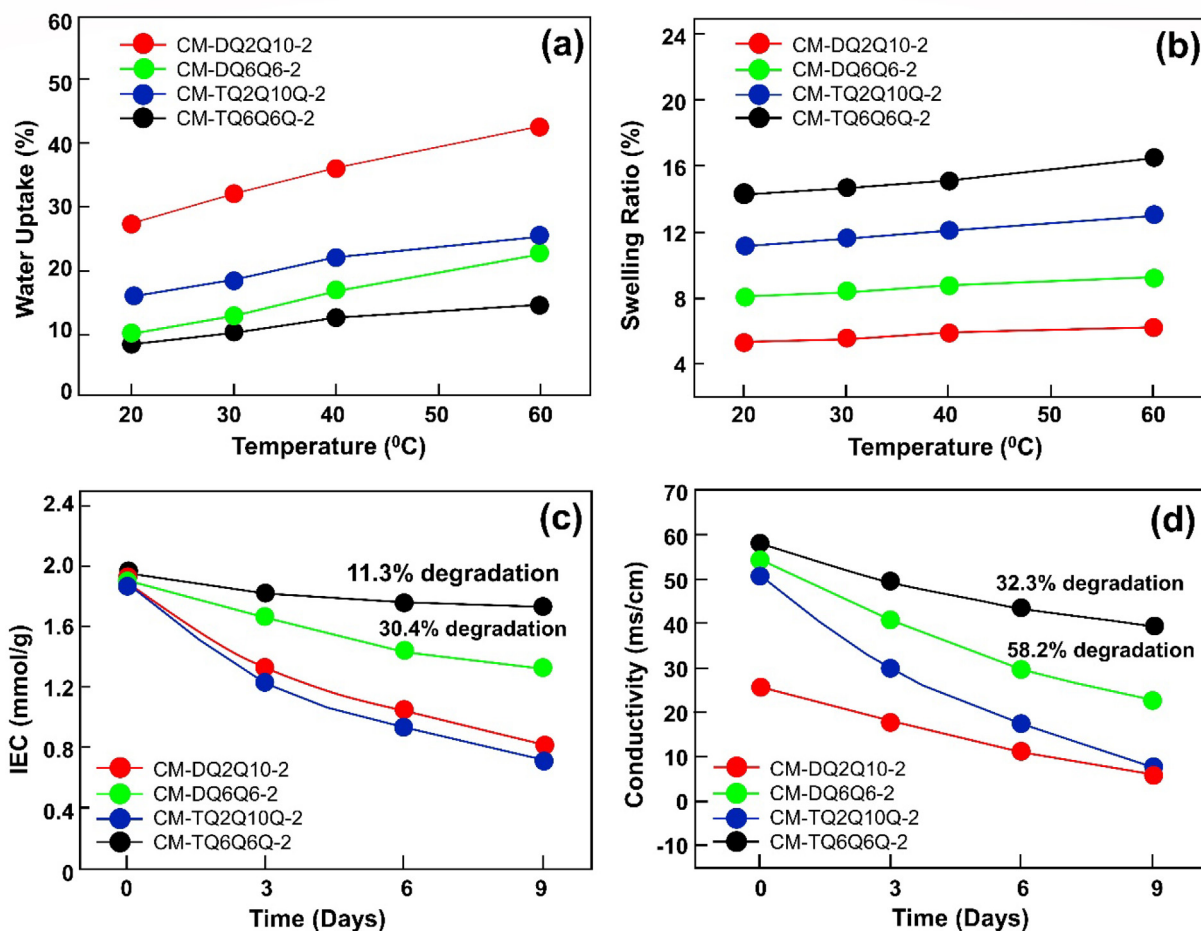


Fig. 9 WU (a), SR (b), temperature testing and IEC retention (c), and OH^- conductivity (d) of CM-DQxQy-2 and CM-TQxQyQ-2 (Immersion of CM-DQxQy-2 and CM-TQxQyQ-2 in 2.0 M NaOH solution for varying amounts of time at room temperature). The image reproduced with the copy right permission of Elsevier 2021 (Wang et al., 2021).

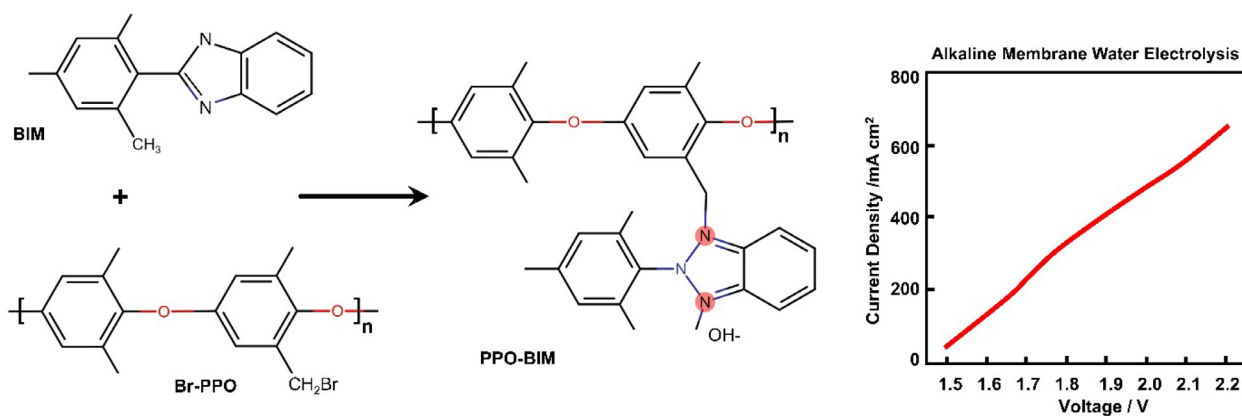


Fig. 10 Chemical synthesis of imidazole containing polymer membranes (PPO-BIM), reproduced with the copyright permission of Elsevier 2018 (Marinkas et al., 2018).

when utilizing potent. A well-known quaternization method for PBI includes a pendant quaternary ammonium moiety and an imidazolium side group (Xia et al., 2012, Jheng et al., 2014, Shin et al., 2020).

AEM can be improved by using different kinds of materials, such as multiwall carbon nanotubes (Hosseini et al., 2013), Chitosan nanoparticles (Liao et al., 2015) or graphene oxide (Zhang et al., 2018). Graphene oxide, however, caught

the eye of researchers due to its large surface area (Wang et al., 2020), good barrier properties, and excellent mechanical strength (Ye et al., 2011).

Among the greatest challenges facing polymer scientists, electrochemists, and membrane scientists is the development of AEMs with highest mechanical properties and higher hydroxide ion conductivity. In order to commercialize a membrane, it needs to meet several requirements, including scalability, the use of cost-effective/economical materials and methods; by controlling morphology and selecting the appropriate cationic ion-exchange groups, the mechanical properties of the polymer can be improved. The polymer backbone of the membranes is tethered to the fixed cationic sites. The phosphonium and quaternary ammonium salts of polysulfone produced via chloromethylation and quaternization followed by reaction with an amine. With potassium hydroxide, the form salt can easily be alkalized to produce an AEM that conducts hydroxyl ions (Arges et al., 2010).

Various kind of cations have been explored for Anion exchange membranes, including imidazolium (Lin et al., 2013), QA (Tuan and Kim 2016), phosphonium (Noonan et al., 2012), pyridinium (Kim et al., 2017), sulfonium (Zhang et al., 2012), and guanidinium (Arges and Ramani 2013). Though QA is commonly used because of its cost competitiveness, high anion conductivity and ease of preparation (Qiu et al., 2012), toxic trimethylamine and low alkali thermochemical stability are serious disadvantages (Ran et al., 2012). A large proportion of recent attention has been paid to imidazolium, since it is easily modified, synthetically convenient, and has comparable ionic conductivities (Wang et al., 2018). Due to its ability to stabilize through charge delocalization, imidazolium can also replace ammonium cations. For long-term applications, however, its stability in strong alkaline environments must be improved. According to several studies the ring opening mechanism led to the decomposition of imidazolium cations via the hydroxide attack at C2 position. Several researchers have used the C2 substitution in order to improve its alkaline stability (Wang et al., 2013, Hugar et al., 2015). Additionally, it has been reported that the addition of N3 alkyl substituents can improve its chemical stability (Gu et al., 2014, Yang et al., 2016). In general, N3-alkyl substituents should have four/five carbon atoms because imidazolium-based AEM had alkaline stability that was about the same (and in some cases even worse) than N3-methyl substituted counterparts if N3 substituents had longer alkyl chains (over six carbon) (Yang et al., 2015, Yang et al., 2016).

A number of properties of poly(arylene ether) ketone-based anion electrolyte membranes were investigated by substituting the imidazolium functional group at the C2 and N3 positions by Duong diem tham et al, as shown in Fig. 11 (Tham and Kim 2019). These membranes were tested in a zero-gap cell to test their electrolysis performance with alkaline water. They found that all membranes outperformed the commercially available membrane (Fumasep FAA-3) in terms of ionic conductivity and electrochemical efficiency. A PAEK-APMBI membrane and a C2 methyl membrane had high voltages and ionic conductivities of 2.63 V and 0.0154 S cm⁻¹, respectively, at 60 °C in KOH solution (10 %) while Fumasep FAA-3 membranes showed voltages and ionic conductivities of 2.63 V and 0.01 S cm⁻¹, respectively. IEC was retained by 96 % in PAEK-APMBI membrane in an alkaline environment for a long period of time, whereas IEC was reduced by 38 % in Fui-

masep FAA-3 membrane after long-term treatment in alkaline environment.

Researchers believe that the PAEK-APMBI membrane is an attractive candidate for electrolyzing anion exchange membranes and Baolong Wang et al (Wang et al., 2016) conducted experiments with QA, C2 substituted, and imidazolium to compare the differences in poly (arylene ether ketone) functionalized with benzyltrimethylammonium, benzylmethylimidazolium, and benzyl dimethylimidazolium. It was found that benzyltrimethylammonium (7 %) degraded in 1 M NaOH at 60 °C, while benzyl dimethylimidazolium and benzylmethylimidazolium had 46 % and 55 % degradation, respectively. Benzyltrimethylammonium > benzyl dimethylimidazolium > benzylmethylimidazolium is the order of stability. In comparison with the other two functionalized polymers immersed in 1 M NaOH and 60 °C, benzyltrimethylammonium showed better stability in the alkaline environment at elevated temperatures.

The structure of poly (arylene-ether) ketone with an aminopropyl moiety at the pendant site (PAEK-APMP) was investigated by 1H NMR in a paper published by Lee et al. In the present work, a series of membranes were synthesized, including PAEK-APMP 50, 75, 100 and 150; among which PAEK-APMP 75 and PAEK-APMP 100 under low water uptake (less than 55 %) exhibited good hydroxide ion conductivity (> 0.011 Scm⁻¹) at 60 °C. In addition to comparing synthetic membranes with commercial ones, they found that hybrid PAEK membranes grafted with quaternary ammonium groups exhibited excellent chemical, mechanical, and hydrolytic stability. The hybrid PAEK-APMP 75 and 100 membranes also performed better on an electrolytic test than PAEK-QA and FAA-3 (Fumasep) membranes (Lee et al., 2018).

Due to the hydration of cationic domain structures, water uptake closely correlates with membrane mechanical properties and ionic conductivity. Fig. 12 (a) shows the membrane's water uptake in relationship to temperature. Due to the ease with which hydration of ionic cluster occurs in PAEK-APMP membranes, water uptake is increased with increasing APMP contents. It was not possible to measure Fumasep FAA-3 membrane's water uptake beyond 60 °C due to membrane decomposition in water above that point. PAEK-QA had a lower water uptake despite a higher IEC value than PAEK-APMP75. In PAEK membranes, APMP groups form strong hydrogen bonds with water. As a result, water uptake increases, leading to higher ionic conductivity. The anion conductivities of a PAEKAPMP, a PAEK-QA, and a Fumasep FAA-3 membrane are shown in Fig. 12 (b). IECs of FAA-3 membranes were higher than PAEK membranes, resulting in higher anion conductivity. In spite of this, FAA-3 exhibited poor hydrolytic stability, preventing measurement of anion conductivity above 60 °C. At 30 °C and 80 °C, the anion conductivity varied from 0.0001 to 0.0054 Scm⁻¹ and 0.0034–0.0184 Scm⁻¹ depending on the amount of APMP substituted in the PAEK-APMP membranes.

Fig. 12 (c) illustrates the tensile behavior of PAEK-APMP membranes after they have been injected with APMP at different doses. APMP is replaced more often, which decreases its tensile strength while increasing its elongation at break. In association with water, the APMP induces a plasticizing effect on the membrane. PAEK-APMP150, which has the highest concentration of APMP, had the best tensile strength of 17.2 MPa and elongation of 73.8 %. However, Fumasep FAA-3 membranes exhibited a much lower elongation than

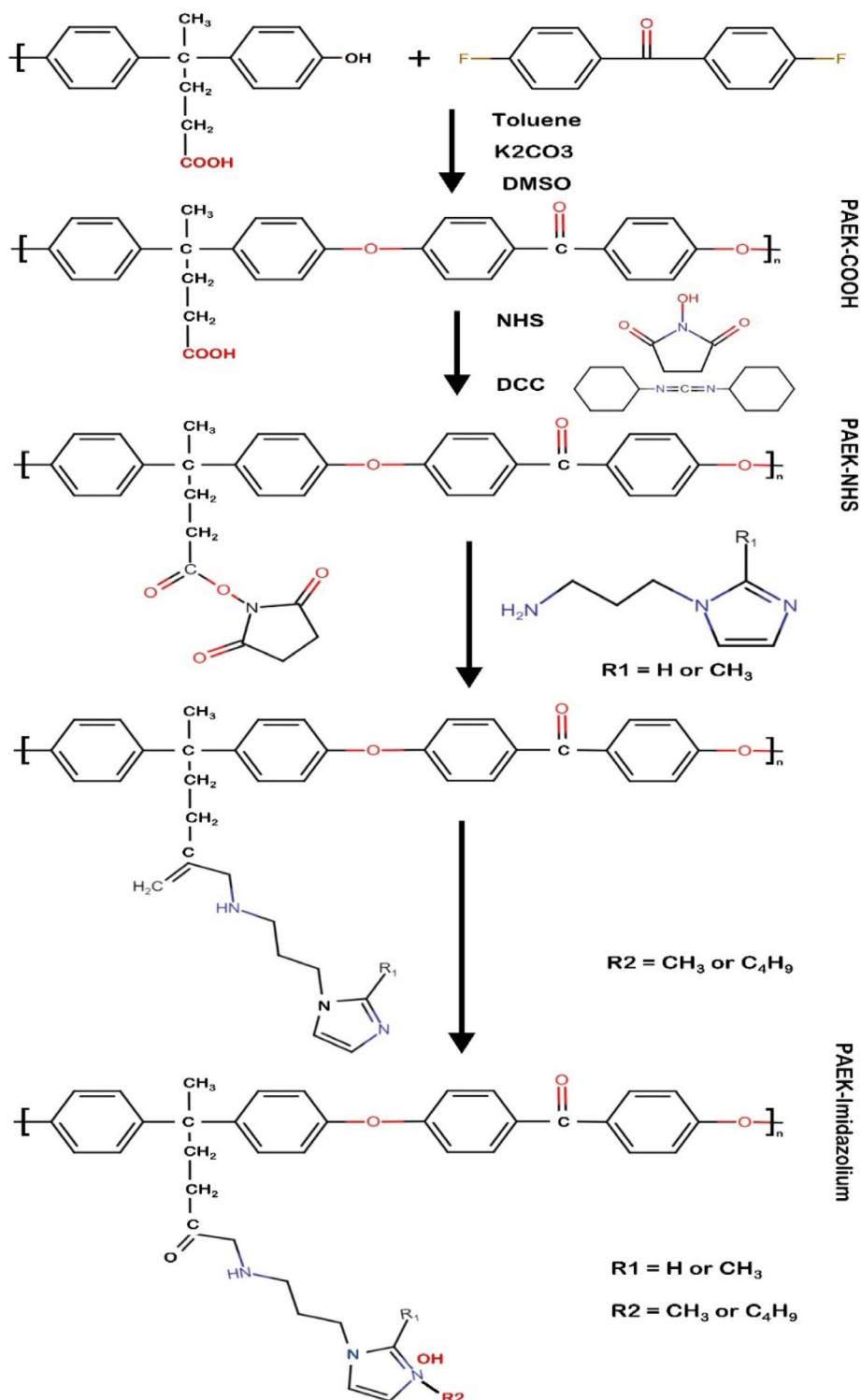


Fig. 11 Schematic representation of PAEK-Imidazolium membranes. Reproduced with the copyright permission of Elsevier 2019 (Tham and Kim 2019).

PAEK membranes despite having a higher tensile strength. Fig. 12 d depicts the IEC changes measured during four weeks in NaOH solution in 10 wt% at 60 °C for PAEK-APMP, Fumasep FAA-3 and PAEK-QA membranes. Due to its frequent operation at lower temperatures, Fumasep FAA-3 was

also tested at 50 °C in addition to 60 °C. Fumasep FAA-3 and PAEK-QA membranes show rapid decreases in IEC as a result of the Hofmann elimination reaction (Mohanty and Bae 2014). While Fumasep FAA-3 had a higher initial IEC value, its degradation rate was also similar to PAEK-QA.

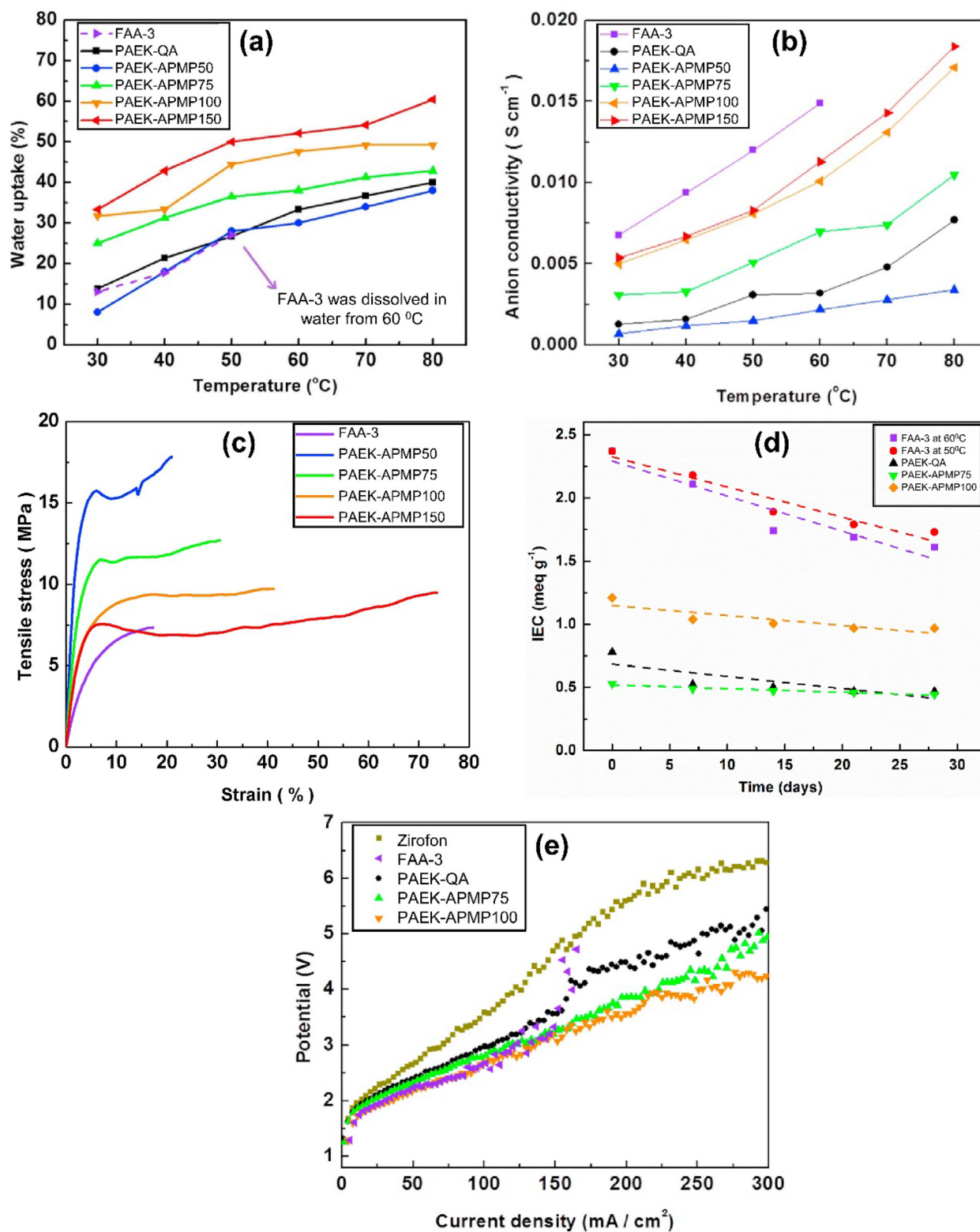


Fig. 12 The water uptake and anion conductivity as a function of temperature of the PAEK-APMP, Fumasep FAA-3, and PAEK-QA membranes (a and b), respectively, tensile stress vs strain behavior of PAEK-APMPs and Fumasep FAA-3 (c), Variation in the IEC of Fumasep FAA-3, PAEK-QA, and PAEK-APMP membranes in a solution of 10 % NaOH at 60 °C (d), and the polarization curves of PAEK-APMP-75 and PAEK-APMP-100 along with Fumasep, FAA-3, PAEK-QA, and zirfon membranes were measured at 60 °C in an electrolysis system composed of 10 wt% KOH solution for all membranes (e), Images were reproduced with permission from Elsevier (2018) under the copyright (Lee et al., 2018).

The degradation rate of PAEK-APMP membranes was substantially lower than other types of membranes regardless of the initial IEC value. In alkaline conditions, APMP suffers from less susceptibility to Hofmann elimination reaction compared to QA PAEKAPMP. This ensures that membranes containing QA can retain ion transport capability under alkaline conditions for a longer period. An electrolyzer constructed with different membranes is illustrated in Fig. 12 (e). PAEK-APMP-75 and PAEK-APMP-100 membranes have lower potentials and maintain higher performance than Zirfon separators (used in AWE). When the current density in PAEK-APMP membranes was low, they performed in a similar way to PAEK-QA membranes. However, when the current density was above 150 mAcm^{-2} regardless of IEC, they performed significantly better. This may be due to the chemical stability of QA ion conductivity. In their early stages of development, FAA-3 membranes showed performance that was similar to that of APMP100, however, they were quite hydrolytically unstable due to weak mechanical and thermal properties. The PAEK membranes synthesized in this study performed well and were durable, without any abnormalities before or after use (Lee et al., 2018).

An electrochemically oriented AEM was fabricated by using a convenient approach by Thomas et al. AEMs containing polysulfone hydroxide anion and negative charge carriers, triazatriangulenium carbonation (4,8,12-triethano-4,8,12-tria-

zatriangulenium tetrafluoroborate), pKR + values > 20 were used. It can be seen from the different results that the polysulfone matrix contains a large carbocation network for 4,8,12-triazatriangulenium, that its ionization capacity is good ($2.44 \pm 0.72 \text{ mew/g}$) and that it can transport hydroxide anions smoothly with an E_a value of 6.56 kJmol^{-1} . The high stability of the triazatriangulenium cation is responsible for 88 % of the initial membrane conductivity in a 3 M KOH at 60°C for 35 days, in addition to the high ion conductivity of 23.5 mS cm^{-1} at 90°C ., shown in Fig. 13 below (Thomas et al., 2021).

Utilizing crosslinking and methylation of polysulfone, Priya Goel et al (Goel et al., 2021) synthesized a series of monovalent anion selective graphene oxide (QGO). QGO cross-linked on membranes provide additional functional sites, as well as a dense polymer matrix. They studied the effects QGO on different properties such as electrochemical and physicochemical properties and using a CrPSf-3 membrane (nano cross-linker at 3 wt%), the researchers determined that it had good mechanical and thermal stability and the best ion exchange capacity with water uptake of 31.20 %, a swelling ratio of 9.90 %, a counter-ions transport coefficient of 0.95, and a chloride ion conductivity of 72 mS cm^{-1} . With 0.05 mol. L^{-1} of mixed salt solution ($\text{NaCl} + \text{Na}_2\text{SO}_4$), electro-dialysis was studied to investigate the membrane permselectivity of Cl^- and SO_4^{2-} . Compared to commercial FAB-PK-130

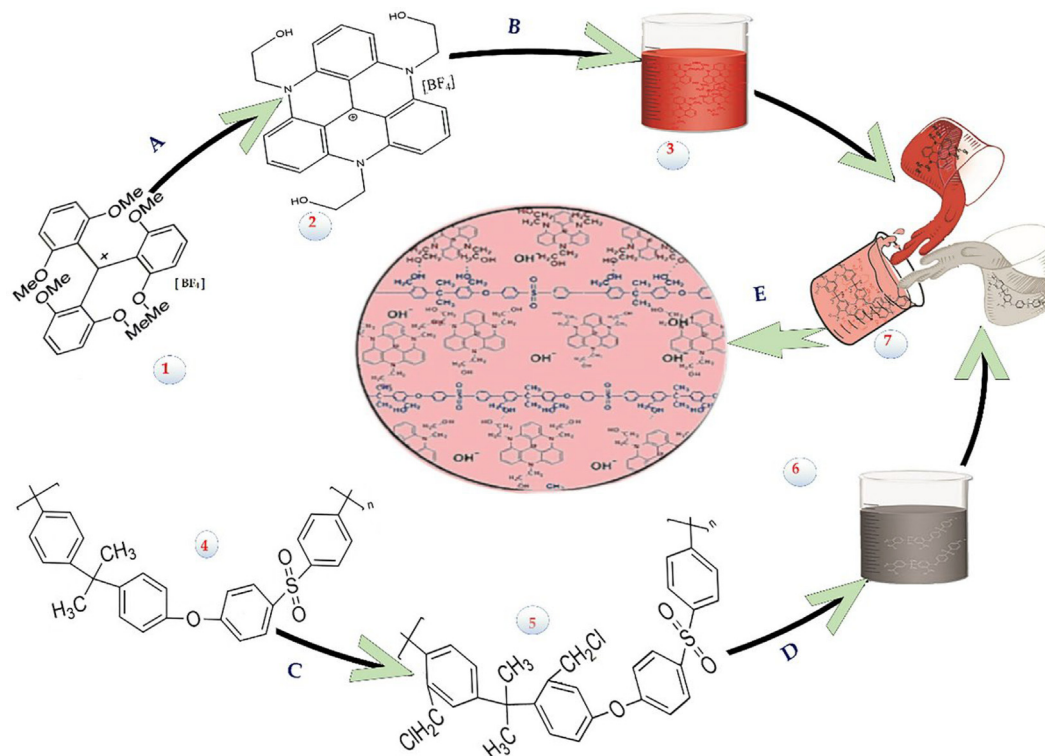


Fig. 13 AEM fabricated by using $\text{TATA}^+ -\text{OH}$. The steps involved; (1) Initial materials used for the fabrication of AEM; tris(2,6-dimethoxyphenyl)-methyl tetrafluoroborate), (2) Addition of (4,8,12 tri-ethano-4,8,12-triazatriangulenium- $\text{TATA}^+ -\text{OH}$), (3) $\text{TATA}^+ -\text{OH}$ dispersion in NMP, (4) PSF, (5) CMPSF, (6) NMP and CMPSF Dispersion, (7) Further, CMPSF and $\text{TATA}^+ -\text{OH}$ solutions are mixed and sonicated on different reaction conditions: (A) Addition of N_2 /Ethanolamine at 190°C ; (B) $\text{TATA}^+ -\text{OH}$ stirred; (C) addition of $(\text{CH}_3)_3\text{SiCl}$, Paraformaldehyde and SnCl_4/N_2 for 72 h; (D) CMPSF was stirred; (E) The final step in the process is to determine the electrochemical synthesis pathway for the $\text{TATA}^+ -\text{OH}$ carbocation AEM using evaporating solvents and drying settled casted membranes. Images were redrawn by with the copyright permission from Elsevier 2021(Thomas et al., 2021).

(2.01) and QPSF (1.7) membranes, the separation factor (SF) of the CrPSf-3 membranes was 5.7 for $\text{Cl}^- / \text{SO}_4^{2-}$. As a consequence, CrPSf-3 membranes displayed a much higher Cl^- flux rate than commercial membranes ($1.6 \text{ mol m}^{-2} \text{ h}^{-1}$) and pristine QPSf ($1.45 \text{ mol m}^{-2} \text{ h}^{-1}$) as shown in Fig. 14.

Chuan Hu et al. examined the ploy (aryl-*co*-aryl piperidinium)-*x* ($\text{PD}_n\text{TP-}x$) with alkyl spacers in five alkyl positions ($n = 0, 1, 2, 6, \text{ and } 10$) to explain their conclusions. A short alkyl chain is more dimensionally stable and gas-tight (H_2 permeability 10 Barrer) than a long chain, whereas long alkyl chains displayed better dimensional stability as mentioned in Fig. 15. $\text{PD}_n\text{TP-}x$ membranes were found to be excellent alkaline and oxidative stabilizers (200 h in Fenton's reagents) on all of the polyaromatic AEMFCs, cells of the long chain type had a greater power output of 1.7 W cm^{-2} . There is a continuous operation time of 220 h for $\text{PD}_n\text{TP-}x$ AEMFCs of the short chain type using a current density of 0.4 A cm^{-2} and a voltage decay rate of $77 \mu\text{V h}^{-1}$ (Hu et al., 2022).

As depicted in Fig. 16, Yang Bai et al. formed nanostructure (CQPSU-X-rGO) supported on quaternized polysulfone

(QPSU) and functionalized with small molecules of varied chain lengths after crosslinking by reduced graphene oxide. A control was prepared with QPSU-*n* cross-linked to organic small molecules. Comparisons of quaternary ammonium groups generated by elastic long chain cross linked membranes and elastic short chain cross linked membranes indicate that membranes with elastic long chain cross linked agents demonstrate superior conductivity. The CQPSU-XLrGO and CQPSU-X-SrGO demonstrated superior chemical stability and conductivity to cross linked AEMs (CQPSU-2 %-LrGO, at 80°C $\sigma_{\text{OH}} = 139.7 \text{ mS/cm}$). AEMs prepared by cross-linking functionalized rGO have therefore been shown to possess improved properties as cross-linkers and fillers (Bai et al., 2019).

PTMHDA (Fig. 17 b) and LrGO (Fig. 17 d) prepared by long-chain cross-linkers demonstrated higher hydroxide conductivities than TMHDA (Fig. 17 a) and SrGO (Fig. 17 c) prepared by short-chain cross-linkers (Bai et al., 2019). PTMHDA and LrGO have been shown to be capable of generating more quaternary ammonium groups, which enhance WU. Further-

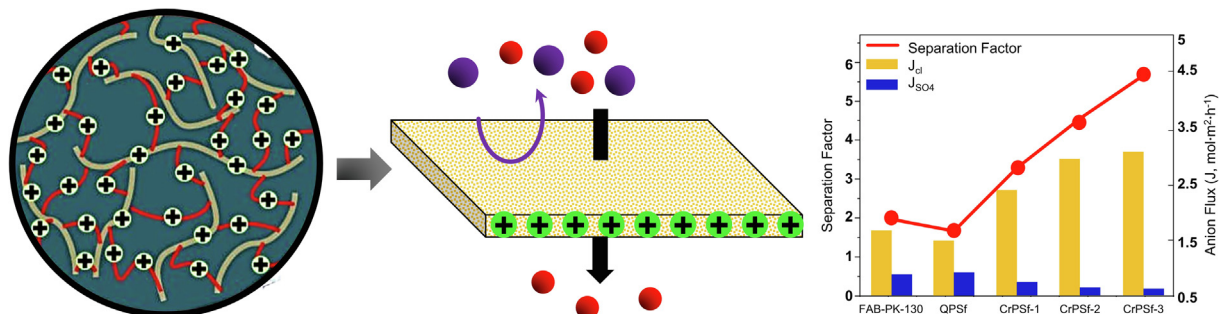


Fig. 14 Multi-cationic cross-linked monovalent selective AEM based on QGO for electro dialysis. Figure reproduced with copyright permission of Elsevier's (2021) permission (Goel et al., 2021).

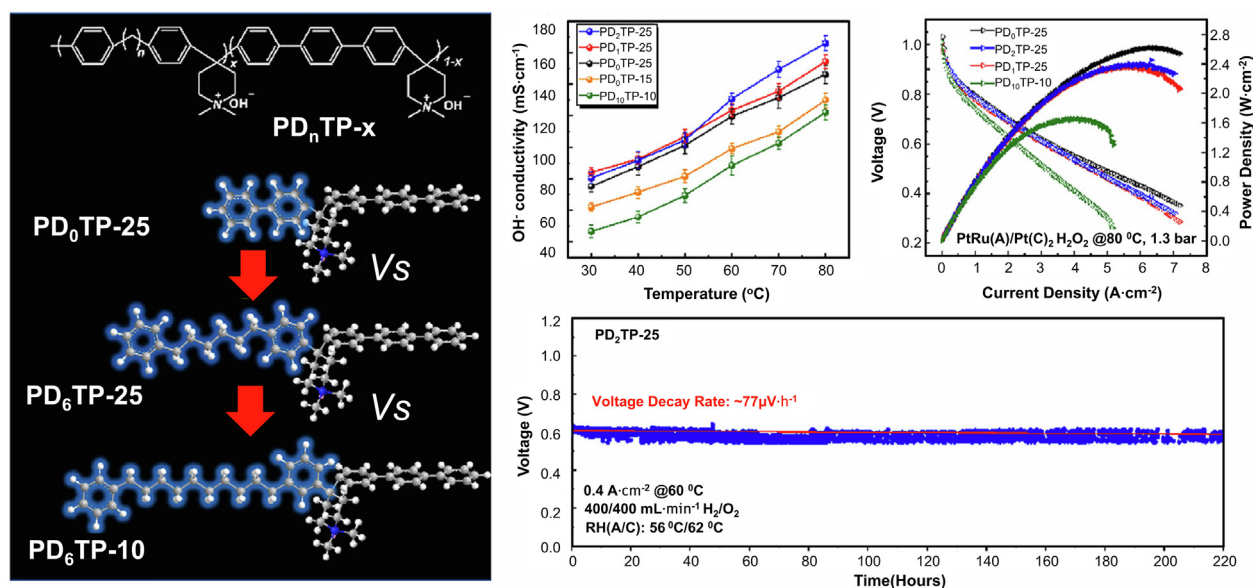


Fig. 15 Performance and durability of membrane(ploy (aryl-*co*-aryl piperidinium)-*x*) based fuel cells based on different test conditions and cathode catalysts and AEMs-water uptake, platinum-cathode, 1.3 bar-backpressure (both sides), and current density of 0.4 A cm^{-2} at 60°C . Figure reproduced with copyright permission of Elsevier's (2022) permission (Hu et al., 2022).



Fig. 16 The chemical synthesis of functionalized rGO and their crosslinked QPSU-based AEMs. Copyright permission was obtained from Elsevier 2019 for the redrawn figure (Bai et al., 2019).

more, modified rGOs cross-linked composite AEMs show greater hydroxide conductivity than small molecules-cross-linked polymers. As a result of this, functionalized rGO in AEMs can disperse ionic clusters with greater uniformity, improving ion conductivity as compared to small molecules-cross-linkers. CQPSU-2 %-SrGO membrane's ion conductivity was further reduced when the SrGO content was increased to 2 %. Inorganic fillers introduced in excess can lead to a decrease of hydroxide conductivity due to the obstruction of ion transport pathways. Despite the higher doping, the CQPSU-2 %-LrGO membrane had the highest conductivity of $139.67 \text{ mS cm}^{-1}$ at 80°C .

The authors also found that the long-chain molecule cross-linker proposed for AEMs which utilized functionalized rGO as a cross-linker can effectively solve the compatibility problem between the filler molecules and the polymer matrix, and further enhance overall performance, including ion conductivity in cross-linked AEMs (Bai et al., 2019). Based on the temperature-dependent ion conductivity plots in Fig. 17(e-h), one can calculate the apparent activation energy (E_a) of OH^- conduction for different AEM samples (Bai et al., 2019). E_a values of modified rGO-cross-linked composite AEMs ($8.1\text{--}14.9 \text{ kJ mol}^{-1}$) were somewhat lower than those of cross-linked polymer membranes ($12.3\text{--}18.9 \text{ kJ mol}^{-1}$). QPSU-2 %-LrGO and QPSU-2 %-SrGO had the highest E_a values, with 9.1 kJ mol^{-1} and 8.2 kJ mol^{-1} , respectively. Based on the fact that the rGO-crosslinked composite membranes had comparable ion conductivity to other membrane samples, the nonionic nature of rGO should contribute to lowering E_a for ion conduction in AEMs [193]. In Fig. 17(i, j), the hydroxide conductivity was plotted as a function of WU and SR to better understand the ion conductivity of different cross-linked AEMs. In comparison to the cross-linked polymer films with similar WU, the modified rGO cross-linked composite films exhibit significantly higher OH^- conductivity (Fig. 17 i). CQPSU-2 %-LrGO membrane has an OH^- conductivity of 75.9 mS cm^{-1} with a controlled WU of 95.5 %. p-CQPSU-3 had a OH^- conductivity of 49.2 mS cm^{-1} even when its WU

reached 103.1 %. AEMs with rGO cross-linked are more uniform in their nanophase separation structures as a result of increased ion transmission through the lamellar structure of rGO. According to Fig. 17 (j), membrane samples prepared by short-chain cross-linker of THMDA exhibited a lower swelling ratio than those prepared with long-chain cross-linker of PTHMDA. Long-chain cross-linkers provide flexibility to the membranes, preventing the inner structure from being tightly packed. Compared to cross-linked polymer membranes with similar SR, the rGO-cross-linked composite membrane had higher OH^- conductivity. Due to the incorporation of rGO, the membranes remained dimensionally stable due to decreased movement of the polymer chain (Bai et al., 2019).

Recently, it has been reported that pendent quaternary ammonium ionomers made of polysulfone (PSf) can dissolve only in solvents having high boiling points, like dimethylformamide (DMF) and dimethylacetamide (DMAc), which are difficult to remove from solution when finely dispersed catalysts are present (Lu et al., 2008, Park et al., 2008, Pan et al., 2010). An ionomer of quaternary phosphonium functionalized PSf with a low boiling point, superior hydroxide conductivity and superior alkaline stability has been created by Yang et al., (Yang et al., 2015) A H_2/O_2 AEMFC outperformed the MEA without ionomers by 3.5 times at 50°C , as measured by its peak power density of 138 mW cm^{-2} at 50°C . In their study, Sun et al. synthesized quaternary ammonium-based ionomers with a wide range of ion exchange capacities using SEBS as the backbone, a thermoplastic elastomer with good thermal, mechanical and chemical stability. With a back pressure of 2 atm and a temperature of 50°C , an AEMFC(H_2/O_2) achieved a peak output of 210 mW cm^{-2} , this is significantly higher than a MEA with PSf-based ionomers (50 mW cm^{-2}) (Sun et al., 2012). However, despite the ion conductivity and solubility of these ionomers being acceptable, their MEA performance did not align with state-of-the-art PEMFCs. The public domain also contains only a limited number of publications discussing AEMFC performance, particularly durability (Varcoe et al., 2006, Wang et al., 2017). The Xueqiang Gao

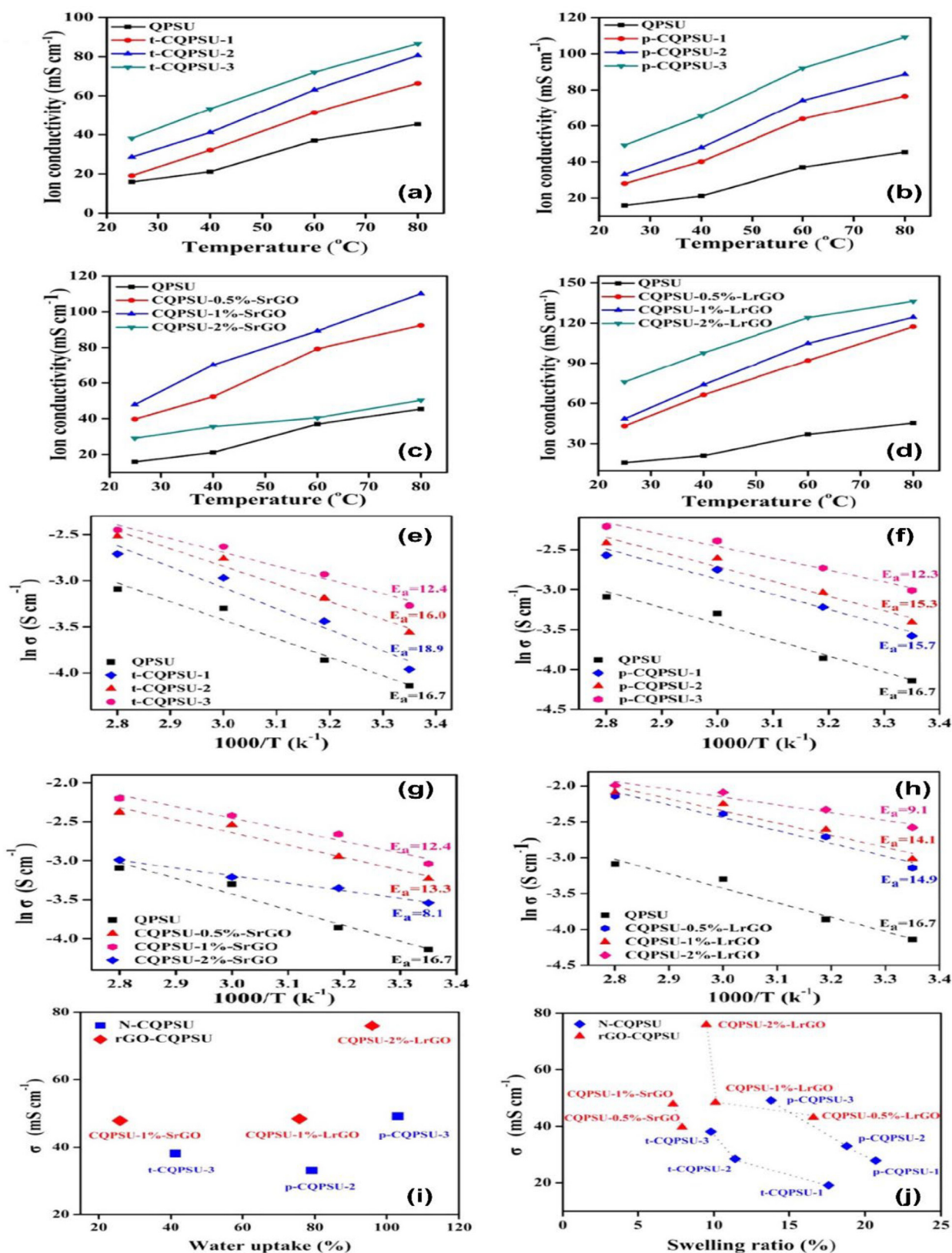


Fig. 17 (a-d) Hydroxide conductivity of different AEMs, (e-h) Arrhenius curves of different AEMs, (i) Water uptake and OH⁻ conductivity, and (j) swelling ratio and hydroxide conductivity of different AEMs at room temperature. Figure reproduced with the copyright permission from Elsevier 2019 (Bai et al., 2019).

et al. study synthesized novel ionomers containing a triblock copolymer that is highly conductive and durable. In this study, the authors showed that poly(styrene-ethylene/butylene-styrene-SEMS) can be grafted with a functional group, and that the OH⁻ conductivity of the ionomer at 75 °C is 30 mS cm⁻¹. In H₂/O₂ AEMFCs, this ionomer also demonstrated excellent durability with a degradation rate of 0.22 mVh⁻¹ over 500 h at a constant current density of 100 mA cm⁻². The performance of the MEA with QASEBS ionomer was also compared to that of the commercially available Acta I2 ionomer. A MEA ionomer with QASEBS reaches 375 mW cm⁻² at 50 °C, which is three times more powerful than an Acta I2 ionomer (124 mW cm⁻²), shown in Fig. 18 (Gao et al., 2017).

Sun Young Kang et al. reported high stability and ionic conductivity of their AEMWE system by using TM1TM membrane combines with a polyphenylene backbone and quaternary ammonium groups as the functional group (Meek et al., 2019). AEMWE performs better due to the hydrophobicity and geometry of the membrane. In their study, they found the Orion TM1TM membrane to be thermally stable and more temperature resistant than the FAA-3 membrane. The Fig. 19 below illustrates the AEMWEs' polarization curves (cl-10, 20, 30, & 40) and the ionomer content of anode was constant (20 %). At 1.9 Vcell, the current density of cl-10, 20, 30, and 40 were 1.72, 1.92, 2.40, and 1.38 A cm⁻², respectively. Here, 10–40 indicates the cathode ionomer content ranges from 10 to 40 wt%. After increasing the content of ions from 10 to 30 wt%, performance gradually increased till 30 %, then decreased at 40 %. The results are shown in Fig. 19(b).

Fig. 19 (c) illustrates the performance of AEMWEs that contained 5 % (al-5), 10 % (al-10), 20 % (al-20), 30 % (al-30), and 40 % (al-40) ionomers. Cathode ionomer (30 %) was fixed. From al-05 to al-10, the performance of AEMWEs increased, while from al-10 to al-40, it decreased. There is a ionomer in a certain amount that facilitates ion movement in the catalyst layer, which assists electrochemical reactions. However, excessive ionomer blocks the catalyst's active sites. Despite its very small ionomer content, al-05 exhibits high activation and mass transport resistance, as shown in Fig. 19(d). A second characteristic of al-05 is that it has dense structures with small secondary pores, increasing the resistance to reac-

tant and product transport. The result of the experiment is that as the percentage of the ionomer increased from 5 to 10 %, activation and mass transport resistance have decreased, and cell performance has improved, this indicates that 10 wt% is sufficient for efficient ionic connections. Moreover, they noted that the cell performance was reduced when the ionomer content was > 10 wt%, possibly due to the larger secondary pores caused by the large ionomer content, and they recommended that the optimal cathode and anode ionomer content should be 30 % and 10 wt% in regard to the catalyst loading. Furthermore, they found that the optimum catalyst loading was 0.4 mg_{pt} cm⁻² and 2.0 mg_{IrO2} cm⁻².

Optimized TM1-MEA's current density is 2.75 A cm⁻², allowing it to operate a 1.9 Vcell. Due to its high stability of 55 mVh⁻¹ and its superior structure, the orion-TM1TM membrane offers superior performance. According to Fig. 20(a), current density at 1.9Vcell is approximately calculated from a graph based on the values reported in the literature for AEMWE (Pavel et al., 2014, Liu et al., 2017, Vincent et al., 2017, Cossar et al., 2019, Park et al., 2019, Fortin et al., 2020, Jang et al., 2020, Thangavel et al., 2020). Compared to the literature, they claimed and demonstrated to have achieved the best results, as seen in Fig. 20 (a). Fig. 20 (b and c) shows the results of evaluating cycling stability using TM1-MEA and FAA-MEA under optimum conditions. Following 200 cycles, the TM1-MEA was significantly more stable than the FAA-MEA, resulting in a reduction in the current density by 32 % and an 85 % reduction in the FAA-MEA. Both showed rapid decreases in current density during the first hundred cycles. According to Fig. 20 (d), TM1-MEA displayed a gradual increase in voltage until about 20 h and then exhibited a constant voltage profile for 50 h, whereas FAA-MEA mounted sharply in 3.4 h to 2.3 Vcell. In comparison with previous studies on commercially available ionomeric anion exchange membranes for AEMWEs, their work provided the highest performance. Consequently, ionomeric AEM for AEMWE can be considered as Orion TM1TM membrane. Overall, it was found that the TM1-MEA performed better than the FAA-MEA in every feeding condition, whether it was pure water or diluted alkaline solution.

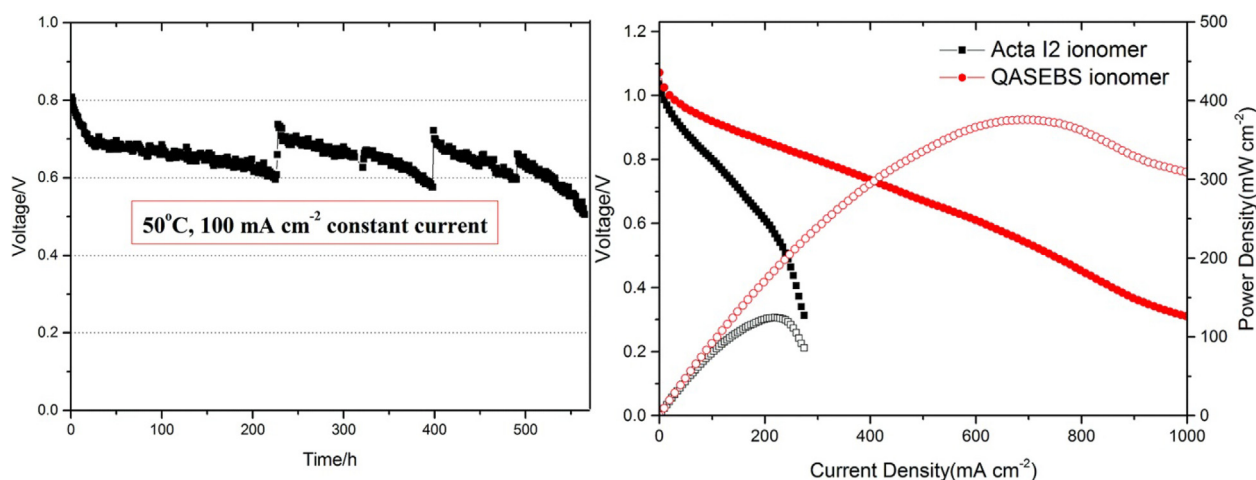


Fig. 18 Portrays the efficacy of various electrode systems utilizing QASEBS and Acta I2 ionomers and the durability of MEA using QASEBS ionomer. The Figure reproduced with the copyright permission of RSC advance 2017 (Gao et al., 2017).

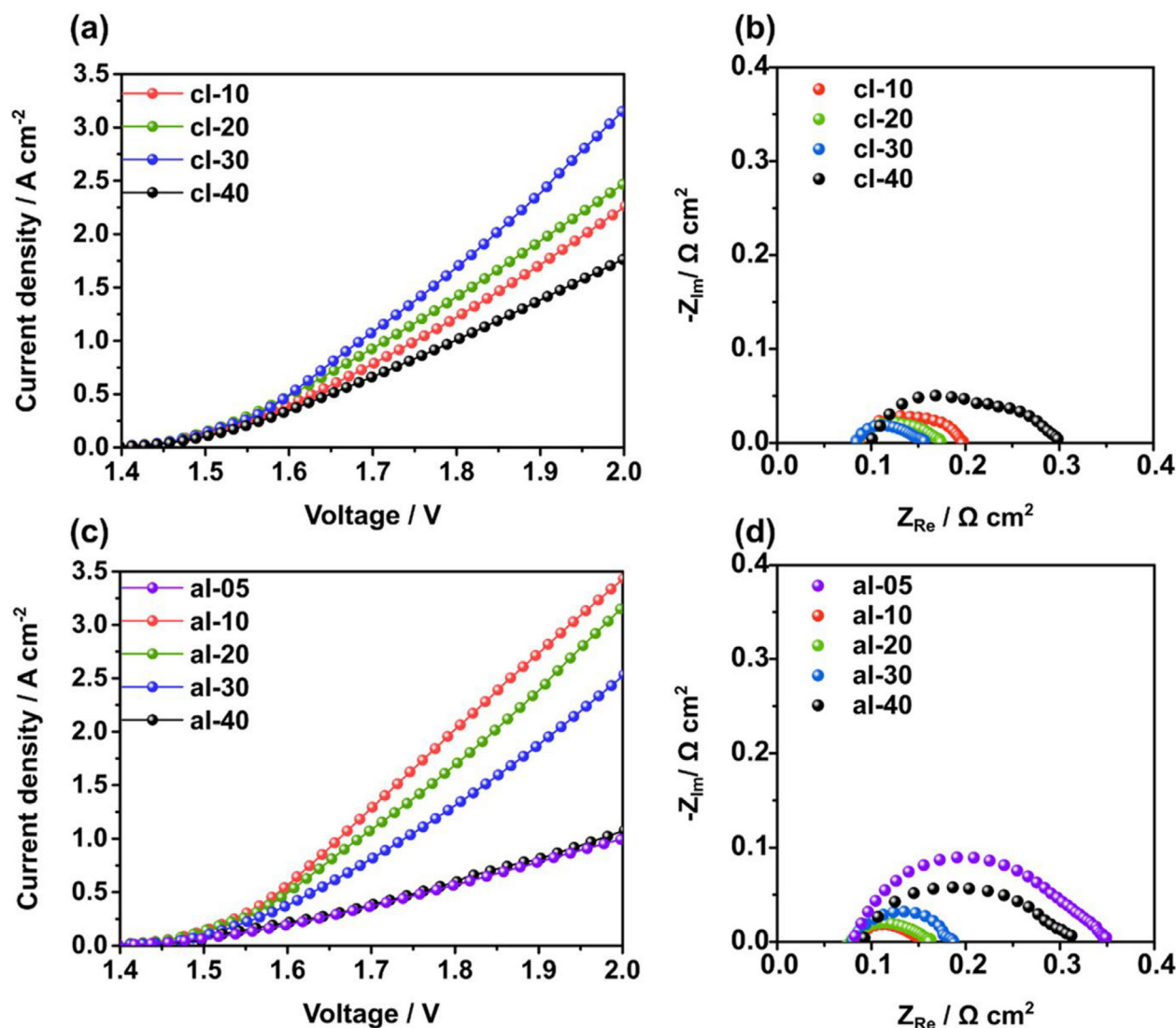


Fig. 19 The polarization curves and Nyquist plot for AEMWEs (cl-10, 20, 30 & 40) along with varying ionomer contents (10-40 wt%) at $1.9 V_{\text{cell}}$ are shown as symbols in (a & b). At 20%, the anode ionomer content remained constant. The polarization curves and Nyquist plots of the AEMWE's (al-05, 10, 20, 30, and 40) were calculated at $1.9 V_{\text{cell}}$ using 5, 10, 20, 30, and 40 wt% as anode ionomer contents. During the experiment, ionomer of cathode concentration was remained same at 30% by weight. This reproduction is permitted with Elsevier's(2022) consent (Kang et al., 2022).

There has been much interest in backbones and cationic head groups. AEMs are largely made up of aromatic polymers because of their high thermal stability, solubility, and chemical resistance (Zarrin et al., 2012, Lee et al., 2015, Mohanty et al., 2015). In addition to aromatic polymers, exploration of several newly discovered structures has been conducted, including poly (biphenyl alkenes) (Lee et al., 2015), poly(terphenylenes) (Lee et al., 2017), *N*-spirocyclic quaternary ammonium ionenes (Pham et al., 2017) and perfluoroalkyl copolymers/quaternized aromatic (Mahmoud et al., 2017). There have also been reports of cationic head-groups such as quaternary ammonium groups (QA) (Zhu et al., 2016, Mahmoud et al., 2017, Zhu et al., 2017), imidazolium ions (Gong et al., 2017, Guo et al., 2017, Lin et al., 2017), guanidinium ions (Xue et al., 2017), phosphonium ions (Noonan et al., 2012), and aliphatic heterocyclic QA head groups (Hahn et al., 2013, Dang

and Jannasch 2016). Due to their availability and reasonable stability, the QAs are among the most popular cationic groups (Mahmoud et al., 2017). Ling Li et al. (Li et al., 2018) used demethylation, polycondensation, and the Williamson reaction to prepare the synthesized poly(ether ketone) bearing multi cation side chains via Poly(ether ketone)s. It has been confirmed by TEM and SAXS that multication side chains promote phase segregated morphologies between hydrophilic and hydrophobic phases. At 80°C , the TQAPEK-0.5 membrane has the highest IEC of 1.94 meq g^{-1} as well as the highest hydroxide conductivity of 132.8 mS cm^{-1} . AEM possesses a high alkaline stability due to hexyleneoxy groups connecting the side chain to the backbone. It took TQAPEK-0.5 only 22.4 % longer to decrease its conductivity at 60°C in a solution of 2 M KOH after 600 h. Moreover, a single cell utilizing TQAPEK-0.5 membrane can generate a peak power density of

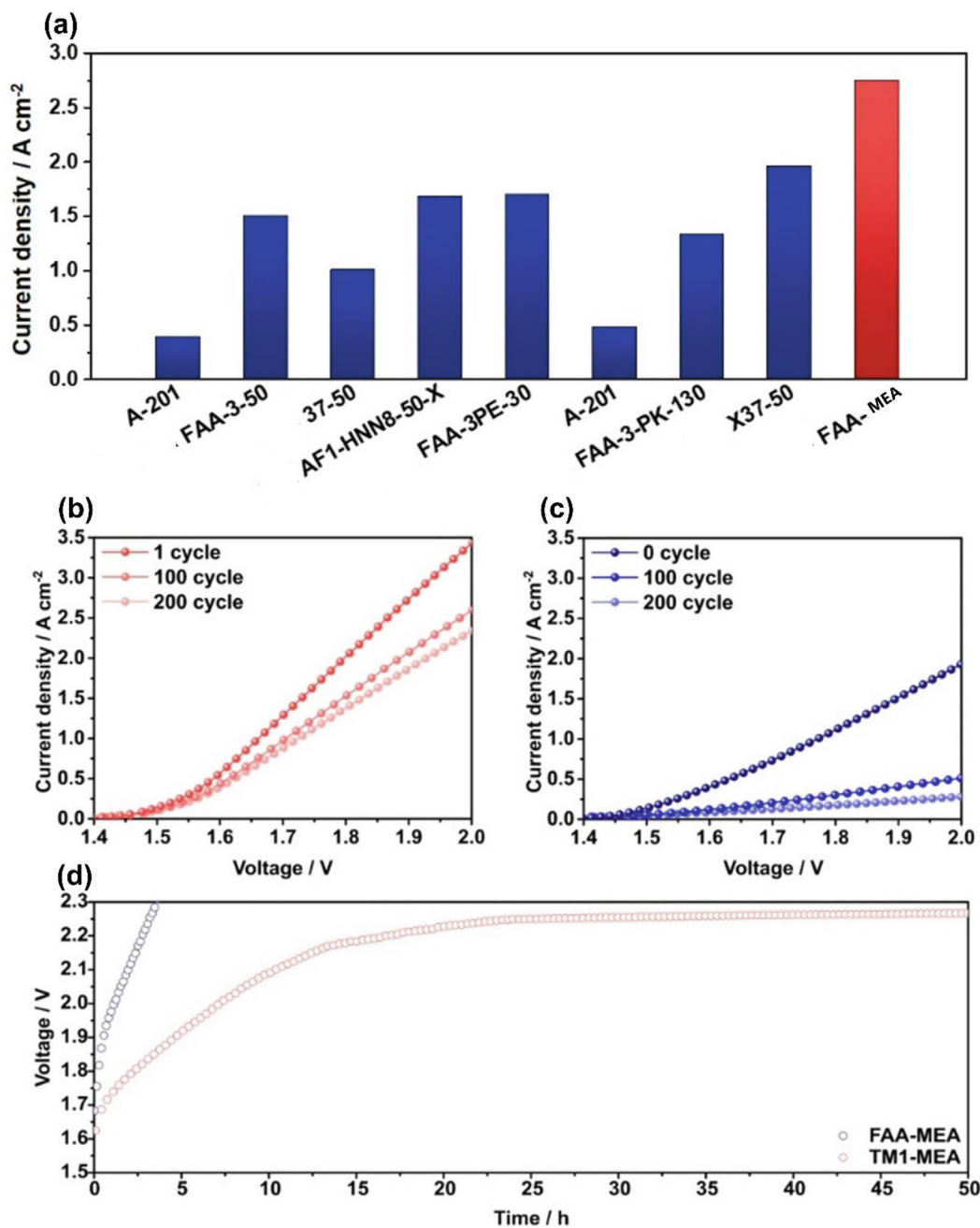


Fig. 20 (a) A comparison between the results of AEMWEs presents in the previous studies (as mentioned on x-axis) (Pavel et al., 2014, Liu et al., 2017, Vincent et al., 2017, Cossar et al., 2019, Park et al., 2019, Fortin et al., 2020, Jang et al., 2020, Thangavel et al., 2020) and the ones developed FAA-MEA (70 °C). (b) Polarization curves of FAA-MEA and (c) TM1-MEA after 100 and 200 cycles. Under optimized conditions at 500 mA cm⁻² stability tests were performed on two types of AEMWE such as TM1-MEA and FAA-MEA (d). The Figure was reproduced with the permission of Elsevier 2022(Kang et al., 2022).

206 mW cm⁻² when the current density is 400 mA cm⁻². Additionally, the as-prepared AEMs exhibit good thermal and mechanical properties, promising their use in FC as shown in Fig. 21.

As depicted in Fig. 22, TQAPEK-x has a better conductivity than other membranes reported for WU and IEC. As shown in the graphs, all membranes of TQAPEK-x appear at the top left, indicating that membranes in Li Liang et al's work have higher transport of OH⁻ efficiencies at lower WU

and IEC. Additionally, membranes with multications on the side chains may be an effective material to increase ionic conductivity by efficiently using water due to the structure-induced segregation of microphases (Li et al., 2018).

According to the literature, AEM base polymers based on ETFE are promising. Polyethylene and polytetrafluoroethylene units alternate in the structure of ETFE, giving it properties that describe in terms of their physicochemical properties, both types of polymers (hydrocarbons and fluoro-

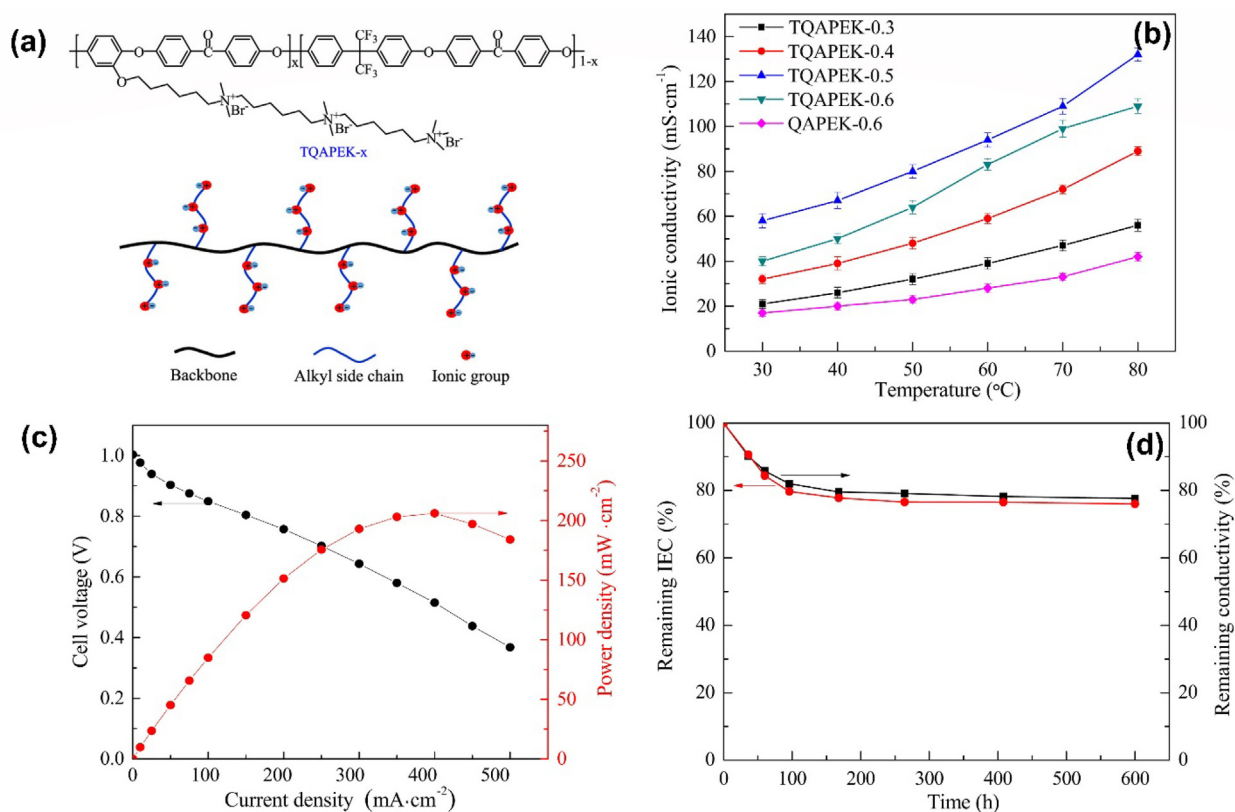


Fig. 21 Nucleophilic polycondensation produces poly(ether ketone)s containing multication side chains(a), temperature dependence of ion conductivity (b), curve of polarization(c), alkaline resistance (d) of TQAPEK-0.5 in a H_2/O_2 single cell at 60 °C, The figure was reproduced with the permission of Elsevier 2018(Li et al., 2018).

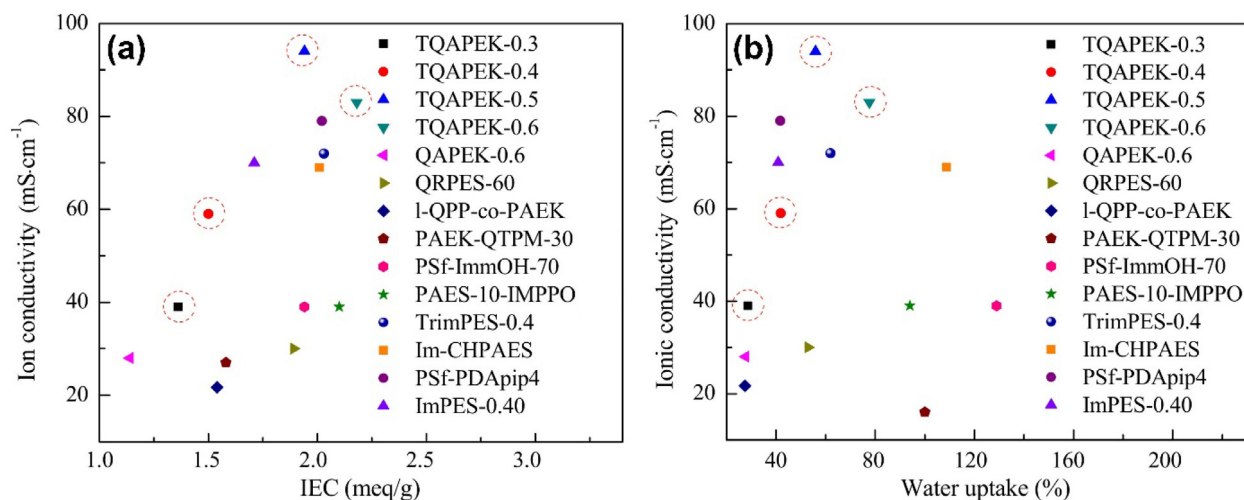


Fig. 22 Study of AEMs' conductivity at 60 °C in relation to (a) IEC and (b) water uptake from previous studies (Yang et al., 2014, Shen et al., 2015, Dong et al., 2016, Guo et al., 2016, Lin et al., 2016, Dong et al., 2017, Guo et al., 2017, Lu et al., 2017, Strasser et al., 2017) and TQAPEK-x. Image was reproduced with the copyright permission Elsevier 2018(Li et al., 2018).

carbons) have excellent chemical and thermal stability (Nasef et al., 2003, Nasef and Hegazy 2004, Kizewski et al., 2013, Douglin et al., 2021). ETFE's C—C, C—H, and C—F bonds in its backbone may detach during irradiation. As a result, macroradicals are formed (reactions (1)–(3) in Fig. 23). Three

competitive reactions occur between these radicals, affecting the structure of the backbone, affecting its mechanical properties, and thereby changing the material's properties (Kizewski et al., 2013). During irradiation with air (reaction 4, Fig. 23), the bonds are split into macroradicals which react with

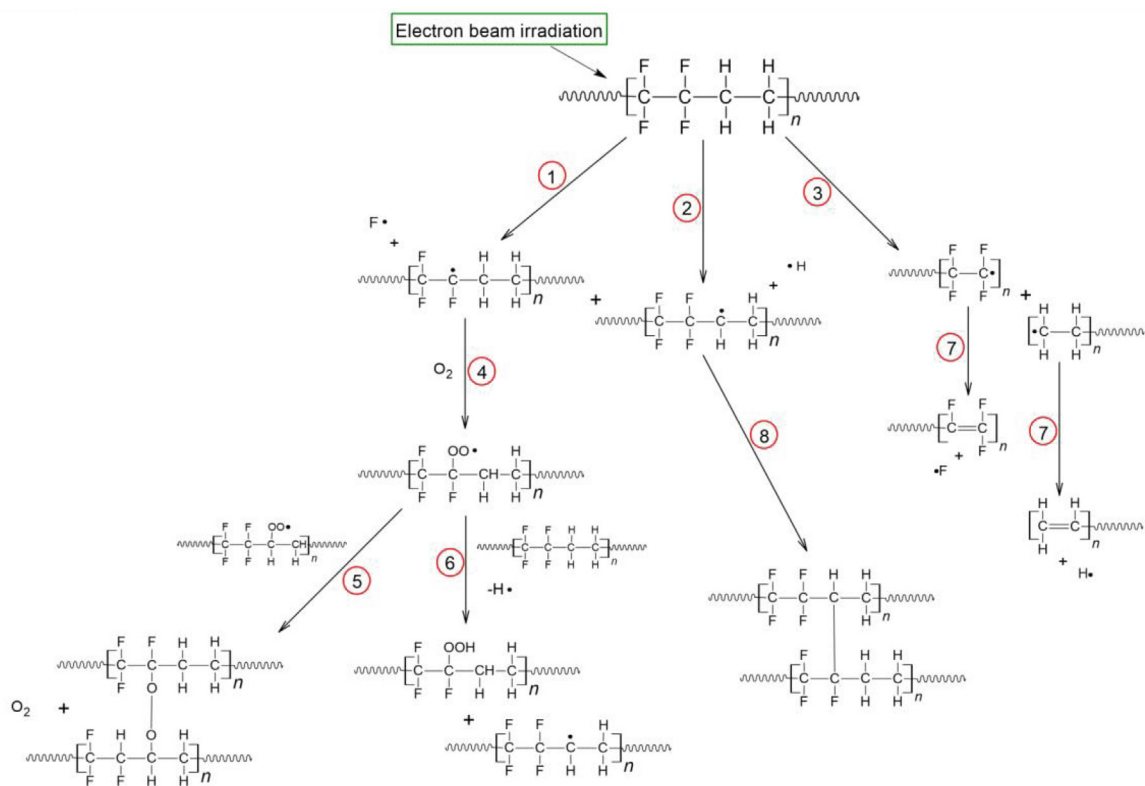


Fig. 23 Reactions (1), 2 and 3: C–F, C–H, C–C bond cleavages, respectively, and formation of macroradicals upon irradiation. Reaction 4: formation of peroxy radicals after contact with O₂. Reaction 5: peroxy radicals reacting to form peroxides. Reaction 6: abstraction of hydrogen and formation of hydroperoxides. Reactions 7: By C–C scission followed by dehydrofluorination, an unsaturated structure is formed, Reaction 8: After dehydrofluorination, the radicals react to form crosslinking structures (reactions (1) and (2)). Figure reproduced with the copyright permission of Elsevier 2022 (Biancolli et al., 2022).

atmospheric oxygen, resulting in peroxide. Upon reaction with peroxy radicals, alkylperoxides can be formed (as shown in reaction-5 of Fig. 23) and/or hydrogen can be abstracted, resulting in hydroperoxides (as shown in reaction-6 of Fig. 20). Additionally, they can undergo more complex changes or undergo other complex reactions that may lead to oxidative degradation (Arakawa et al., 1982), causing the chain to cleave (Dawes et al., 2007). Afterwards, unsaturated structures are produced by C–C scission followed by dehydrofluorination (reaction-7 in Fig. 23), another reaction indicating degradation. Finally, following dehydrofluorination, two adjacent radicals react to form crosslinks (reaction-8 in Fig. 23) (Nasef et al., 2003). Crosslinking and degradation caused by scission processes can result in a conflict between chemical and mechanical reinforcement (Chapiro 1964). For ion exchange membranes, ETFE films are commonly used as the basis polymer, particularly for PEMFC applications (Gürsel et al., 2007, Ben youcef et al., 2009, Ben youcef et al., 2010, Lappan et al., 2010, Nasef 2014, Nasef et al., 2016, Sproll et al., 2016). Recent studies have also reported the performance of AEMs in single fuel cell tests (Fang et al., 2012, Mamlouk et al., 2012, Wang et al., 2017, Gonçalves Biancolli et al., 2018, Omasta et al., 2018).

In this regard researchers Ana Laura Biancolli et al. (Biancolli et al., 2022) present an overview of the effect of electron beam grafted ETFE-AEMs on their final properties. Considering ETFE-based AEMs, the findings support the use of

low absorbed doses (less than 40 kGy) during irradiation to obtain a better backbone stability as well as a greater degree of AEMFC durability. There have been a number of factors that influence the degree of grafting and the backbone structure during irradiation, such as crosslinking or chain scission. In addition to affecting crystallinity and mechanical, chemical, and electrochemical properties, irradiation parameters were found to affect chemical and electrochemical properties as well. The conductivity decay rate is less than 0.018 % h⁻¹ under harsh alkaline conditions. H₂/O₂ AEMFC performance at 70 °C with selected AEM is 1350 mW cm⁻² as shown in Fig. 24.

As AEMs materials for AEMWE applications, Xu Hu et al. (Hu et al., 2021) synthesized a series of quaternized poly[(terphenyl piperidinium)-co-oxyindole terphenylene] (PTP). As a result of copolymerizing with superacid and quaternizing with methyl iodide, isatin, *N*-methyl-4-piperidone, and *P*-terphenyl for the synthesis of quaternized poly[(terphenyl piperidinium)-co-oxyindole terphenylene] (PTP) membranes. PTP AEMs had tensile strengths of 29.2–36.5 MPa due to their aryl ether-free polyaromatic polymer backbone. Conductivity values of 64.4 and 128.1 mS/cm were observed with PTP-90 membranes at 20 and 80 °C (IEC of 2.52 mmol/g, respectively). Under alkaline conditions, the PTP-85 membranes degraded in 1 M NaOH at 80 °C, and NMR experiments revealed that Hofmann elimination and nucleophilic substitution contributed to the degradation of the DMPs in

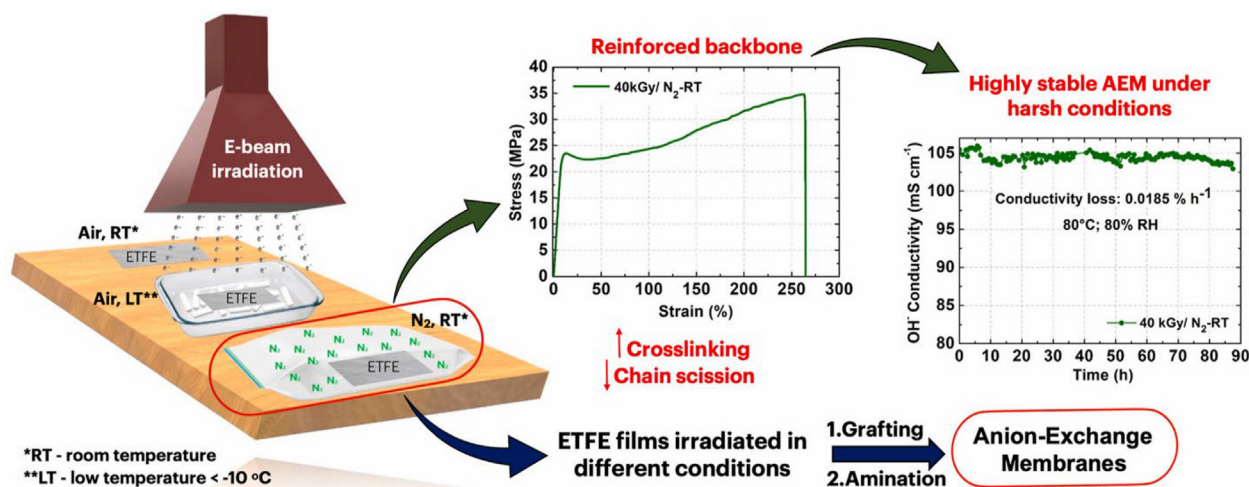


Fig. 24 AEM preparation and applications using ETFE-MPRD, Figure reproduced with the copyright permission of Elsevier 2022 (Biancolli et al., 2022).

the PTP membranes after 934 h. To run the MEA with PTP membrane, they used an AEM alkaline electrolyser fed with 1 M NaOH. MEAs using PTP-90 membranes showed 910 mA/cm² conductivity at 2.2 V at 55 °C and 1,000 mA/cm² at 75 °C. After 120 h at 55 °C, NMR spectroscopy analysis of PTP membrane post-cell reveals significant chemical degradation due to Hofmann elimination reaction and nucleophilic substitution reaction. In contrast, the PTP membrane did not degrade in ex situ 10 M NaOH for 200 h at 55 °C.

AEMs with PTP were investigated for their temperature-dependence of water uptake as shown in Fig. 25 (a). A temperature increase of 20 to 80 °C increased water uptake in all membranes as expected. For PTP-90 membranes with the highest IEC values, water uptake is more sensitive to temperature, with 86.9 % uptake at 80 °C (about 2.2 times higher than at 20 °C). At 80 °C, the WU of the PTP-75 membrane was 1.5 times greater than at 20 °C. An increase in swelling ratio was also seen at elevated temperatures. Even at 80 °C (S.R. = 15.4 %), in terms of dimensional stability, the PTP-90 membrane performed well, despite its high IEC value and high-water uptake, which is critical for the design of water electrolysers.

When PTP AEMs are immersed in 1 M NaOH at 80 °C, they are found to be alkaline stable. According to Fig. 25 (b), predetermined intervals were used to monitor the hydroxide conductivity. During the entire testing period, the AEMs continuously lost conductivity. With high IEC values, PTP-90 AEM showed poor stability under alkaline conditions. Furthermore, after 934 h of alkaline testing, the hydroxide conductivity of aged PTP-90 AEM decreased by 73 %. Comparatively, the PTP-75 membrane lost 41 % of its hydroxide conductivity under identical test conditions. PTP-75 might have low initial IEC and low water uptake due to its higher alkaline stability.

The performance of electrochemical devices using anion exchange membranes is directly affected by their high ion transport properties. Using the two-probe method, EIS was used to measure the hydroxide conductivity of PTP AEMs in water. A function of temperature and IEC was used to calculate hydroxide conductivity in Fig. 25 (c and d). Due to the

greater number of sites for ion transport, AEM conductivity increases with IEC values. Due to this, the hydroxide conductivity of PTP-90 membranes with IECs of 2.52 mmol/g at 20 °C was 64.4 mS/cm, which was 1.3 times more than PTP-75 membranes with IECs of 2.10 mmol/g. PTP membrane's hydroxide conductivity increased sharply between 20 °C and 80 °C as the ions moved more rapidly and water moved faster. Hydroxide conductivity was measured at 80 °C to be 128.9 mS/cm on PTP-90 membrane. Hydroxide conductivity of PTP-90 membranes compares favorably with that of other membranes at 20 °C and 80 °C due to their high IEC and medium dimensional stability. In spite of having a lower swelling ratio, a higher conductivity, and IEC values higher than those of PBPA membrane, the PTP-90 performed better than PBPA membrane. As a function of temperature, the hydroxide conductivity of PTP membranes exhibited an Arrhenius-like behavior. Based on the slope of $\ln(\sigma)$ vs $1/T$, they calculated the effective activation energy to be 10.9–12.6 kJ/mol, consistent with other reports (Pham et al., 2018, Chu et al., 2019, Zhang et al., 2019).

It has been shown that chloromethylation-functionalization is an effective and simple way to synthesize AEM materials (Hickner et al., 2013). A chloromethylation reaction is used to introduce chloromethyl groups to the polymer's benzene ring. A chloromethylated polymer is reacted with hydrazine, 1-alkylimidazole, tertiary amine, or tertiary phosphine to form a functionalized polymer (Xiong et al., 2009, Wang et al., 2010, Yan et al., 2011, Sajjad et al., 2015, Sherazi et al., 2015). AEM properties such as solubility, conductivity, and stability are greatly influenced by hydroxide conducting functional groups (Arges and Ramani 2013, Hnát et al., 2017). As a result of their excellent thermal stability, low volatility, and good electrochemical performance, imidazole-functionalized poly(ether ether ketone)-AEMs have excellent mechanical properties and good hydroxide conductivity as well (Awad et al., 2004, Arges and Ramani 2013). Thermal stability, dimensional stability, and conductivity of polymers are also influenced by their matrix. In addition to polyfluorene (Lin et al., 2011, Lee et al., 2015), polyether-ether-ketone (Yan et al., 2011, Yan et al., 2014), polysulfone (Zhang et al., 2011, Yan et al., 2012, Liu

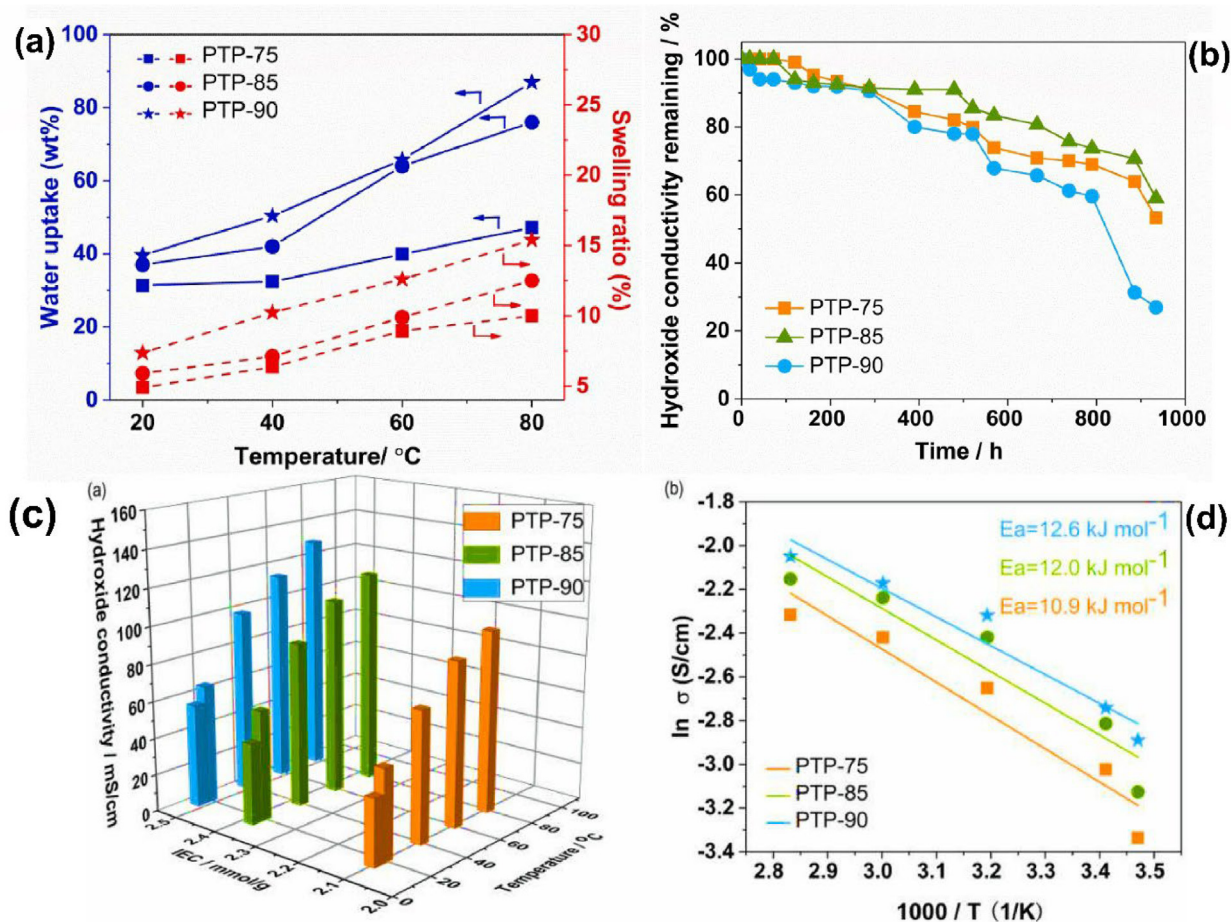


Fig. 25 (a) A temperature-dependent study of the PTP membranes' water uptake and swelling ratio, (b) PTP-AEM s' alkaline stability in 1 M NaOH at 80 °C, (c) The influence of temperature and IEC on PTP-x's hydrogen conductivity, and (d) Arrhenius type behaviors between Temperature-Inσ relationship. The Figure is reproduced with the copyright permission of Elsevier(2021) (Hu et al., 2021).

et al., 2015, Weiber and Jannasch 2015, Chen et al., 2017), and fluorinated poly (arylether oxadiazole)s(Hahn et al., 2013), and chloromethylated aromatic polymers were utilized to prepare imidazole-functionalized AEMs.

In this regards Taintian Li et al., (Li et al., 2018) developed a poly (ether ether ketone ketone)-functionalized poly (ether ether ketone ketone)-diol-stabilized anion exchange membrane (AEM) that is readily soluble in certain low-boiling-point solvents (isopropanol) as shown in Fig. 26. Based on molecular dynamics simulations, the solubility results are consistent. PEEKK-DImOH AEMs with IECs of 1.14–1.65 mmol·g⁻¹ can be produced by adjusting the temperature of the chloromethylation reaction or the concentration of sulfuric acid. At 60 °C, the hydroxide conductivity of the PEEKK-DImOH-92 % AEM is very high (31 mS⁻¹cm⁻¹) and the water uptake (94 %) and the swelling ratio (39 %) are acceptable. Additionally, PEEKK-DImOH AEMs exhibit good alkaline stability and thermal stability. PEEKK-DImOH 92 % AEM-prepared fuel cells have a higher power density (46.16 mW·cm⁻²) than those with commercial AHA membranes. In this study, the findings of the PEEKK study point towards the potential use of PEEKK as an AEM matrix material for alkaline fuel cells.

Several side-chain-type-AEMs were prepared using bromination, functionalization, chemical grafting and alkalization by Chen Xiao Lin and coworkers at 80 °C based on poly (arylene ether sulfone) and imidazolium-functionalized polyphenylene oxide (PPO)(Lin et al., 2016). Fig. 27 shows the hydroxide conductivity of the PAES-x-IMPPO membranes as 78.8 mS cm⁻¹. The AEMs are also mechanically sound, thermally stable, and have a moderate alkaline stability. A PAES-15-IMPPO at 60 °C with an open circuit voltage of 0.98 V can indicate low fuel crossover in H₂/O₂ alkaline fuel cells. The maximum power density of 56.8 mW/cm² was achieved without optimization with a current density of 125 mA cm⁻².

AEMs use water as a fundamental component that dissociates ions and forms hydroxide conductor channels. For AEMs to maintain their mechanical properties, a moderate rate of water uptake must be maintained. Too much water will cause over swelling. Fig. 28(a) shows the temperature-dependent uptake of water by PAES-x-IMPPO membranes in their hydroxide form. A higher temperature resulted in a higher water uptake. It may be that at high temperatures, polymer chains move more freely, allowing more space for water to accumulate. To overcome the differences in IEC, they calculated the number of absorbed water molecules (designated as

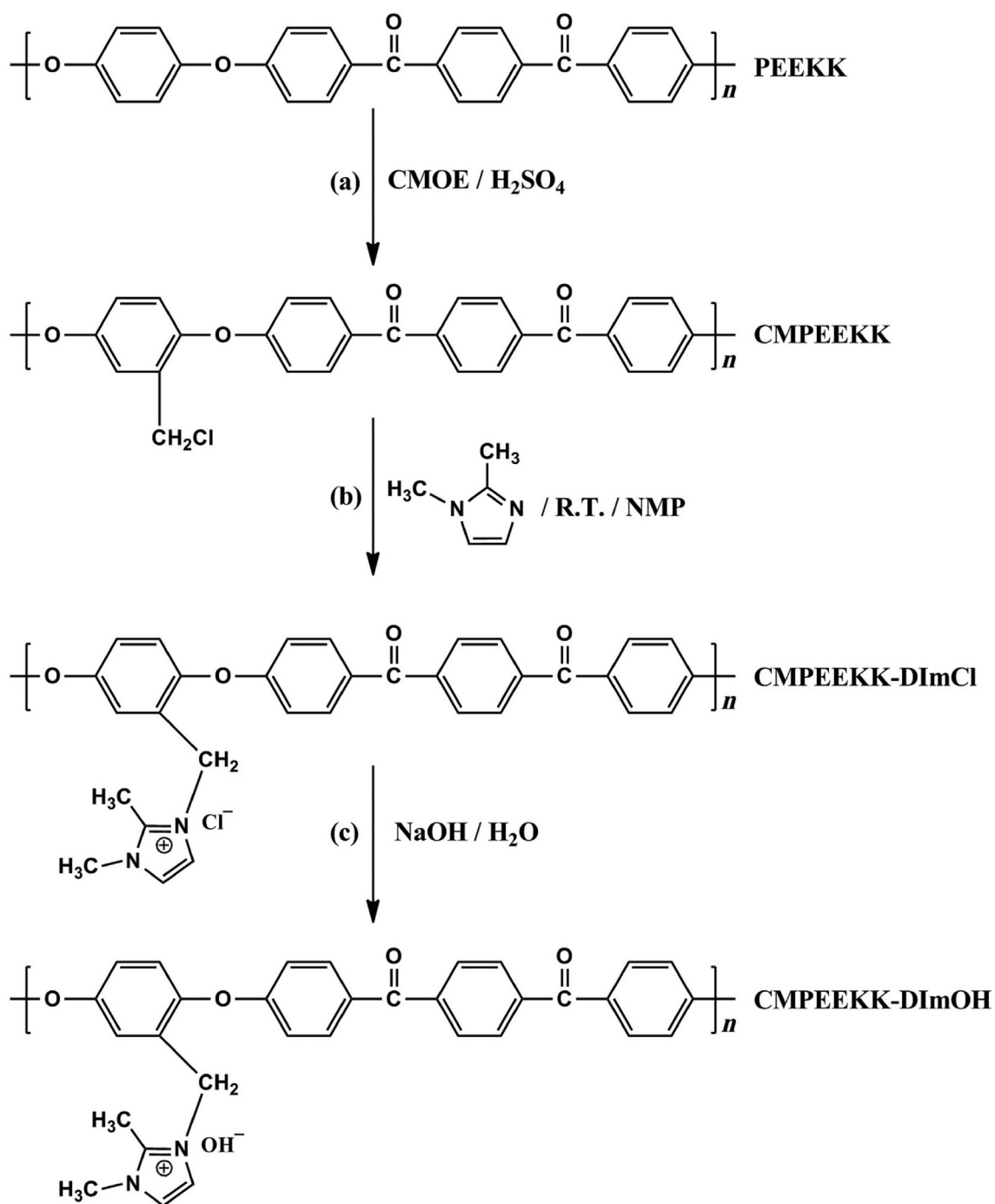


Fig. 26 AEM preparation with PEEKK-DImOH. The images reproduced with the copyright permission of Elsevier(2018) (Li et al., 2018).

λ). λ range of PAES-x-IMPPO measurements was observed at 30 °C between 10.9 and 26. The PAES-10-IMPPO membrane have WU = 70.1 %, $\lambda = 18.5$, and IEC = 2.05 meq/g slightly lower than the reported block F-QPES, that have WU = 109.4 %, IEC = 1.89 meq⁻¹ and $\lambda = 32.2$ (219) and QPE-X₁₆Y₁₁ having $\lambda = 32.2$, water uptake = 112 % and IEC = 2.05 meq/g with a similar IEC at 30 °C. According to Fig. 28(b), the tendency of the PAES-x-IMPPO's swelling

ratio versus temperature is in accordance with water uptake. The in-plane SR, measured at 30 °C and 80 °C, is 7.8 % for PAES-5-IMPPO, while it is 28 % at 30 °C and 39.1 % at 80 °C for PAES-15-IMPPO. In the in-plane and through-plane directions, PAES-x-IMPPO membrane swelling ratios were observed at 30 °C. There was a small amount of anisotropy in the PAES-x-IMPPO membranes as indicated by their through-plane swelling ratio, which was 1.6 times larger than

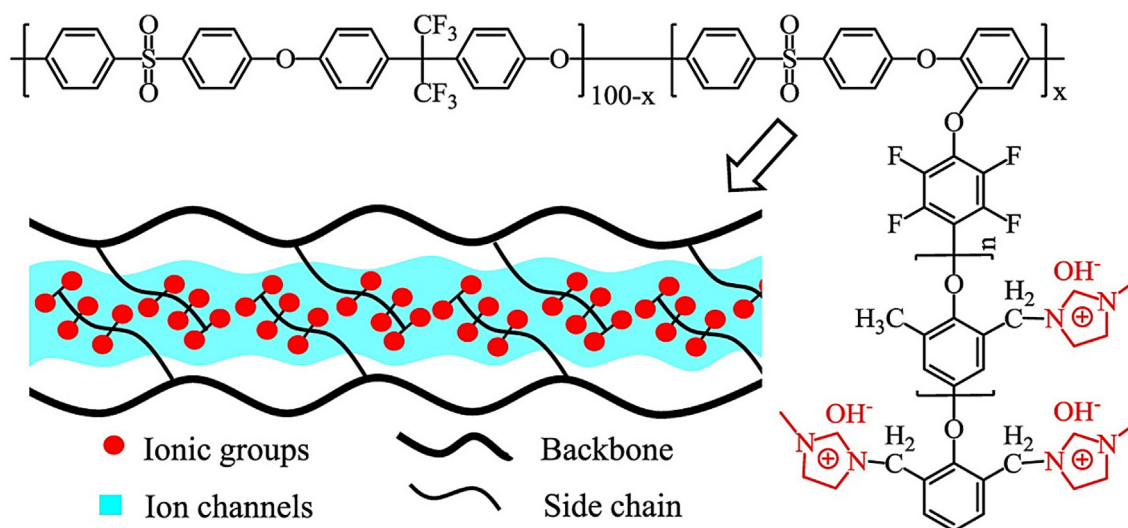


Fig. 27 Synthesis of membrane with hydroxyl conducting channels and sidechain-type PAES-x-IMPO copolymer. Image reproduced with the copyright permission by Elsevier(2016) (Lin et al., 2016).

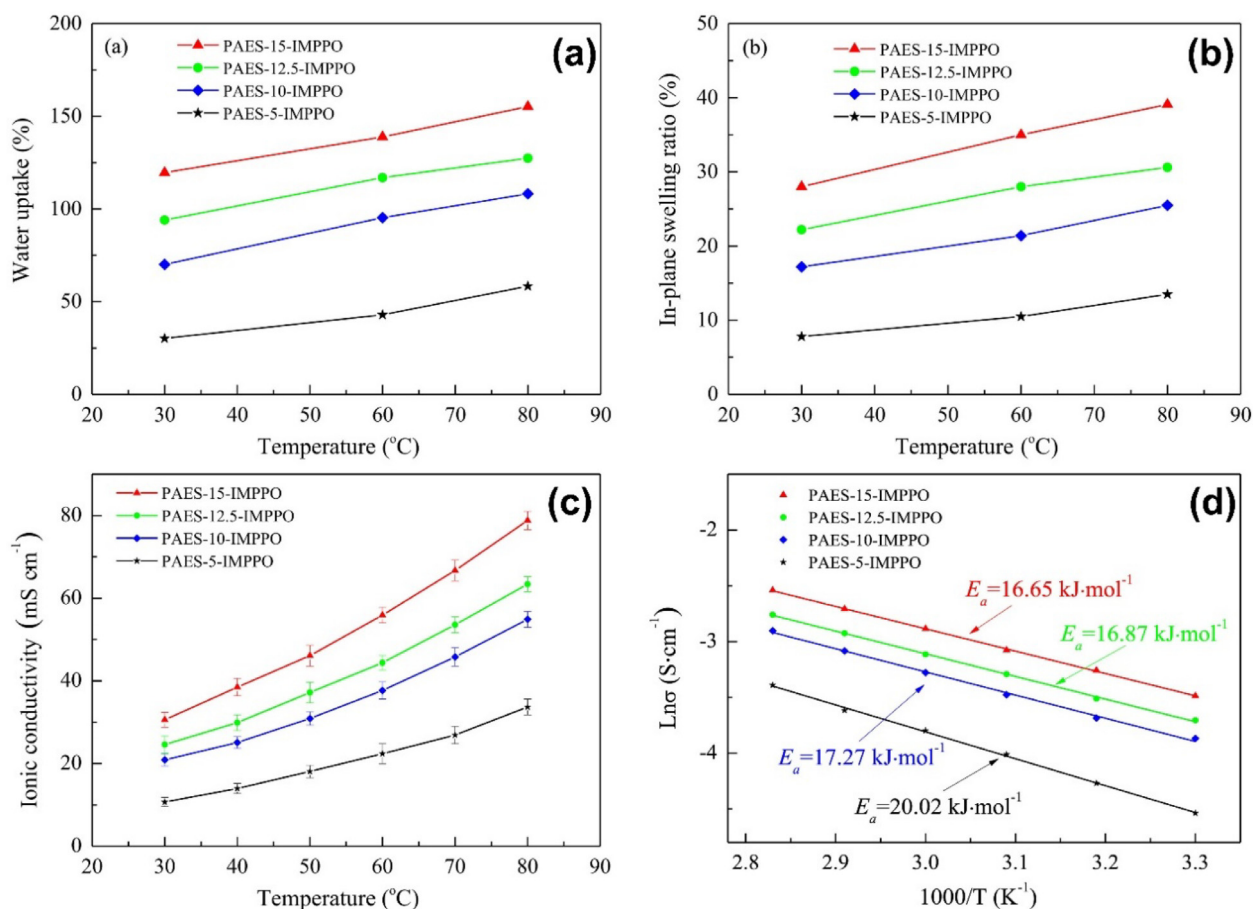


Fig. 28 In-plane swelling ratio and water uptake with respect to temperature (a and b), hydroxide conductivity with respect to temperature (c) and Arrhenius plots (d) of PAES-x-IMPO membranes, Figure is reproduced with the copyright permission of the Elsevier 2016 (Lin et al., 2016).

their in-plane swelling ratio. Temperature-dependent hydroxide conductivity of PAES-x-IMPPO membrane is shown in Fig. 28(c).

Due to the increasing concentration of imidazolium groups in the AEMs, the hydroxide conductivity increased with increasing IEC. Increasing the temperature also increases the hydroxide conductivity of PAES-x-IMPPO membranes. Hydrogen conductivity was measured at 30 °C and 80 °C and ranged from 10.7 to 30.6 mS cm⁻¹ and 33.7 to 78.8 mS cm⁻¹ respectively, suggesting that the as-developed AEMs can be used in fuel cells. Hydroxide conductivity is high when ion clusters with large sizes form effective ion conducting channels. Additionally, Fig. 28(d) illustrates the relationship between hydroxide conductivity ($\ln \sigma$) and temperature ($1000/T$) using the Arrhenius equation. As-synthesised membranes' activation energies for hydroxide transport were calculated by a linear regressed plot by $E_a = -b.R$, here b = slope of the $\ln \sigma - 1000/T$ plot, and R = universal gas constant (8.314 J mol⁻¹ K⁻¹) (Xu et al., 2014).

Hydroxide conductivity and E_a value show similar variation trends. PAES-5-IMPPO demonstrated highest E_a for lowest hydroxide conductivity. Apparently, the membrane required additional energy in order to transport the hydroxide ions. WU in the membrane is increased by increased IEC, which results in more ion conducting channels and a lower E_a (Lin et al., 2010). The E_a values for all membranes range from 16.65 to 20.05 kJ mol⁻¹, which is consistent with the AEMs reported (Jheng et al., 2014, Sherazi et al., 2015, Zhang et al., 2016).

In Fig. 29, Hue Wang et al. (Wang et al., 2021) report the preparation of quaternary ammonium salt poly(ether ether ketone)-AEMs containing long ether substituents. A PEEK-DABDA-80 membrane with 80 % methylhydroquinone reaches a hydroxide conductivity of 0.052 S/cm at 80 °C. In addition, it has excellent mechanical properties and anti-

swelling properties. Elongation at break is 8.12 percent, tensile strength is 25 MPa, and swelling ratio at 80 °C degrees is 17.4 percent. Furthermore, these AEMs are more thermally stable. PEEK-DABDA-80 membranes exhibit an acceptable ion conductivity of 0.021 S/cm after 30 days of soaking in 1 M NaOH. Due to these properties, PEEK-DABDA-x(x = 20, 40, 60, 80) AEMs may be suitable for use as alkaline AEMs.

AEMs have been synthesized from the copolymerization of low ionic liquid imidazolium substances-1-vinyl-3-methylimidazolium iodide [VMI]I and 1-vinyl-3-butylimidazolium bromide [VBI]Br, by Jun Fang et al (Fang et al., 2015) (see Fig. 30). Membranes obtained from this process are characterized by IEC, water uptake, ionic conductivity, thermal stability and chemical stability. At 30 °C, conductivity reached 0.0226 S cm⁻¹. Alkaline fuel cell membranes demonstrate excellent prospects for future applications. Polymerization of Sample A, B, and C was carried out using [VBI]Br with styrene, whereas Samples D, E, and F were carried out using [VMI]I with styrene. The obtained WU and IEC values are A(56.8 %, 1.26 mmol g⁻¹), B(42.9 %, 1.10 mmol g⁻¹), C(30.2 %, 0.98 mmol g⁻¹), D(82.7 %, 1.52 mmol g⁻¹), E (54.8 %, 1.48 mmol g⁻¹) and F(43.6 %, 1.04 mmol g⁻¹). In ionic exchange membranes, water uptake reflects the hydrophilicity of imidazolium salts due to their strong hydrophilicity. As a result, imidazolium cation groups present in the membrane enhance the membrane's ability to absorb water. With the highest imidazolium cation content, membrane D shows an uptake of water of 82.7 %. In conclusion, increasing imidazole group content results in increased IEC as well as an increase in water uptake. Water uptake of 82.7 % was shown by membrane D with a IEC of 1.52 mmol g⁻¹. As a function of temperature, the ionic conductivities of the six OH⁻ form membranes are shown in Fig. 30 (a and b). It is found that the ionic conductivity increases with increasing imidazolium cation content at

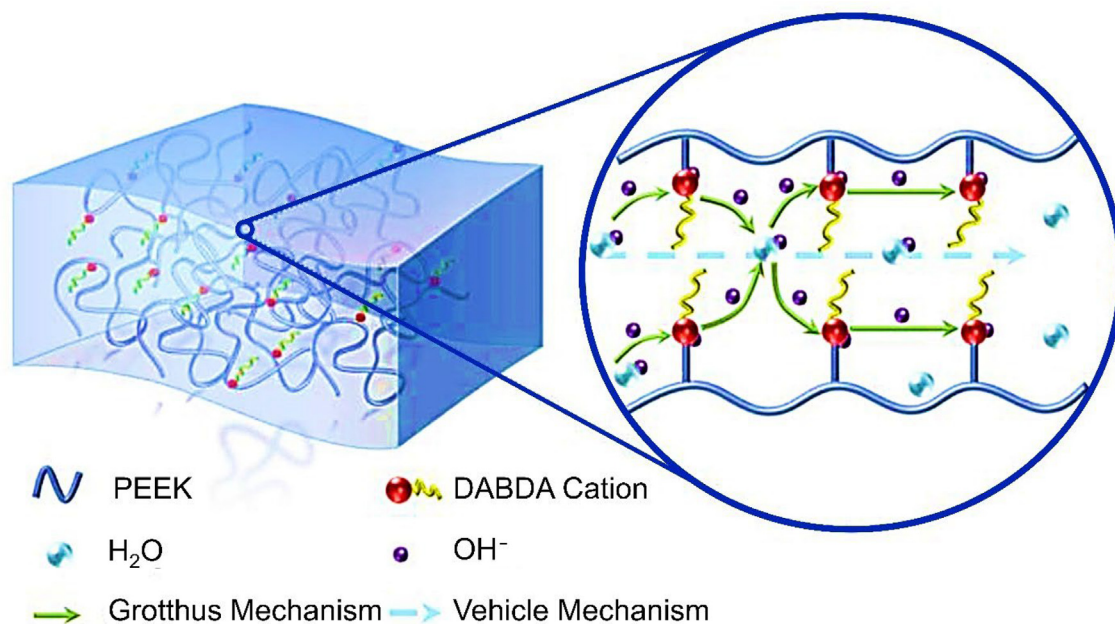


Fig. 29 Schematic diagram of long side chain type quaternary ammonium functionalized poly(ether-ether ketone) based AEM, Figure was redrawn with the copyright permission Elsevier 2021 (Wang et al., 2021).

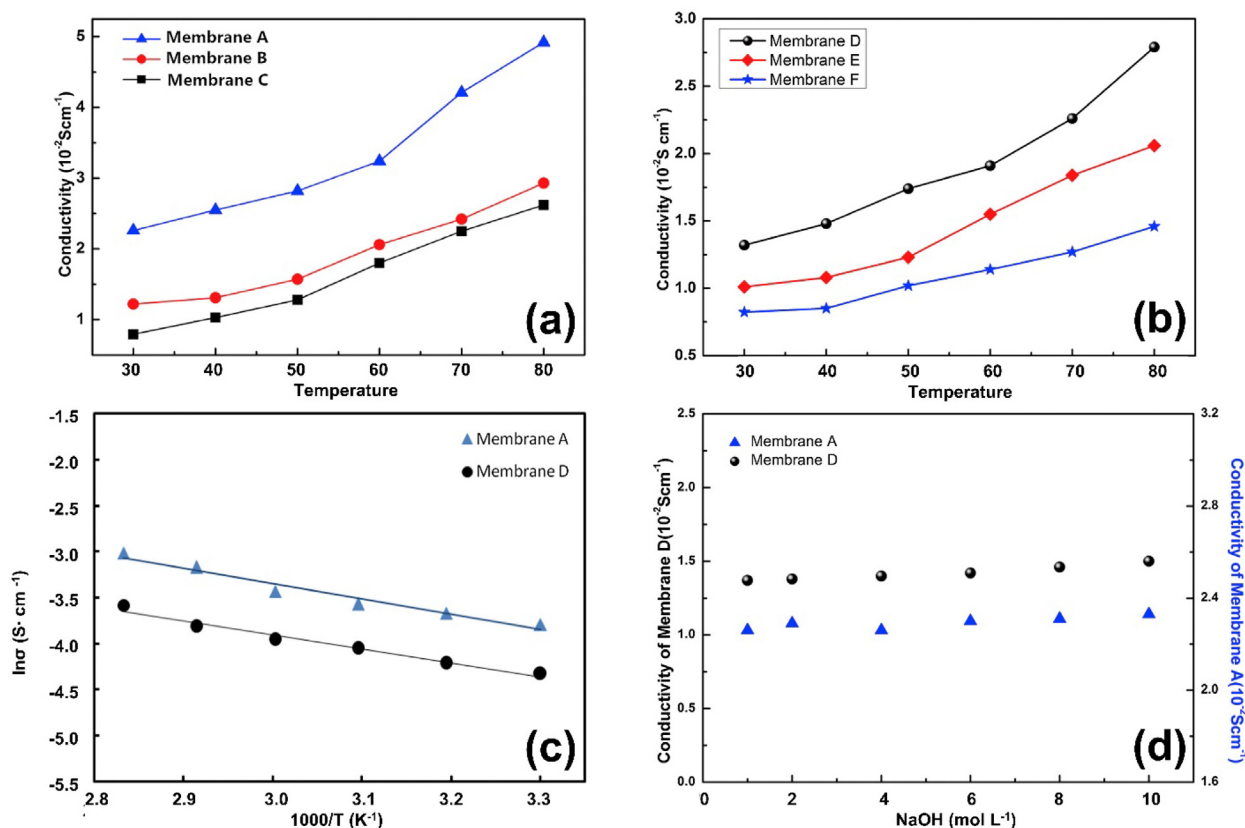


Fig. 30 Ion conductivities of membranes A, B, and C (a), membranes D, E, and F (b) with respect to temperature, Ionic conductivity plots (Arrhenius plots) of OH^- , utilizing AEM (c), and performance of membranes A and D after treatment with NaOH solution at 60 °C at different concentrations (d). Figure was redrawn with the copyright permission Elsevier 2015 (Fang et al., 2015).

30 °C. The higher the amount of OH^- charge carriers, the greater the imidazolium cation group content.

Membrane conductivity will be decreased due to insufficient imidazole functional groups, while membrane dimensional stability and mechanical properties will be severely affected by the high imidazole content. When a membrane's temperature goes up, its ionic conductivity increases. As the temperature increases from 30 °C to 80 °C, membrane A's ionic conductivity varies between $2.26 \times 10^{-2} \text{ S cm}^{-1}$ and $4.92 \times 10^{-2} \text{ S cm}^{-1}$. An association between $1000/T$ and $\ln(\sigma)$ can be seen in Fig. 30 (c). Furthermore, in Fig. 30 (c), the temperature dependence of hydroxide conductivity can also be calculated using the Arrhenius equation. Arrhenius' law was used to calculate the apparent activation energies of the membranes. Ten membranes were treated with 2, 4, 6, 8 and 10 mol/L NaOH solution at 60 °C for 120 h to determine their conductivity. Membrane A has an E_a value of $12.765 \text{ kJ mol}^{-1}$, and membrane D has an E_a value of $11.240 \text{ kJ mol}^{-1}$ as shown in Fig. 30 (d). Membrane A had a conductivity ranging from 2.26 to $2.34 \times 10^{-1} \text{ S cm}^{-1}$. Increasing concentration led to increased conductivities, which may be explained by the precipitation of more OH^- in the membranes at higher pH levels. Contrast samples with conductivities of $1.37 \times 10^{-2} \text{ S cm}^{-1}$ and $2.26 \times 10^{-2} \text{ S cm}^{-1}$ do not differ from each other in any respect. Membranes have been found to be capable of withstanding high pH conditions at temperatures as high as 60 °C.

It is important to know, water is produced by AEMs when hydroxyl ions travel from the cathode to the anode. This simplifies the process of managing water in the AEMFC. Furthermore, the hydroxyl ions in the fuel move in opposite directions, reducing fuel permeability and costs in other aspects (Spendelov et al., 2006, Tang et al., 2010). In recent years, AEMFC has become one of the hottest research topics, despite developing relatively late. Various types of AEMs have been synthesized using chemically modified polymers, including PSF (Park et al., 2008), PPESK (Fang and Shen 2006), poly(ether sulfone cardo (Li and Wang 2005), and poly(arylene ether sulfone) (Zhou et al., 2009). Preparation of AEMs was also accomplished using the radio grafting method (Fang et al., 2012), and polymerization route (Wu et al., 2011, Luo et al., 2012). The process of chloromethylation, followed by quaternization, was integral to the preparation of quaternized polymers in many earlier studies. It is also considered that the chloromethylation reagents are highly toxic and cancerous. In addition, Hofmann elimination reactions and/or nucleophilic substitution may also degrade the alkyl quaternary ammonium groups on the side chains at high pH and high temperatures.

Materials developed by the Dupont Company, including PFSA membranes and ionomers, are considered benchmark materials for membranes, electrochemical devices, and ionomers (Valdes et al., 2008, Cai et al., 2012, Chu and Majumdar 2012). PFSA is a hydrophobic ionic compound with a Teflon like backbone. Furthermore, PFSA membranes

have excellent mechanical and chemical properties as a result of their perfluorinated backbone (Matsui et al., 1986, Tang et al., 2007). Due to PFSA's unique structure and its success in PEMFCs, there have been numerous attempts to implement Teflon-like backbones into AEMFCs (Arges et al., 2011, Jung et al., 2011). Perfluorinated AEMs seem the most promising AEMs for AEMFCs because of the perfluorinated backbone's extreme hydrophobicity, which drives phase separation necessary for improving ion conductivity (Li and Guiver 2014).

AEMs containing short side chain perfluoro-sulfonamide polymers have been synthesized by Xubdao Liu et al., (Liu et al., 2016) which consist of (S-PFSO₂NH-GCL-OH). By reacting S-PFSO₂NH-GCI-OH ions with various solvents, especially low-boiling point solvents, a transparent solution was formed. The IEC, perm-selectivity, and transport numbers for Tokuyama® A201 and S-PFSO₂NH-GCI membranes are compared; with S-PFSO₂NH-GCI membrane, the Cl⁻ transport numbers are 0.93 (>0.8) and Na⁺ transport numbers are 0.04 (less than 0.2). Its selectivity is 95.8 %, which is comparable to Tokuyama® A201 (Krol et al., 1999)[310]. There is no doubt that this is an alkaline membrane. S-PFSO₂NH-GCI-OH membranes have a temperature-dependent hydroxide conductivity, as shown in Fig. 31(a). Additionally, the conductivity of fully hydrate Tokuyama A201 was measured for comparison. The conductivity increased with temperature as shown in Fig. 31 (a). At higher temperatures, ions have a higher mobility, which leads to increased conductivity. Water absorbed by the membrane may be beneficial to ion transport and mobility, which leads to increased conductivity. S-PFSO₂NH-GCI-OH had better conductivity even though Tokuyama A201 had a higher IEC value. With temperature rising from 30 °C to 80 °C, S-PFSO₂NH-GCI-OH conducted better, rising from 49.7 to 102.4 mS cm⁻¹. Furthermore, the temperature-dependent conductivity of the membrane in Cl⁻ form (S-PFSO₂NH-GCI-Cl) was recorded (Fig. 31a, green dot). At 80 °C, the membrane conductivity is 37.6 mS cm⁻¹ in Cl⁻ form, which is 2.67–2.74 times lower than in OH⁻ form. Although OH⁻ may be transported with a high Grotthuss component, Cl⁻ is evidently not (Tuckerman et al., 2002, Liu et al., 2016). A LER value below 5 %, as shown in Fig. 31 (b), demonstrates superior length dimension stability in water for S-PFSO₂NH-GCI-OH membranes. Vs% increases almost

linearly as WU% increases as shown in Fig. 31(c). When WU% is raised from 7.6 % to 15.2 %, the membrane's Vs% varies from 5.5 % to 17.6 %. A comparison between S-PFSO₂NH-GCI-OH membrane and perfluorinated sulfonic membrane showed that the S-PFSO₂NH-GCI-OH membrane demonstrated minimal swelling in the presence of water, low water uptake, and high dimensional stability.

In conclusion, as a replacement for AWE and PEM water electrolyzers, AEM water electrolyzers can be developed. An Anion Exchange Membrane is used as the solid polymer electrolyte in AEM water electrolyzer systems, which can produce high-purity hydrogen while having the advantages of both PEMWE and AWE. Their use with non-noble metals is enabled by their ability to operate in an alkaline environment. Nevertheless, AEM water electrolyzers (200–400 mA cm⁻² at 1.8–2.4 V) perform worse than PEM (600–2000 mA cm⁻² at 1.8–2.2 V) water electrolyzers. The lower performance of the non-noble metal electrocatalysts can be attributed to their insufficient OER and HER. Electrocatalysts or electrodes for the OER and HER in AEMWE must be highly efficient and cost-effective to overcome this barrier. There has been much interest in backbones and cationic head groups. AEMs are largely made up of aromatic polymers because of their high thermal stability, solubility, and chemical resistance (Zarrin et al., 2012, Lee et al., 2015, Mohanty et al., 2015). In addition to aromatic polymers, exploration of several newly discovered structures has been conducted, including poly (biphenyl alkylene)s (Lee et al., 2015), poly(terphenylenes) (Lee et al., 2017), *N*-spirocyclic quaternary ammonium ionenes (Pham et al., 2017), and perfluoroalkyl copolymers/ quaternized aromatic (Mahmoud et al., 2017). There have also been reports of cationic head-groups such as quaternary ammonium groups (QA) (Zhu et al., 2016, Mahmoud et al., 2017, Zhu et al., 2017, Li et al., 2018), imidazolium ions (Gong et al., 2017, Guo et al., 2017, Lin et al., 2017), guanidinium ions (Xue et al., 2017), phosphonium ions (Noonan et al., 2012), and aliphatic heterocyclic QA head groups (Hahn et al., 2013, Dang and Jannasch 2016). Due to their availability and reasonable stability, the QAs are among the most popular cationic groups (Mahmoud et al., 2017). There is a ionomer in a certain amount that facilitates ion movement in the catalyst layer, which assists electrochemical reactions, However, excessive

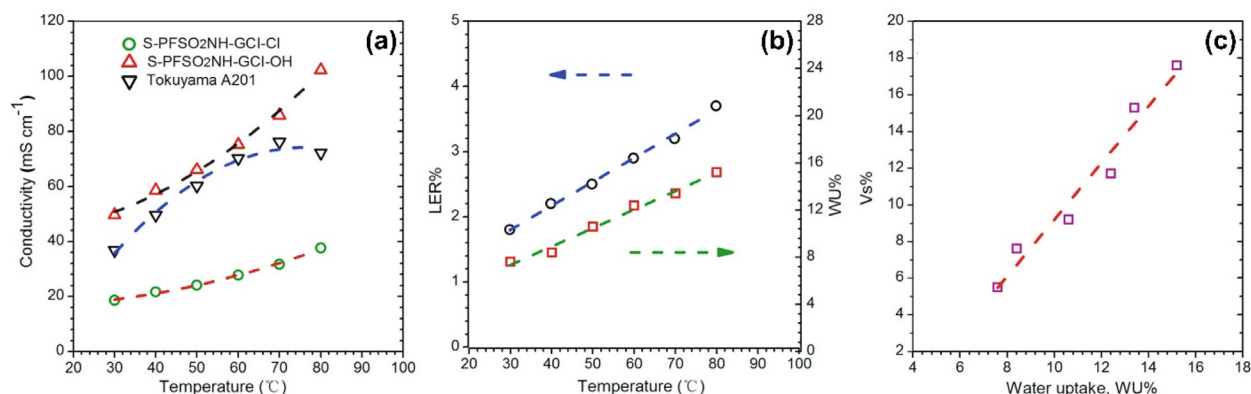


Fig. 31 Temperature dependence of membrane conductivity in water. S-PFSO₂NH-GCI and Tokuyama A 201 membranes measured in water were 28 and 15 μm thick, respectively (a), S-PFSO₂NH-GCI-OH membrane's LER% and WU% with different temperatures (b), the Vs% versus WU%. Elsevier 2016 has granted permission to reproduce the Figures (Liu et al., 2016).

ionomer blocks the catalyst's active sites. According to the literature as the percentage of the ionomer increased, activation and mass transport resistance have decreased, and cell performance has improved, this indicates that minimal weight percent will be sufficient for efficient ionic connections. NMR spectroscopy analysis of membrane post-cell reveals significant chemical degradation due to Hofmann elimination reaction and nucleophilic substitution reaction. It has been shown that chloromethylation-functionalization is an effective and simple way to synthesize AEM materials (Hickner et al., 2013). A chloromethylation reaction is used to introduce chloromethyl groups to the polymer's benzene ring. A chloromethylated polymer is reacted with hydrazine, 1-alkylimidazole, tertiary amine, or tertiary phosphine to form a functionalized polymer (Wang et al., 2010, Yan et al., 2011, Sajjad et al., 2015). AEM properties such as solubility, conductivity, and stability are greatly influenced by hydroxide conducting functional groups (Arges and Ramani 2013, Hickner et al., 2013). Imidazole-functionalized poly(ether ether ketone)-AEMs have excellent mechanical properties, good hydroxide conductivity, excellent thermal stability, low volatility, and good electrochemical performance. Thermal stability, dimensional stability, and conductivity of polymers are also influenced by their matrix (Awad et al., 2004). In addition to polyfluorene (Lin et al., 2011, Lee et al., 2015), polyether-ether-ketone (Yan et al., 2014), polysulfone (Chen et al., 2017), fluorinated poly(arylether oxadiazole)s (Lee et al., 2015), and chloromethylated aromatic polymers were utilized to prepare imidazole-functionalized AEMs.

Study comparison of various AEM, anode, and cathode materials for water electrolysis is shown in Table 1.

5. Overview of the electrodes (HER and OER) in AEMWEs

As a replacement for AWE and PEM water electrolyzers, anion exchange membrane (AEM) water electrolyzers have been developed. An Anion Exchange Membrane is used as the solid polymer electrolyte in AEM water electrolyzer systems, which are capable of producing high-purity hydrogen while having the advantages of both PEM and AWE water electrolyzer systems. Their use on non-noble metals is enabled by their ability to operate in an alkaline environment. The performance of non-noble metal electrocatalysts can be attributed to their insufficient OER and HER. Electrocatalysts or electrodes for the OER and HER must be highly efficient and cost-effective to overcome this barrier.

Researchers have been working to develop inexpensive and efficient components for alkaline water electrolysis for decades to improve hydrogen and oxygen evolution reaction (HER and OER) kinetics. In alkaline conditions, ion-conducting membranes and non-noble catalysts have been studied extensively. Researchers have studied different catalysts that are not noble, exhibiting high electrocatalytic activity, such as NiFeOx, Ni-Zn, Ni-Co, and Ni-Mo based composites, under alkaline conditions (Gong et al., 2016, Babar et al., 2019). As non-noble OER catalysts, metal oxides such as CoOx, MnOx, NiOx, $\text{Co}_{0.81}\text{Co}_{2.19}\text{O}_4$ and NiFe-OS (Frydendal et al., 2014, Babar et al., 2018, Choi et al., 2018), FeOOH (Lee et al., 2018), and NiFe-OS (Kim et al., 2019) have been studied; a voltage overpotential of less than 0.5 V has also been achieved at 10 mA cm^{-2} in alkali media. There has also been the develop-

ment of alkaline-exchange membranes that demonstrate anionic conducting properties in the range of 7 to 100 mS cm^{-1} , similar to Nafion's proton conducting properties (Chen and Hickner 2012, Duan et al., 2013, Ren et al., 2014, Zeng and Zhao 2015, Aili et al., 2017, Konovalova et al., 2018, Marinkas et al., 2018). However, AEMWE still performs poorly compared with PEMWE in terms of state of operation. Anion-conducting polymer electrolytes despite adding large amounts of catalysts exhibit lower performances than PEMWE (Xu and Scott 2010, Cho et al., 2017). Low performance of AEM is due to several factors, including the instability of AEM at high temperatures and pressures (e.g., Nafion), which prevents AEMWE from scaling up to a commercial level (Chen and Hickner 2012).

A gold microgrid, electrochemically deposited with nonprecious-metal catalysts (MnO nanowires), was prepared by Jiao Jin et al. and it is shown in Fig. 32. In a liquid-phase electrochemical reaction, microgrids produce high-coating uniformity MnO nanowires with discontinuous solid-liquid contact lines. A super aero phobic/super hydrophilic electrode exhibits an OER current density of 10 mA cm^{-2} at 530 mV overpotential in 0.1 M KOH thanks to its ability to synergize electrolyte wetting and gas release; this makes it a good MnO catalyst for OER. This study paves the way for the development of synergistic synthesis approaches (gas bubble formation and electrolyte wetting in a synergistic manner), towards high-performance OER electrodes (Jin et al., 2022).

NiCoO-NiCo-C was synthesized by Yoo Sei Park et al. Initially, Ni/C electrocatalyst was alloyed with Co, then supported on carbon cloth layered with microporous carbon layers in order to improve electrocatalytic activity; then, oxide (Ni/Co-O) was formed in order to improve the NiCo/C catalyst's performance. In order to determine whether the electrocatalyst can be utilized in a real AEMWE system, it has also been evaluated as a cathode for single-cell AEMWE and for a stack of five cells. AEMWE systems (64 cm^2) use same-sized electrodes as those used in some commercially available prototypes. For the 5-cell AEMWE stack, the results yielded a current density of 440 mA/ cm^2 over 150 h at 9.25 Vstack (1.85 Vcell) and 69 % efficiency (Park et al., 2021). With nano-island arrays consisting of $\text{Fe}_{0.2}\text{Ni}_{0.8}\text{-P}_{0.5}\text{S}_{0.5}$ as a bifunctional catalyst, Lei Wan et al. achieved current density of 10 mA cm^{-2} and overpotentials of 180 mV (for OER) and 85 mV (for HER). DFT study revealed that doping $\text{Fe}_{0.2}\text{Ni}_{0.8}\text{-P}_{0.5}\text{S}_{0.5}$ with bimetallics could increase intrinsic activity. $\text{Fe}_{0.2}\text{Ni}_{0.8}\text{-P}_{0.5}\text{S}_{0.5}$ electrodes are characterized by superhydrophilicity, capable of exposing active sites and enhancing electrolyte and gas diffusion at high current densities. Thus, the $\text{Fe}_{0.2}\text{Ni}_{0.8}\text{-P}_{0.5}\text{S}_{0.5}$ bifunctional electrodes of the AEMWE maintained performance without apparent degradation for 300 h while maintaining 2.5 A cm^{-2} at 2.0 V (Wan et al., 2022).

The CoZn/NC-Ti₃C₂ electrocatalyst was prepared by Zhongwei Fang et al. (Fang et al., 2022) using ZIF-67/ZIF-8 on the Ti₃C₂ surface. CoZn/NC-Ti₃C₂ exhibits significant kinetics at 0.847 V and 245 mW cm^{-2} power density, with a half-wave potential ($E_{1/2}$) of 0.847 V. Further, it is quite stable, losing only 4.83 percent of its relative current after 30000 s cycles of testing. MXene-Ti₃C₂ is expected to have a high specific surface area, which will allow it to provide more active sites while reducing the collapsing of carbon-based active particles, thereby improving catalytic stability. AEMFCs could

Table 1 Study comparison of various AEM, anode, and cathode materials for water electrolysis conducted by different researchers.

Name of membranes	Anode and cathode materials used	IEC (mmol/g)	Ionic conductivity mScm ⁻¹	A/C flowrate (L min ⁻¹)	Gas(anode and cathode)	Materials loading anode/cathode [mg _{metal} cm ⁻²]	T (°C)	Current density	Electrolytes used	Ref
A-201(Tokuyama)	Acta3030(CuCoO _x)/Acta3040(Ni (CeO ₂ -La ₂ O ₃)/C)	N/A	42 & 45	N/A	H ₂ /O ₂	30/7.4	60	500 mA.cm ⁻²	1 % K ₂ CO ₃ to anode	(Vincent et al., 2017)
FAA-3	IrO ₂ 40 wt% /Pt/C	N/A	N/A	1, 2.5, 5 and 10 ml/min	H ₂ /O ₂	2/0.4	70	1.5 A.cm ⁻²	1 M KOH for both electrode	(Park et al., 2019)
37-60 (Fumatech)	NiFe ₂ O ₄ /NiFeCO	N/A	N/A	2 ml/min	H ₂ /O ₂	2/2	60	1 A.cm ⁻²	1 M KOH for both electrode	(Liu et al., 2017)
(Sustanion®)										
AF1-HNN8-50-X (Aemion ®)	Ir black/ Pt/C	1.4-		N/A	H ₂ /O ₂	3.5-3.8/1	50	2 A.cm ⁻²	1 M KOH for both electrode	(Fortin et al., 2020)
FAA-3PE-30 (Fumatech)	Ir Black/Pt/C	1.7	40 ± 2							
	Ni ₉₀ Fe ₁₀ /CeO ₂ /60 wt% Pt/C	N/A	N/A	N/A	H ₂ /O ₂	6/3	50	2 A.cm ⁻²	1 M KOH for both electrode	(Cossar et al., 2019)
A-201(Tokuyama)	Acta 3030/Acta3040	1.8	12 (HCO ₃ form)	N/A	H ₂ /O ₂	36/7.4	50	470 mA.cm ⁻²	1 % K ₂ CO ₃ to anode	(Pavel et al., 2014)
X37-50 (Sustanion®)	Cu _{0.5} Co _{2.5} O ₄ / Pt/C	N/A	N/A	50 ml/min	H ₂ /O ₂	10/1	45	1.3 A.cm ⁻²	1 M KOH	(Jang et al., 2020)
Orion-TM1 (Orion)	IrO ₂ /40 wt% Pt/C	N/A	N/A	1 ml/min	H ₂ /O ₂	2/0.4	70	2.75 A.cm ⁻²	1 M KOH for both electrode	(Kang et al., 2022)
A-201 (Tokuyama)	46 % Pt/C	> 1.5	38	N/A	H ₂ /air (CO ₂ -free)	0.5/0.5	50	0.28 A.cm ⁻²	0.1 M KOH	(Ramaswamy and Mukerjee 2019)
PD ₀ TP-25Poly (aryl-co-aryl piperidinium)	PtRu/C—Pt/C	2.98	146	1.0/1.0	H ₂ /O ₂	0.39/0.26	80	0.4 A.cm ⁻²	1 M NaOH	(Hu et al., 2022)
PD ₁ TP-25	PtRu/C—Pt/C	2.95	154.3	1.0/1.0	H ₂ /O ₂	0.39/0.26	80	0.4 A.cm ⁻²	1 M NaOH	(Hu et al., 2022)
Phosphonium-based ionomer	Ni/C and Ag	N/A	N/A	N/A	H ₂ /O ₂	5.0/0.5	70	N/A	0.1 M KOH	(Gu et al., 2013)
PD ₂ TP-25	PtRu/C—Pt/C	2.91	166	1.0/1.0	H ₂ /O ₂	0.39/0.26	80	0.4 A.cm ⁻²	1 M NaOH	(Hu et al., 2022)
PD ₁₀ TP-10	PtRu/C—Pt/C	2.71	122.1	1.0/1.0	H ₂ /O ₂	0.39/0.26	80	0.4 A.cm ⁻²	1 M NaOH	(Hu et al., 2022)
PFTP-13	PtRu/C—Pt/C	2.82	175	1.0/1.0	H ₂ /O ₂	0.42/0.33	80	0.2 A.cm ⁻²	1 M NaOH	(Chen et al., 2021)
QAPPT	Pt/C—Pt/C	2.49	137	0.12/0.12	H ₂ /O ₂	0.4/0.4	60	0.2 A.cm ⁻²	1 M KOH	(Peng et al., 2018)
QAPPT	Pt/C—Pt/C	2.49	137	0.12/0.12	H ₂ /O ₂	0.4/0.4	80	0.2 A.cm ⁻²	1 M KOH	(Peng et al., 2018)

Table 1 (continued)

Name of membranes	Anode and cathode materials used	IEC (mmol/g)	Ionic conductivity mScm ⁻¹	A/C flowrate (L min ⁻¹)	Gas(anode and cathode)	Materials loading anode/cathode [mg _{metal} cm ⁻²]	T (°C)	Current density	Electrolytes used	Ref
QAPPT	PtRu/C—Pt/C	2.49	137	1.0/1.0	H ₂ /O ₂	0.4/0.4	80	770 mA cm ⁻²	—	(Li et al., 2019a)
m-TPN	PtRu/C—Pt/C	2.1	112	1.0/1.0	H ₂ /O ₂	0.5/0.6	80	0.6 A cm ⁻²	1 M NaOH	(Park et al., 2019)
m-TPN	PtRu/C—Pt/C	2.1	112	1.0/2.0	H ₂ /O ₂	0.6/0.6	60	0.6	1 M NaOH	(Maurya et al., 2018)
PAP-TP-85	Pt/C—Ag/C	2.37	193(95)	0.15/0.95	H ₂ /Air (CO ₂ free)	0.15/1.0	95	500 mA cm ⁻²	2 M NaOH	(Wang et al., 2019)
20 μm QA radiation-grafted	20 % Pt/C	1.49 + - 1.8 %	N/A	400 cm ³ min ⁻¹	H ₂ /O ₂	0.40 ± 0.02 mg _{pt} cm ⁻²	50	Power peak density 240 W cm ⁻²	1 mol dm ⁻³ KOH	(Poynton et al., 2014)
ETFE PAP-TP-85	PtRu/C—Pt/C	2.37	193(95)	1.0/2.0	H ₂ /O ₂	0.4/0.4	95	Power peak density PPD 1.89 W cm ⁻²	0.1 M KOH	(Wang et al., 2019)
PAP-TP-85	PtRu/C—Pt/C	2.37	193(95)	1.0/1.0	H ₂ /Air	0.4/0.4	95	PPD 1.31 W cm ⁻²	0.1 M KOH	(Wang et al., 2019)
PFBA-QA-0.4	Pt/C—Pt/C	2.15	135	0.6/0.6	H ₂ /O ₂	0.4/0.4	80	PPD 559 W cm ⁻²	5 mol/L NaOH	(Yang et al., 2020)
GT82-15	PtRu/C—Pt/C	3.7	147	1.0/1.0	H ₂ /O ₂	0.7/0.6	80	PPD 3.5 W cm ⁻² And 9.7 A/cm ⁻²	1 M NaOH	(Mandal et al., 2019)
LDPE15-AEM	PtRu/C—Pt/C	2.54	208	1.0/1.0	H ₂ /O ₂ (10 ppm CO ₂)	0.6/0.4	80	PPD 2.0 W cm ⁻²	1 M KOH	(Wang et al., 2018)
LDPE15-AEM	PtRu/C—Pt/C	2.54	208	1.0/1.0	H ₂ /O ₂	0.6/0.4	80	PPD 2.4 W cm ⁻²	N/A	(Wang et al., 2019)
GT78	PtRu/C—Pt/C	3.28	N/A	1.0/1.0	H ₂ /O ₂	0.7/0.6	80	PPD 3.2 W cm ⁻² And 9.4 A cm ⁻²	1 M KOH	(Ul Hassan et al., 2020)
HDPE-AEM	PtRu/C—Pt/C	2.44	214	1.0/1.0	H ₂ /O ₂	0.7/0.6	—	600 mA cm ⁻²	1 M KOH	(Peng et al., 2020)
LDPE-BTMA	PtRu/C—Pt/C	2.49	N/A	1.0/1.0	H ₂ /O ₂	0.7/0.7	105	PPD 1.14 W cm ⁻² And 2.4 A cm ⁻²	1 M KOH	(Douglin et al., 2021)

(continued on next page)

Table 1 (continued)

Name of membranes	Anode and cathode materials used	IEC (mmol/g)	Ionic conductivity mScm ⁻¹	A/C flowrate (L min ⁻¹)	Gas(anode and cathode)	Materials loading anode/cathode [mg _{metal} cm ⁻²]	T (°C)	Current density	Electrolytes used	Ref
Tokuyama A201	Pt/C and CoO/rGO (N)	N/A	N/A	1.5/0.75	H ₂ /O ₂	1.5 and n/a	60	260 & 190 W cm ⁻² and 430 & 320 mA cm ⁻²	0.1 M KOH	(He et al., 2013)
Alkylammonium tethered poly (fluorene) 80 μm QA radiation grafted	PtRu and Pt 20 % Pt/C	2.6 1.25 ± 11	127 N/A	0.6/0.1 N/A	H ₂ /O ₂ H ₂ /O ₂	0.5/0.6 0.5/0.5	80 50	less than 1.46 W cm ⁻² PPD 230 mW cm ⁻²	1 M NaOH 1 M KOH	(Maurya et al., 2018) (Poynton et al., 2010)
ETFE A-901, thickness 9 μm; Tokuyama Corp.)	Acta 3030/Acta 3040	1.8	29 mS cm ⁻²	N/A	H ₂ /O ₂	30/7.4	60	400 mA cm ⁻²	1 % K ₂ CO ₃	(Vincent 2018)
QA polysulfone	Ni-Cr/Ag				H ₂ /O ₂ (1.3 barg)	5/1	60		1 M KOH	(Lu et al., 2008)
Cranfield-membrane	Cu _x Co _{3-x} O ₄ /Pt	N/A	N/A	N/A	H ₂ /O ₂	1/3	25	1 A.cm ⁻²	1 mol dm ⁻³ KOH	(Wu and Scott 2011)
YAB membrane,	CoP/CoP	N/A	N/A	5/5	H ₂ /O ₂	5/5	50	335 mA cm ⁻²	1 M KOH	(Chang et al., 2016)
Foma Co. HMT-PMBI	NiAlMo/NiAlMo	2.52	103	42.7	H ₂ /O ₂	42.7/42.7	60	2 A cm ⁻²	1 M NaOH	(Wang et al., 2019)
Cranfield-membrane	Li _{0.21} Co _{2.79} O ₄ /Ni nanopowder	N/A	N/A	N/A	H ₂ /O ₂	2.5/2	45	300 mA cm ⁻²	DI	(Wu and Scott 2013)
A201, Tokuyama	CuCoO _x / Ni-CeO ₂ -La ₂ O ₃ /C	1.8	12 mScm ⁻¹	N/A	H ₂ /O ₂	36/7.4	55	470 mA cm ⁻²	1 M KOH	(Pavel et al., 2014)
X37-50 T, Dioxide	Ni _{0.27} Fe _{2.27} O ₄ /Pt/C	N/A	N/A	N/A	H ₂ /O ₂	-/1	45	2.0 A cm ⁻²	1 M KOH	(Lee et al., 2021)
Materials PAP-TP-85	Fe _x Ni _y OOH-20F/ Pt/C	N/A	N/A	N/A	H ₂ /O ₂	4.8/2	80	N/A	1 M KOH	(Li et al., 2019b)
PPO/QGO and QPPO/QGO	graphene supported	N/A	1.2 and 1.5 104 S cm ⁻¹	N/A	H ₂ /O ₂	3/0.5	60	0.25–0.35 A cm ⁻²	1 M KOH f	(Manjula et al., 2020)
Tokuyama A201	palladium (Pd/NG)/ 20 % Pt/C IrO ₂ /PtC	N/A	190 at 0.5 M of KOH, 7.4 at 18 mm etc	22 ml/min	H ₂ /O ₂	2/1	60	N/A	1 M KOH and using different concentrations	(Kießling et al., 2022)

Table 1 (continued)

Name of membranes	Anode and cathode materials used	IEC (mmol/g)	Ionic conductivity mScm ⁻¹	A/C flowrate (L min ⁻¹)	Gas(anode and cathode)	Materials loading anode/cathode [mg _{metal} cm ⁻²]	T (°C)	Current density	Electrolytes used	Ref
PBI membrane	Ni-Fe-Ox and Ni-Fe-Co	N/A	N/A	60 ml·min ⁻¹	N/A	5	60	500 mA cm ⁻²	1 M KOH	(Vincent et al., 2021)
Tokuyama A201 membrane	Ni(OH) ₂ -Fe and NiMo	1.8	12 in HCO ₃ ⁻	N/A	N/A	4/25.2	50	2 A cm ⁻²	1 M KOH	(Wang et al., 2022)
HMT-PMBI membrane	NiAlMo as an anode and cathode or NiAl as anode and NiAlMo as a cathode	2.52	N/A	N/A	N/A	42.7/47.9	60	2 A cm ⁻²	1 M KOH	(Wang et al., 2019)

employ CoZn/NC–Ti₃C₂ catalysts as ORR catalysts due to their high activity and stability.

There has been much interest in AEMFCs in recent years because the non-noble metal can be used as a catalyst for ORRs (Praats et al., 2020). AEMFCs use non-noble metal catalysts, such as chalcogenides and transition-metal oxides, because they are cheap and easy to prepare. Unfortunately, their low catalytic activity makes further application difficult. The ORR/OER bifunctional catalyst described by Liu et al. is composed of multivalent nanoparticles of CoS_x and NCNT catalytically active nickel (Lu et al., 2022). Materials (Ni, Fe, Cu, Co, and Mn) doped with transition metals and nitrogen have received attention as promising catalysts. The specific activity of co-doped carbon catalysts with Fe (Co) and nitrogen is unprecedented for ORR. Using the hard template method, Wu et al. (Wu et al., 2021) synthesized a hollow FeN/C catalyst with similar activity to the Pt/C. Rui Gao et al synthesized non noble metal FeSe₂ by hydrothermal process and applied for the OER and compared with the results of CuSe₂ nanoplatelets and commercially available RuO₂ and they found that synthesized FeSe₂ showed better results as compared to the CuSe₂ nanoplatelets and commercially available RuO₂ (Gao et al., 2017). The M–N–C catalysts' high performance is attributed to the regulated electronic structure governed by carbon-based heteroatoms (Xue et al., 2019). As for creating active sites on carbon catalysts, this is an effective method for doping of heteroatoms (like P, S, and N) (Paraknowitsch and Thomas 2013). Additionally, a variety of heteroatoms could be introduced in order to improve the catalytic activity (Najam et al., 2020). It is inevitable that more carbon defects will result in corrosion and oxidation of the carbon support, thereby reducing the catalyst's durability (Wang et al., 2019, Asset and Atanassov 2020). During high-temperature pyrolysis, the low surface area of the carbon matrix will increase the growth of NPs (M–Nx). Therefore, materials with ultrahigh surface areas are ideal for obtaining the M–N × sites (Fang et al., 2022).

Several studies have suggested that MOFs can be used for the synthesis of carbon-based catalysts following pyrolysis (Lai et al., 2017, Guan et al., 2020). The ORR process creates materials with large surfaces, high porosity, clear microstructures, and homoatom decoration which allow for rapid mass transfer and electron migration (Wei et al., 2017). By pyrolyzing (ZIF)-67, Co–N–C catalyst was synthesized, and it showed high activity as a nonprecious metal-based catalyst containing abundant micropores (Lv et al., 2019). In contrast, carbon nanoparticles derived from MOFs are usually dispersible and cannot be synthesized into continuous frameworks, which is insufficient for continuous conductivity in ORR applications (Chen et al., 2015). MOFs are being proposed as conductive materials to solve this problem (Xiao et al., 2020). The fabrication of metal nitrogen carbon materials using Fe-doped ZIF-8 and Ti₃C₂T_x MXene was demonstrated by Wang et al. (Wang et al., 2021). There are abundant activity sites for electrocatalytic species in MXenes with surface terminal groups (Yu et al., 2018, Peng et al., 2020). Moreover, interaction of MXene with electrocatalytic active species may result in strong interfacial coupling, which further alters its electronic structure and catalytic activity (Zhang et al., 2017, He et al., 2019).

Cao et al. (Cao et al., 2012) developed a polyvinyl benzyl chloride membrane grafted with quaternary ammonium for

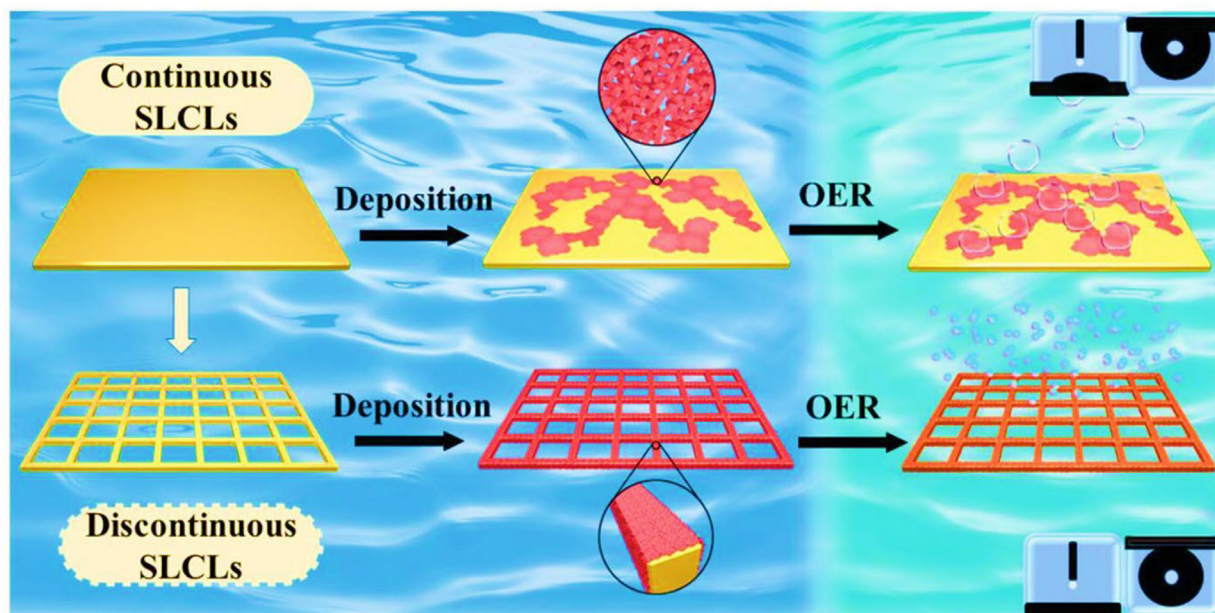


Fig. 32 Illustration of a gold microgrid embedded with MnO nanowires and a flat gold foil deposited by electrodeposition for OER. An uneven coating of MnO nanowires was observed on a gold-foil substrate, demonstrating the nonporous surface's hydrophilicity and aerophobicity. A MnO nanowire coating, formed by the discontinuous SLCLs in the gold microgrid substrate, showed a highly hydrophilic/aerophobic surface, Copyright permission was granted by Elsevier 2022 for redrawn figures (Jin et al., 2022).

AEMWEs, using powder of Ni and $\text{Cu}_{0.7}\text{Co}_{2.3}\text{O}_4$ as hydrogen and oxygen evolution catalysts respectively and a current density of 100 mA/cm^2 was obtained at $55\text{ }^\circ\text{C}$ and 1.99 V . According to Wu et al. (Wu and Scott 2012), they have developed a polymethacrylate-based polyquaternary ammonium OH^- ionomer that is suitable to bond nonprecious metal alkaline AEMWE, which has been demonstrated to provide 100 mA/cm^2 at 1.9 V under deionized water.

The device has also been reported to perform well for 300 min at 1.8 V with a current density of 50 mA/cm^2 . Water electrolysis cells have been made from a membrane electrolyte made of quaternary ammonia polysulfone membranes by Xiao et al. (Xiao et al., 2012). Anodes and cathodes are made of Ni-Fe and Ni-Mo. Using iridium oxide and Pt black as catalysts for the anode and cathode of solid-state water electrolysis cells, a solid-state water electrolysis cell using an alkaline membrane electrode has been demonstrated by Long et al. (Leng et al., 2012). 1.8 V and $50\text{ }^\circ\text{C}$ were used to measure the cell's current density in the absence of liquid electrolyte, the cell showed a current density of 399 mAcm^{-2} . Several studies have suggested that hydroxide-containing polymers perform well in water electrolysis cells when they come into contact with alkaline aqueous solutions (Pletcher and Li 2011). Corrosion in cells and auxiliary equipment can be aggravated by alkaline solutions. Performance could be improved in alkali solutions either by improving membrane conductivity or by improving electrode-to-membrane contact (Pletcher and Li 2011, Seetharaman et al., 2013). As stable electrocatalysts for alkaline water electrolysis (AWE), several nickel oxides and hydroxides have been developed (Ferreira et al., 1988, Pletcher et al., 2012). The alkaline water electrolysis performance of nickel electrodes is improved with several

types of surface coatings such as Pt, NiMo, RuO_2 etc (Li et al., 2011). Graphene is a two-dimensional sheet made up of carbon atoms that are sp^2 bonded and arranged in hexagons in a hexagonal pattern (similar to a honeycomb) with excellent conductivity and chemical and thermal stability. A chemical process in which graphite (weak intermolecular forces join stacked graphene sheets in 3D) is oxidized by strong oxidants (exfoliates and oxidizes) to form graphene oxides with carboxy, hydroxyl, carbonyl, and other functional groups on the surface is presented in (Schniepp et al., 2006). Researchers have found that graphene sheets significantly affect Pt clusters on their surface in electrocatalytic experiments (Yoo et al., 2009). A composite of graphene, metal oxides, and transition metal oxides with improved electrocatalytic properties has been found to be useful for supercapacitors, Li-ion batteries, and electrochromic windows (Li et al., 2011, Cai et al., 2012, Kouchachvili et al., 2018, Gao et al., 2021). By forming electrostatic bonds between metal ions and carboxyl groups in graphene oxide, it is possible to stabilize the active form of the catalyst, thus improving its activity. Li et al. (Li et al., 2011) synthesized MoS_2 nanoparticles on rGO sheets using solvothermal synthesis for the application of electrocatalysis in hydrogen evolution reactions. A good electrical coupling to graphene and an increase in catalytic edge sites are credited with the enhanced properties.

The high electronic conductivity of nickel foam (NF) and the desirable 3-D structure have made this material a popular choice for HER and OER in recent years. The research related to the nickel foam include the application of non-noble metals or their hydrides and oxides to NF as single metals such as Ni, NiO, and Co_3O_4 (Esswein et al., 2009, Kim et al., 2015, Yan et al., 2015), binary metal alloys such as Ni-Mo (Tang et al.,

2014), Ni-Co (Pérez-Alonso et al., 2015), NiFe₂O₄ (Chanda et al., 2015), ternary metal alloys (Yuan et al., 2007, Li et al., 2016), and NiCo LDH (Jiang et al., 2015). Brewer-Engle theory suggests that alloying transition metals on the left half of the periodic table with their counterparts on the right side of the periodic table will provide a stronger synergetic effect than a single noble metal (Jakšić 1987). NF has been deposited with noble metals (for example, Pd and Ru) presented as single alloys (Pierozynski et al., 2014, Zhang et al., 2015) for increased electrocatalytic activity and stability, as well as for improved electrochemical activity. Using nickel substrates, as well as added materials, the authors have enhanced the catalytic activity of Ni meshes (Jović et al., 2013, Tasić et al., 2013), Ni nanofibers (Wu et al., 2016) and Ni foils (Marceta Kaninski et al., 2011), which have been employed as catalyst supports for water electrolysis.

In this regard, in an experiment with alkaline AEMWEs, Mohammad Zhiani et al. modified Ni foam by using NPs with low content of Ni, Pd, Co, and Fe metals NPs (Pd-Ni-Fe-Co/C-Ceria-NF) and applied it as a cathode. As shown in Fig. 33, they examined the electrochemical activity of the electrode using LSV and CV. In an AAEM electrolyzer single cell, the cathode performance of catalyst was studied by separating its anode and cathode polarizations. A high level of catalytic activity was observed for Pd-Ni-Fe-Co/C-Ceria-NF in the HER and A-AEM cathode reactions. When the current density was 10 mA cm⁻² (-14 mV) in HER, the Tafel slope of Pd-Ni-Fe-Co/C-Ceria-NF was low (-79 mV dec⁻¹). Additionally, Pd-Ni-Fe-Co/C-Ceria-NF electrodes performed well and have good stability during 30 h of alkaline treatment. Pd-Ni-Fe-Co/C-Ceria-NF membrane electrode assembly (MEA) at 300 mA cm⁻² exhibited a cell voltage of 2.31 V versus 2.22 V for Pt/Con Ni foam (Pt/C - NF) (Zhiani et al., 2017).

NiCu is reported to be an active HER catalyst in alkaline electrolytes. Synthesis of NiCu catalysts has been accomplished by a variety of methods, including electrodeposition (Cardoso et al., 2015), powder metallurgy (Wang et al., 2017) and freeze casting (He et al., 2019). He et al. reported a current of -10 mA/cm² at 117 mV using galvanostatic deposition of NiCu and atomic ratios Ni:Cu equal to one (He et al., 2017). HER activity was enhanced by electrodeposited NiCu nanosheets with a 48-mV onset potential compared to RHE

(Gao et al., 2016). As Solmaz et al. have reported (Solmaz et al., 2009), NiCu has a roughness effect and synergistic interactions between Ni and Cu atoms lead to a higher HER activity than Ni and Cu. Oshchepkov et al. reported that Ni_{0.95}Cu_{0.05}/C possesses high mass activity due to the electronic influence of Cu on Ni. Unfortunately, there are few publications that demonstrate the use of NiCu catalysts as cathodes in alkaline electrolyzers. Composite structures made up of TMO and Ni/NiO display higher activity of HER. The Volmer step of HER lowers the free energy of the first step, adsorption of hydrogen, through NiO's attraction to OH_{ads} and Ni's attraction to H_{ads} intermediates. The composite NiO component is also stabilized under HER conditions by TMO oxides like Cr₂O₃ or Fe₃O₄. In order to facilitate the stability of mixed oxidation states, HER catalysts contain both a catalytic element and an element (or oxide) that stabilizes the mixed oxidation state. To catalyze HER, the researchers propose mixing NiCu with MMO. NiO and Ni (both of which have a strong affinity for OH_{ad} and H_{ad}) will be contained in this catalyst, and both will be stabilized by CuO under HER conditions simultaneously (Bates et al., 2015, Gong et al., 2015, Oshchepkov et al., 2015, Xie et al., 2018).

According to Alaa Y. Faid et al., nickel-copper catalysts were optimized for cathode catalysis in anion exchange membranes. During the Volmer step, Ni Cu mixed metal oxide nanosheets consist of NiO, Ni metallic, and Cu oxides, resulting in a rapid HER. For NiCu MMO nanosheets, HER activity increased from 0.1 M to 1 M KOH in alkaline electrolytes. Under alkaline HER conditions, NiCu MMO nanosheets demonstrated superior stability for 30 h. An ink containing a Nafion ionomer displayed a higher HER current density than an ink containing a Fumion anion ionomer. Nafion ionomers gave the best HER performance when 0.5 catalyst was used. When Ir black was used as an anode, 1.85 A/cm² was obtained with NiCu MMO cathodes in 1 M KOH at 50 °C. AEM performance of the NiCu MMO catalysts produced here is comparable to that of PEM, as shown in Fig. 34 (Faid et al., 2021).

Ink uniformity and coating quality are achieved through the use of ionomers in electrochemical testing (Jervis et al., 2017). Additionally, the ionomer increases ionic conductivity and minimizes the effects of diffusion limitation on mass-transport. Anion exchange ionomers are more efficient at pro-

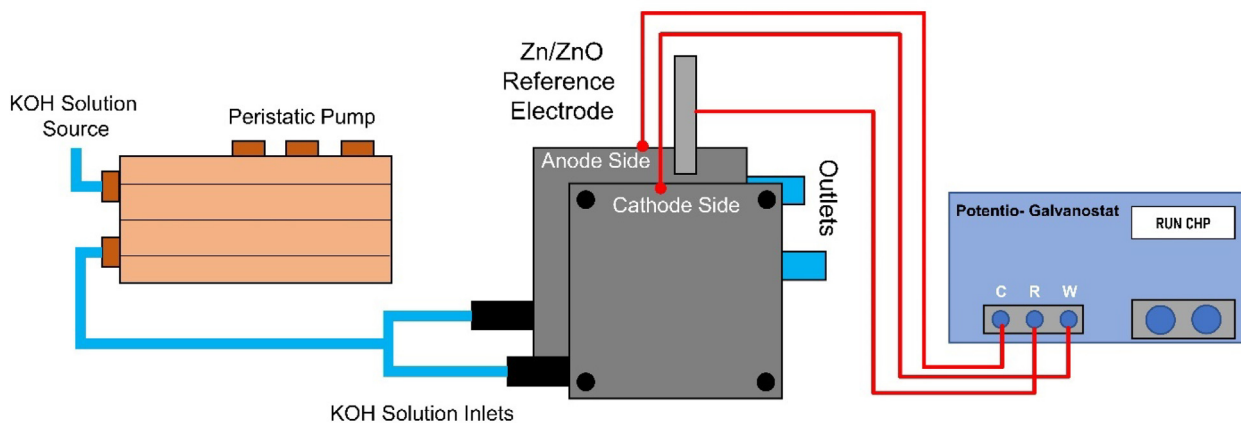


Fig. 33 This figure shows the polarization measurements setup of cell in-situ. Copyright permission was obtained from Elsevier 2017 for reproduction of this Figure (Zhiani et al., 2017).

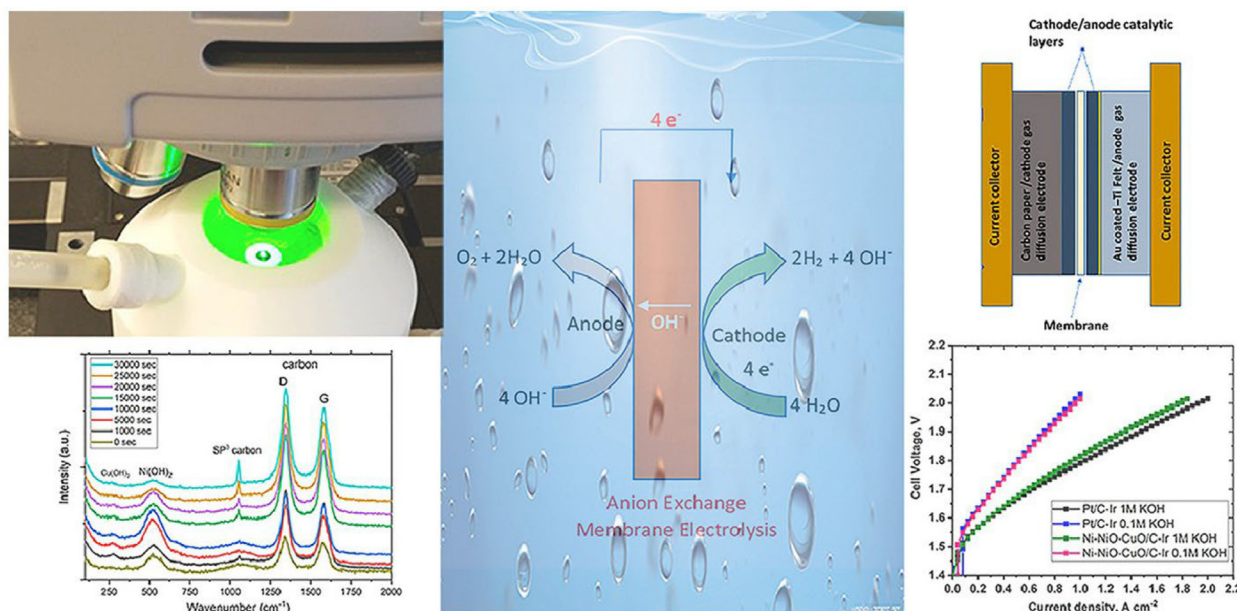


Fig. 34 MEA diagram for AEM water electrolysis by using Ni-Cu mixed metal oxide catalyst. Copyright permission for images was obtained from Elsevier 2021 (Faid et al., 2021).

ducing HER than Nafion ionomers, according to literature reports (Bates et al., 2015, Faid et al., 2019). A variety of factors have been attributed to the difference in activity, including ionomer head groups and ionomer backbone chemistry (Bates et al., 2015). For optimum catalyst utilization, the ionomer-catalyst ratio must be adjusted, as a part of the upscaling of AEM water electrolyzer devices. If NiCu metal mixed oxide catalyst is adopted, it must also be able to interact with ionomers and be tested both as an aqueous electrolyte and an aqueous catalyzer. Therefore, it is essential to include both aqueous and electrolyte tests within experiments (Alia and Pivovar 2018). Therefore, Emily Cossar et al. (Cossar et al., 2021) prepared nickel nanoparticles by chemical reduction in order to optimize the commercial Fumatech fumion ionomer content in AEMWE anodes. In the same way, Ni-iron-based NPs with or without ceria (CeO₂) are prepared after determining the optimal ionomer content. The AEMWE is tested in various concentrations of KOH, with the Ni₉₀Fe₁₀ electrode providing 1.72 V at 0.8 A cm⁻² with a degradation rate of 3.3 mV h⁻¹ in 1 M KOH after IR-correction. When ceria is added to Ni-based catalysts, mass transfer is predicted to be more consistent as a result of more efficient water transport and bubble release, as shown in Fig. 35.

Water electrolysis technology using anion exchange membranes (AEM) presents one of the major challenges of developing high-efficiency, low-cost oxygen-evolving electrodes. Research shows conventional Ni foam electrodes can be converted into electrodes with high OER performances by using surface corrosion of Fe³⁺ and V³⁺ cations. On Ni foam, a ternary array of NiFeV-LDH nanosheets supports the corroded electrode, as proposed in (Lee et al., 2021), the NiFeV-LDH electrode produces a 100-mA cm⁻² OER current density in 1 M KOH at an overpotential of 272 mV, outperforming the IrO₂ catalyst by 180 mV. According to DFT calculation, the unique structure of NiFeV LDH and the presence of vanadium play a key role in improving OER activity.

The resulting AEMWEs, coupled with a commercial Pt/C cathode catalyst, could achieve a cell current density of 2.1 A cm⁻² at 1.8V_{cell} in 1 M KOH, which would be comparable to that achieved by the PEMWEs using IrO₂ and Pt/C catalysts. Through corrosion of Ni foam electrodes with NiFeV-LDH Jooyoung, Lee, et al. (Lee et al., 2021) have demonstrated a highly stable and active OER electrode. When the binary NiFeV LDH electrode was tested at 10 mA cm⁻² in 1 M KOH, it exhibited a 224 mV overpotential. These OER electrodes were coupled with Pt/C HER electrocatalysts to create an AEM water electrolyzer. In 1 M KOH at 50 °C, they achieved 1.8 V only with 2.1 A cm⁻² of current density without iR compensation, which is about 0.9 A cm⁻² better than the class-leading IrO₂ and Pt/C pair. The Schematic diagram is shown in the Fig. 36.

It has been reported that a wide range of non-precious-metals based OER electrocatalysts have excellent activities, including transition metal sulfides (Fu et al., 2018, Jiang et al., 2018, Xu et al., 2018, Hong et al., 2019), phosphides (Xiao et al., 2017, Yu et al., 2018, Sanchez et al., 2019) /oxides (Choi et al., 2018, Xu et al., 2018), and layers and double hydroxides (Yang et al., 2018, Zhou et al., 2018, Kuai et al., 2019). It is expected that the very low overpotential (≤300 mV at 10 mA/cm²) and durability of these catalysts will facilitate the commercialization of water electrolyzers. The majority of studies on these catalysts in commercial devices, however, fail to report performance because it depends on parameters such as cell fabrication pressure, conditions for MEA fabrication, cell operation temperature and electrolyte flow (Pavel et al., 2014, Cho et al., 2018, Lim et al., 2019, Park et al., 2019, Li et al., 2021). The high performance of an experimental catalyst is not necessarily indicative of the high performance of the commercial device (Xu et al., 2019). Electrocatalysts traditionally have been synthesized from powders, which limits the fabrication process of electrodes and thereby the electrode efficiency. Numerous parameters can

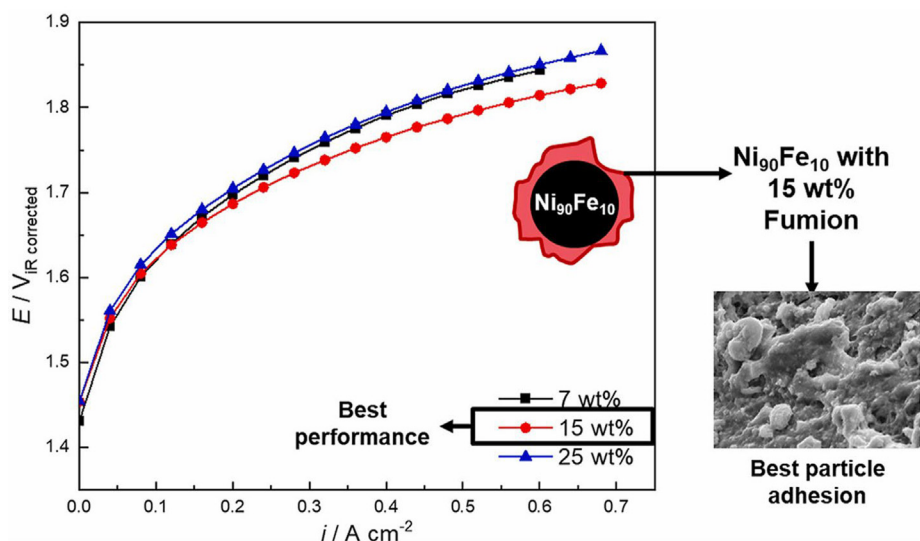


Fig. 35 Incorporates Fumatech fumion ions into AEMWE anodes synthesized by chemical reduction of nickel based nanoparticles and their polarization curve (different wt %). This figure has been reproduced with copyright permission from Elsevier (2021) (Cossar et al., 2021).

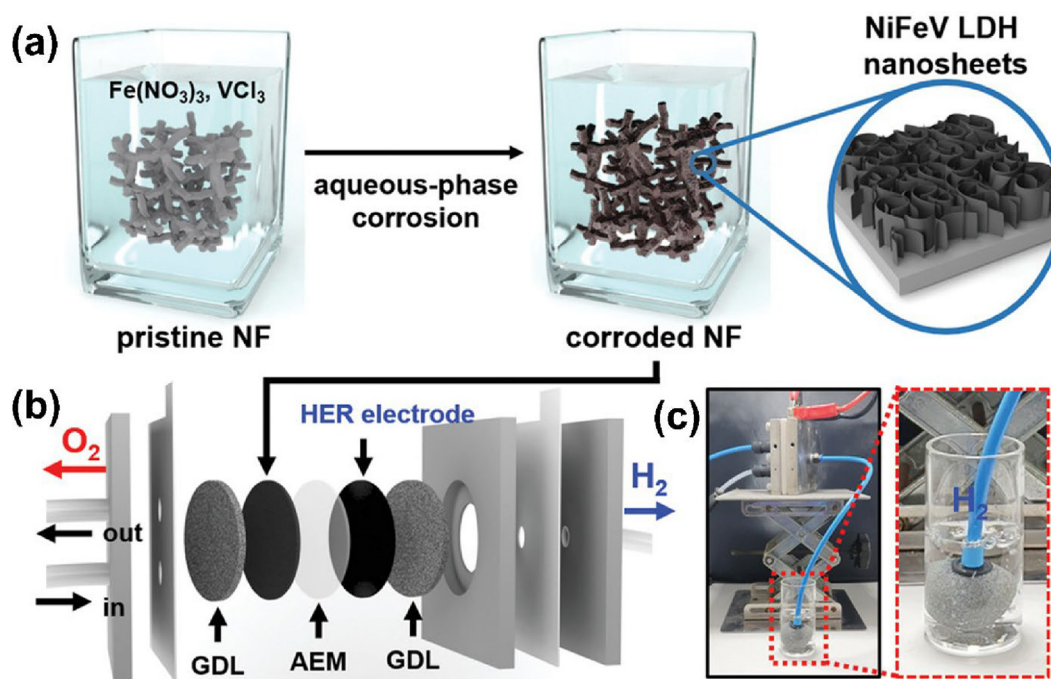
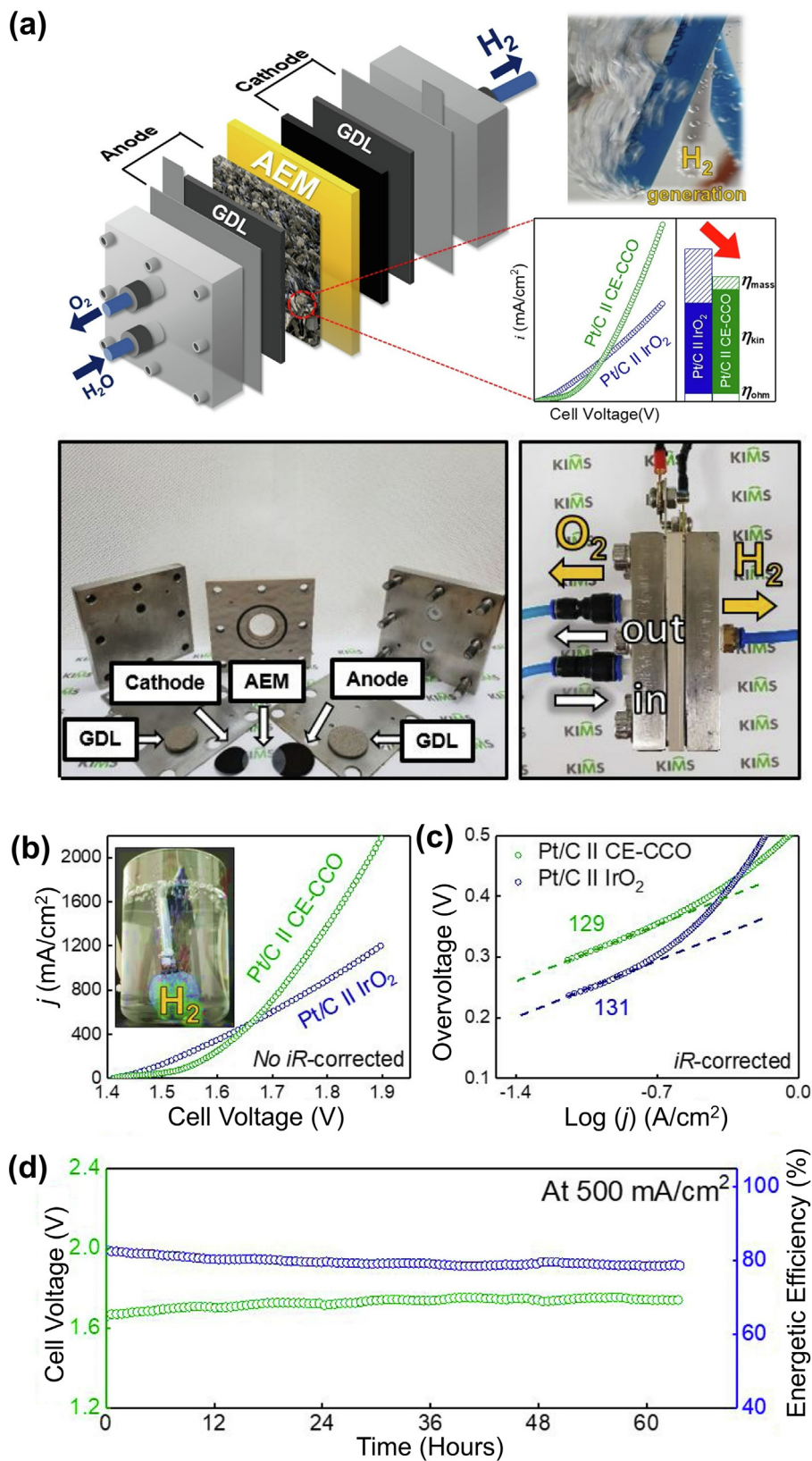


Fig. 36 This schematic shows; (a) corrosion process of NiFeV LDH onto NF, (b) design of the water electrolyzer. (c) development of hydrogen in the water electrolyzer, Wiley 2021 has granted permission to reproduce this Figure (Lee et al., 2021).

affect electrode fabrication, including composition of slurry (binder, catalyst, and solvent) and method of coating. Additionally, electrodes are commonly subjected to high temperature pressing or heat treatment (Lim et al., 2019, Park et al., 2019). In order to optimize the electrode fabrication process due to the variety of variables, simple techniques for producing high-performance electrodes are in highly demand. Among these techniques, electrodeposition can be used to deposit electrocatalysts directly on conductive substrates. This eliminates

the need for optimizing electrode fabrication procedures, which ensures that commercially available electrodeposited catalysts work properly (Lu and Zhao 2015, Sanchez et al., 2019). Using a chemical etching-based method for introducing oxygen defects into CCO, Yoo Sei Park et al. prepared an alkaline electrocatalyst for the OER as shown in Fig. 37. Despite the etching process decreasing the electrochemical surface area of Cu and Co, chemically etched CCO displays excellent OER performance and remarkable durability over 3600 h.



AEMWE fuel cells characterized by high performance (1390 mA/cm² at 1.8 V_{cell}) were directly constructed from the above material(anode) due to its low mass transfer resistance, especially at high current densities (Park et al., 2020).

Researchers have been working for decades and are still actively working to develop cost-effective and efficient materials and components for alkaline water electrolysis with the aim of to improve the kinetics of hydrogen and oxygen evolution reaction (HER and OER). In alkaline conditions, ion-conducting membranes and non-noble catalysts have been studied extensively. Researchers have studied different catalysts that are not noble, exhibiting high electrocatalytic activity, such as NiFeOx, Ni-Zn, Ni-Co, ZnCo LDH and Ni-Mo based composites, under alkaline conditions (Li et al., 2014, Gong et al., 2016, Babar et al., 2019). As non-noble OER catalysts, metal oxides such as CoOx, MnOx, NiOx, Co_{0.81}Co_{2.19}O₄ and NiFe-OS (Frydendal et al., 2014, Babar et al., 2018, Choi et al., 2018), FeOOH (Lee et al., 2018) and NiFe-OS (Kim et al., 2019) have been studied; a voltage overpotential of less than 0.5 V has also been achieved at 10 mA cm⁻² in alkali media. MXene-Ti₃C₂ and rGOs are expected to have a high specific surface area, which will allow it to provide more active sites while reducing the collapsing of carbon-based active particles, thereby improving catalytic stability (Fang et al., 2022). Also, AEMFCs can use non-noble metal catalysts, such as chalcogenides and transition-metal oxides, because they are cheap and easy to prepare. Unfortunately, their low catalytic activity makes further application difficult therefore, nitrogen doping/functionalization of NPs can improve the catalytic efficiency for HER/OER such as materials (Ni, Fe, Cu, Co, and Mn) doped with transition metals and nitrogen have received attention as promising catalysts for OER/ORRs, so as nitrogen-doped carbon nanotubes, nanocomposites with MXene and reduced graphene oxide. The high electronic conductivity of nickel foam (NF) and the desirable 3-D structure have made this material a popular choice for HER and OER in recent years. The research related to the nickel foam include the application of non-noble metals or their hydrides and oxides to NF as single metals such as Ni, NiO, and Co₃O₄ (Esswein et al., 2009, Kim et al., 2015, Yan et al., 2015), binary metal alloys such as Ni-Mo (Tang et al., 2014), Ni-Co (Pérez-Alonso et al., 2015), NiFe₂O₄ (Chanda et al., 2015), Ni/Fe base micro/nanostructures (Gao and Yan 2019), ternary metal alloys (Yuan et al., 2007, Li et al., 2016), and NiCo LDH (Jiang et al., 2015) by using nickel substrates, as well as added materials enhanced the catalytic activity of Ni meshes (Jović et al., 2013, Tasić et al., 2013), Ni nanofibers (Wu et al., 2016) and Ni foils (Marceta Kaninski et al., 2011), NiCu (Cardoso et al., 2015), which have been employed as catalyst supports for the water electrolysis. Further, a summary based on the type of materials reported in

the literature for electrolysis activity of AEMWE is shown in Table 2.

6. Challenges and summary

The technology of AEM electrolysis is still in its infancy. This report depicts the current status of the AEM electrolysis process' ability to produce low-cost hydrogen. AEM electrolyzer, Ionomers, Membranes, and Electrodes have been discussed in this paper, along with methods for producing hydrogen. We have critically reviewed recent developments.

Upon reviewing the articles, we discovered that the best results achieved by using AEM electrolysis are:

- i. At potential of 1.8 V in 0.1 M K₂CO₃, using membrane (A-201), Acta 3030 and Acta 4030 were used as catalyst for OER and HER, achieving current density of 500 mA cm⁻² at 45 °C (Vincent et al., 2017).
- ii. A Sustainion® 37–60 membrane was used in an alkaline water electrolyzer at 60 °C and 1.9 V for 2000 h using nickel, iron, and cobalt catalysts; they achieved at 1.82 V a current density of 1 A cm⁻² (Liu et al., 2017).
- iii. At a potential of 1.82 V with 1 M KOH at 60 °C, membrane AF1-HNN8-50 exhibiting an ion exchange capacity of 2.1–2.5 meq OH⁻ g⁻¹ achieved current density of 2 A cm⁻² (Fortin et al., 2020).
- iv. At potential of 1.8 V in 1 moldm⁻³ KOH, cranfield-membrane and 3 mg cm⁻² of Cu_{0.7}Co_{2.3}O₄ as a anode and Pt as cathode achieved current density of 1 A cm⁻² at 25 °C (Wu and Scott 2011).
- v. At potential of 2.046 V in 1 M KOH, using Tokuyama A201 membrane and 4 mg cm⁻² of Ni(OH)₂-Fe as a anode and 25.2 mg cm⁻² NiMo as cathode achieved current density of 2 A cm⁻² at 50 °C (Wang et al., 2022).
- vi. At potential of 2.046 V in 1 M KOH, using HMT-PMBI membrane and NiAlMo as an anode and cathode or NiAl as anode and NiAlMo as a cathode achieved current density of 2 A cm⁻² at 60 °C (Wang et al., 2019).

Even so, the AEM electrolysis technology still faces several challenges in terms of achieving low-cost hydrogen production; there are many issues to resolve in this respect. Current AEM electrolysis technology has the following features/weak points, which require improvement:

1. Ionic exchange capacity of a membrane can be increased by adding charged groups to the membrane.
2. Nucleophilic attack on the attached cationic groups and Hoffmann elimination can cause degradation of AEM.
3. A quaternary ammonium functional group degradation deforms membranes and electrodes.

Fig. 37 Shows the AEMWE configuration and performance. MEA is made up of a GDL_Pt/C used a cathode_AEM_CE-CCO and IrO₂ were used as an anode_GDL. Anodes are wet electrodes and cathodes are dry electrodes, the electrolytes are supplied towards the anode. (b) (Without iR correction) polarization curves (at 45 °C in 1 M KOH by using Pt/C + CE-CCO & Pt/C for AEMWEs). In Inset diagram of (b), shows a developed bubble of hydrogen from the cathode, (c) Figure of the polarization curve (at 45 °C in 1 M KOH by using Pt/C + CE-CCO & Pt/C for AEMWEs), (d) durability from 500 mA/cm² in 1 M KOH at 45 °C during 64 h for the AEMWE. Copyright permission was granted by Elsevier 2020 for redrawn figures (Park et al., 2020).

Table 2 Based on the type of materials reported in the literature for electrolysis activity of AEMWE.

Cathode and anode materials	Catalyst loading ($\text{mg}_{\text{metal}} \text{cm}^{-2}$)	Temperature	Cell voltage (V)	Current density (mA cm^{-2})	Electrolyte	References
NiCoO-NiCo/C & $\text{Cu}_{0.75}\text{Co}_{2.25}\text{O}_4$	1.5/30	50	9.25 stack (1.85V _{cell} per cell)	504 mA cm^{-2}	1 M KOH	(Park et al., 2021)
Pt/C & $\text{Cu}_{0.7}\text{Co}_{2.3}\text{O}_4$	1.0/3.0	25	2.0	1 A cm^{-2}	1 mol dm^{-1} KOH	(Wu and Scott 2011)
NiCoO-NiCo/C & $\text{Cu}_{0.75}\text{Co}_{2.25}\text{O}_4$	1.5/30	50	9.25 stack (1.85V _{cell} per cell)	740.23 mA cm^{-2}	1 M KOH	(Park et al., 2021)
Ni/CeO ₂ -La ₂ O ₃ /C & CuCoO_x	0.6–7.4	316 K	2.01, 1.89 &	~0.60	1 wt% K ₂ CO ₃ , 1 wt% K ₂ CO ₃ /KHCO ₃ (0.67 wt% K ₂ CO ₃ and 0.33 % KHCO ₃) and 1 M KOH	(Pavel et al., 2014)
NiFeCo & NiFe ₂ O ₄	N/A	40–60		~0.377	0.1–1 M KOH	(Pushkareva et al., 2020)
CeO ₂ -La ₂ O ₃ (Acta 4030) & CuCoO_x (Acta 3030)	Varies 2.9/3.9 0.4/2.8 4.4/2.4			~0.70	K ₂ CO ₃	(Ito et al., 2018)
Ni & Ce _{0.2} MnFe _{1.8} O ₄	3.5/3.5	25	1.8	325 mA cm^{-2}	0.1 M KOH	(Pandiarajan et al., 2015)
Ni & Li _{0.21} Co _{2.79} O ₄	2.5/2.5	20–45	2.2–2.05	300 mA cm^{-2}	0.2 M KOH	(Wu and Scott 2013)
CO ₃ S ₄ NS/NF & $\text{C}_{i0.81}\text{Co}_{2.19}\text{O}_4$	N/A	40–45	1.863	~431 mA cm^{-2}	1 M KOH	(Park et al., 2020)
CoP/CoP	5.0/5.0	–	1.8	335 mA cm^{-2}	0.1 M KOH	(Chang et al., 2016)
Ni/Carbon Paper & Ni Carbon Paper	N/A	70	1.9	150 mA cm^{-2}	1 M KOH	(Ahn et al., 2014)
NiMO & Ir	5.0/3.0	50	1.8	1 A cm^{-2}	1 M KOH	(Faid et al., 2018)
NiFe ₂ O ₄ /NF & Ni foam	C = 10	50	1.85	125 mA cm^{-2}	10 % KOH	(Chanda et al., 2015)
Ni & $\text{Cu}_x\text{Co}_{3-x}\text{O}_4$	0.4/0.18	40	2.0	100 mA cm^{-2}	1.0 M KOH	(López-Fernández et al., 2019)
Ni & CuCoO	0.38/0.4	30–70	1.5	300 mA cm^{-2}	1 M KOH	(López-Fernández et al., 2021)
Pt/C & $\text{Cu}_{0.7}\text{Co}_{2.3}\text{O}_4$	20 % Pt/3	25	1.7	1 A cm^{-2}	1 mol dm^{-3} KOH	(Wu and Scott 2011)
NiCoS & IrO ₂	N/A	50	1.7	~1.84 A cm^{-2}	1.0 M KOH	(Guo et al., 2020)
Ni & $\text{Cu}_{0.7}\text{Co}_{2.3}\text{O}_4$	2.0/3.0	55	1.99	100 mA cm^{-2}	Water	(Cao et al., 2012)
Ni/(CeO ₂ -La ₂ O ₃) & NiCo ₂ O ₄ @MnOx	4.00	60	1.86	400 mA cm^{-2}	0.1 M KOH	(Zeng et al., 2018)
Ni/(CeO ₂ -La ₂ O ₃)/C (Acta 4030) & CuCoO_x (Acta 3030)	7.4/30	60	1.95	500 mA cm^{-2}	1 % K ₂ CO ₃	(Vincent et al., 2017)
NiFeS/NF	N/A	25	2	274 mA cm^{-2}	1 M KOH	(Ganesan et al., 2016)
Ni/Li _{0.21} Co _{2.79} O ₄	2.0/2.0	20	2.2	300 mA cm^{-2}	Water	(Wu and Scott 2013)
Nickel Plate	N/A	80	2	100 mA cm^{-2}	30 wt% KOH	(Aili et al., 2015)
Ni-NiPx/Ni Mesh & Ni NiCo ₂ O ₄ /Ni mesh	N/A	25	1.85	100 mA cm^{-2}	30 wt% KOH	(Kuleshov et al., 2016)
PdNiFeCo/C-Ceria-Nf & Pt/C-CC	C = 0.3	25	1.82	100 mA cm^{-2}	1 M KOH	(Zhiani et al., 2017)
Pt/Ti & IrO ₂ /Carbon Paper	2.4/2.6	50	1.8	399 mA cm^{-2}	Water	(Leng et al., 2012)

Table 2 (continued)

Cathode and anode materials	Catalyst loading (mg _{metal} cm ⁻²)	Temperature	Cell voltage (V)	Current density (mA cm ⁻²)	Electrolyte	References
Ni Plate & Ni plate	0.5	80	2	200 mA cm ⁻²	30 wt% KOH	(Aili et al., 2013)
Ni foam & Ni Foam	0.5/0.5	70	1.9	260 mA cm ⁻²	10 wt% KOH	(Hnát et al., 2012)
Pt/C & NiCu MMO	1/5	50	2	1.85 A.cm ⁻²	1 M KOH	(Faid et al., 2021)
Pt/C & CuX Mn _{0.9-x} Co _{2.1} O ₄	1/3	45	1.82	100 mA.cm ⁻²	1 M KOH	(Wu and Scott 2012)
PdNiFeCo/C-Ceria-NF & Ni Pt/C-CC	C = 0.3	25	2.31	300 mA.cm ⁻²	1 M KOH	(Zhiani et al., 2017)
Pt & Ni/Fe	N/A	60	2.3	1 A.cm ⁻²	4 M NaOH	(Li et al., 2011)
Pt/Cu & Pt/Cu	C/A = 2.0/2.0	75	1.84	2.69 mA.cm ⁻²	3 M HCOOH	(Li et al., 2022)
Ni-MoO ₂ & Ni _{0.6} Co _{0.2} Fe _{0.2}	C/A = 3/5	50	2.0	1.15 A.cm ⁻²	1 M KOH	(Faid et al., 2021)
Pt/C & NiCo ₂ O ₄	0.3/2.5	70	1.75	266 mA.cm ⁻²	1 M KOH	(Hnát et al., 2014)
Pt & Ir	3.2/2.9	50	1.8	399 mA.cm ⁻²	Water	(Leng et al., 2012)
Pt/C & Cu _{0.7} Co _{2.3} O ₄	1/3	25	2	0.2	Water	(Wu and Scott 2012)
Pt/IrO ₂	3/2	60	1.63	1 A.cm ⁻²	1 M KOH	(Liu et al., 2017)
Pt black & Pb ₂ Ru ₂ O _{6.5}	2.5/2.5	50	1.84	400 mA.cm ⁻²	Ultra-pure water	(Parrondo et al., 2014)
Pt & IrO ₂	2.4/2.6	50	1.8	399 mA.cm ⁻²	Water	(Leng et al., 2012)
Pt/C & CuMnCoO ₄	C/A = 1/3	40	2.2	0.3 mA.cm ⁻²	Water	(Wu and Scott 2012)
Ni & Cu _{0.7} Co _{2.3} O ₄	2/3	50	2.3	100 mA.cm ⁻²	Water	(Cao et al., 2012)
PGM & PGM	C/A = 2/2	50	2	0.5	Water	(Park et al., 2018)
NiMo & Ni-Fe	N/A	70	1.95	0.4 A.cm ⁻²	Water	(Xiao et al., 2012)
Ni & Cu _{0.7} Co _{2.3} O ₄	2/3	22	1.9	100 mA.cm ⁻²	Water	(Wu and Scott 2012)
CeO ₂ La ₂ O ₃ /C(ACTA 4030) CuCoOx(ACTA 3030)	0.6–7.4/36	55	2	470 mA.cm ⁻²	K ₂ CO ₃	(Pavel et al., 2014)
ACTA SpA Catalyst	N/A	45	2.2	600 mA.cm ⁻²	K ₂ CO ₃	(Faraj et al., 2012)
Polished Nickel Plate & Polished Nickel Plate	N/A	80	2.3	700 mA.cm ⁻²	30 % KOH	(Aili et al., 2013)
Ni & Li _{0.21} Co _{2.79} O ₄	2/2.5	45	2.1	300 mA.cm ⁻²	Water	(Wu and Scott 2013)
Ni/(CeO ₂ -La ₂ O ₃)/C (ACTA 4030)& CuCoOx(ACTA 3030)	7.4/36	60	1.95	500 mA.cm ⁻²	1 % K ₂ CO ₃	(Vincent et al., 2017)
NiFeO ₄ & NiCo ₂ O ₄	10/10	40	2	150 mA.cm ⁻²	1 wt% KOH	(Hnát et al., 2017)
Electroplated Ni/ Electroplated Ni	N/A	70	1.9	300 mA.cm ⁻²	1 M KOH	(Ahn et al., 2014)
NiCuMMO & Ir Black	5/1	50	1.85	1.85 A.cm ⁻²	1 M KOH	(Faid et al., 2021)

(continued on next page)

Table 2 (continued)

Cathode and anode materials	Catalyst loading ($\text{mg}_{\text{metal}} \text{cm}^{-2}$)	Temperature	Cell voltage (V)	Current density (mA cm^{-2})	Electrolyte	References
Platinum Black & IrOx	3.0/3.0	50	2.29	500 mA cm^{-2}	1 M KOH	(Xu et al., 2019)
Ni-Mo-Al & NiFeCO & NiFe ₂ O ₄	N/A N/A	80 60	1.8 2	1.7 2 A cm^{-2}	24 % KOH 1 M KOH	(Pushkareva et al., 2020)
Pt/C & Ir Black	1/3.5–3.8	50	2	2 A cm^{-2}	1 M KOH	(Fortin et al., 2020)
NiMo/X72 & Ir Black	C = 5	50	1.9	1 A cm^{-2}	1 M KOH	(Faid et al., 2018)
Pt/C & IrO ₂	N/A	50	1.9	1.5 A cm^{-2}	1 M KOH	(Park et al., 2019)
Co ₂ P@Co ₃ O ₄ / Co ₂ P@Co ₃ O ₄	0.285/0.285	N/A	1.57	10 mA cm^{-2}	1 M KOH	(Yao et al., 2018)

- Hydroxyl ions have a lower conductivity than proton ions.
- In the MEA, ionomers degrade.
- Potential drop resulting from unsatisfactory anode load due to non-noble metal catalysts.
- In comparison with noble metal catalysts, transition metal catalysts are less effective, as well as having a lower catalyst utilization rate.
- When the electrolyte contains fewer hydroxyl ions, there is a slowing down of OER reactions.
- By trapping hydrogen and oxygen in MEA, at high pressure, hydrogen and oxygen block the catalyst's active sites.
- Despite the MEA's higher internal resistance, AEM electrolysis still results in lower performance than PEM electrolysis.
- Hofmann elimination reactions and/or nucleophilic substitution may also degrade the alkyl quaternary ammonium groups on the side chains at high pH and high temperatures.
- Similar to distilled water and ultrapure water, other electrolytes are ineffective compared to 1 M KOH.
- Cross-linked AEMs that use functionalized rGO as a cross-linker effectively solve compatibility issues between filler molecules and the matrix, and also enhance overall performance, such as ion conductivity, and the membranes have maintained their dimensional stability due to decreased motion of the polymer chain, while the nonionic nature of rGO should contribute toward lowering the ion conduction Ea (Bai et al., 2019).
- If nucleophilic attack and Hoffmann elimination are to be avoided, it is necessary to understand how the hydroxyl ions interact with the quaternary ammonium functional groups and polymer backbones.
- The following novel AEMs are suggested: Membrane AF1-HNN8-50, AEMs grafted with radiation red membrane (A-201), Sustainion® 37–60, Poly(ether ether ketone) sulfonated and imidazolium-functionalized AEM blends, Orion TM1TM membrane.
- hydrophilic quaternary-ammonium functionalized styrenic copolymer and hydrophobic hydrophilic block cross-linked AEM can be used to achieve the higher performance for AMEWs.
- An analysis of polarization, gas crossover, electrochemical impedance, and chronoamperometry is required to characterize the properties of AEMs in AEM water electrolysis conditions.
- Membranes with multi-cations on the side chains may be an effective material to increase ionic conductivity by efficiently using water due to the structure-induced segregation of microphases.
- Increasing imidazole group content results in increased IEC as well as an increase in water uptake.
- Addition of nanoparticle fillers and blends could increase the conductivity of hydroxyl ions. A lot of ionomers are toxic, which means development of ionomers may be slow. The development of an ionomer characterized by chemical stability, high ionic conductivity, and thermal stability should be pursued for AEM electrolysis.
- Ni and a rare earth metal form the basis of most of the OER catalysts.
- For the OER, a variety of metal alloy based catalysts, CO₃O₄ nanorods anchored on multiwalled carbon nanotubes, and the growth of CO₃O₄ nanocrystals on GO/rGO MXene may be considered. In addition, HER catalysts require further development. To improve the catalyst efficiency, catalytic activity, and stability of HER, low-cost catalysts are necessary.

6.1. Prospects for future research

AEM electrolysis still faces several development challenges before it is widely accepted and implemented on a large scale.

- Ionomers and membranes (conductive polymers must be developed with high stability, high conductivity, and low gas crossover, in particular > 60 °C).

11. Brewer-Engle theory suggests that alloying transition metals on the left half of the periodic table with their counterparts on the right side of the periodic table will provide a stronger synergetic effect than a single noble metal (Jakšić 1987)

Overall, the capital cost of the entire system will be reduced by AEM electrolysis with non-noble metal and non-platinum group metal catalysts. For the total cost of hydrogen production to be further reduced, it is necessary to improve the overall performance of AEM electrolyzer.

Declaration of Competing Interest

The authors declare that they have no known competing financial interests or personal relationships that could have appeared to influence the work reported in this paper.

Acknowledgement

This work was supported by Ph.D. Grant: FSE - REACT EU, Programma Operativo Nazionale Ricerca e innovazione 2014-2020 at University of Genova, Italy. This work was developed within the Project NEMESI, ID: RSH2B_000002, funded by PNRR- Next Generation Eu, MITE (Ministero della Transizione Ecologica).

References

- Abbasi, R., Setzler, B.P., Lin, S., et al, 2019. A Roadmap to Low-Cost Hydrogen with Hydroxide Exchange Membrane Electrolyzers. *Adv. Mater.* 31, 1805876. <https://doi.org/10.1002/adma.201805876>.
- Acar, C., Ghosh, S., Dincer, I., et al, 2015. Evaluation of a new continuous type hybrid photo-electrochemical system. *Int. J. Hydrog. Energy.* 40, 11112–11124. <https://doi.org/10.1016/j.ijhydene.2014.12.036>.
- Ahn, S.H., Lee, B.-S., Choi, I., et al, 2014. Development of a membrane electrode assembly for alkaline water electrolysis by direct electrodeposition of nickel on carbon papers. *Appl Catal B* 154–155, 197–205. <https://doi.org/10.1016/j.apcatb.2014.02.021>.
- Aili, D., Hansen, M.K., Renzaho, R.F., et al, 2013. Heterogeneous anion conducting membranes based on linear and crosslinked KOH doped polybenzimidazole for alkaline water electrolysis. *J. Membr. Sci.* 447, 424–432. <https://doi.org/10.1016/j.memsci.2013.07.054>.
- Aili, D., Hansen, M.K., Andreasen, J.W., et al, 2015. Porous poly(perfluorosulfonic acid) membranes for alkaline water electrolysis. *J. Membr. Sci.* 493, 589–598. <https://doi.org/10.1016/j.memsci.2015.06.057>.
- Aili, D., Wright, A.G., Kraglund, M.R., et al, 2017. Towards a stable ion-solvating polymer electrolyte for advanced alkaline water electrolysis. *J. Mater. Chem. A* 5, 5055–5066. <https://doi.org/10.1039/C6TA10680C>.
- Al Munsur, A.Z., Goo, B.-H., Kim, Y., et al, 2021. Nafion-Based Proton-Exchange Membranes Built on Cross-Linked Semi-Interpenetrating Polymer Networks between Poly(acrylic acid) and Poly(vinyl alcohol). *ACS Appl. Mater. Interfaces* 13, 28188–28200. <https://doi.org/10.1021/acsami.1c05662>.
- Alia, S.M., Pivovar, B.S., 2018. Evaluating Hydrogen Evolution and Oxidation in Alkaline Media to Establish Baselines. *J. Electrochem. Soc.* 165, F441–F455. <https://doi.org/10.1149/2.0361807jes>.
- Arakawa, K., Seguchi, T., Watanabe, Y., et al, 1982. Radiation-induced oxidation of polyethylene, ethylene-butene copolymer, and ethylene-propylene copolymer. *J. Polym. Sci., Polym. Chem. Ed.* 20, 2681–2692. <https://doi.org/10.1002/pol.1982.170200926>.
- Arges, C.G., Ramani, V.K., Pintauro, P.N., 2010. The Chalkboard: Anion Exchange Membrane Fuel Cells. *The Electrochemical Society Interface.* 19, 31–35. <https://doi.org/10.1149/2.f03102if>.
- Arges, C.G., Ramani, V., 2013a. Investigation of Cation Degradation in Anion Exchange Membranes Using Multi-Dimensional NMR Spectroscopy. *J. Electrochem. Soc.* 160, F1006–F1021. <https://doi.org/10.1149/2.056309jes>.
- Arges, C.G., Ramani, V., 2013b. Two-dimensional NMR spectroscopy reveals cation-triggered backbone degradation in polysulfone-based anion exchange membranes. *Proc. Natl. Acad. Sci.* 110, 2490–2495. <https://doi.org/10.1073/pnas.1217215110>.
- Arges, C.G., Jung, M.-S., Johnson, G., et al, 2011. Anion Exchange Membranes (AEMs) with Perfluorinated and Polysulfone Backbones with Different Cation Chemistries. *ECS Trans.* 41, 1795–1816. <https://doi.org/10.1149/1.3635711>.
- Asset, T., Atanassov, P., 2020. Iron-Nitrogen-Carbon Catalysts for Proton Exchange Membrane Fuel Cells. *Joule.* 4, 33–44. <https://doi.org/10.1016/j.joule.2019.12.002>.
- Awad, W.H., Gilman, J.W., Nyden, M., et al, 2004. Thermal degradation studies of alkyl-imidazolium salts and their application in nanocomposites. *Thermochim Acta* 409, 3–11. [https://doi.org/10.1016/S0040-6031\(03\)00334-4](https://doi.org/10.1016/S0040-6031(03)00334-4).
- Ayers, K.E., Anderson, E.B., Capuano, C., et al, 2010. Research Advances towards Low Cost, High Efficiency PEM Electrolysis. *ECS Trans.* 33, 3–15. <https://doi.org/10.1149/1.3484496>.
- Babar, P.T., Lokhande, A.C., Gang, M.G., et al, 2018. Thermally oxidized porous NiO as an efficient oxygen evolution reaction (OER) electrocatalyst for electrochemical water splitting application. *J. Ind. Eng. Chem.* 60, 493–497. <https://doi.org/10.1016/j.jiec.2017.11.037>.
- Babar, P.T., Lokhande, A.C., Jo, E., et al, 2019. Facile electrosynthesis of Fe (Ni/Co) hydroxyphosphate as a bifunctional electrocatalyst for efficient water splitting. *J. Ind. Eng. Chem.* 70, 116–123. <https://doi.org/10.1016/j.jiec.2018.09.041>.
- Bai, Y., Yuan, Y., Miao, L., et al, 2019. Functionalized rGO as covalent crosslinkers for constructing chemically stable polysulfone-based anion exchange membranes with enhanced ion conductivity. *J. Membr. Sci.* 570–571, 481–493. <https://doi.org/10.1016/j.memsci.2018.10.030>.
- Bates, M.K., Jia, Q., Ramaswamy, N., et al, 2015. Composite Ni/NiO-Cr₂O₃ Catalyst for Alkaline Hydrogen Evolution Reaction. *J. Phys. Chem. C* 119, 5467–5477. <https://doi.org/10.1021/jp512311c>.
- Ben youcef, H., Gubler, L., Gürsel, S.A., et al, 2009. Novel ETFE based radiation grafted poly(styrene sulfonic acid-co-methacrylonitrile) proton conducting membranes with increased stability. *Electrochem. Commun.* 11, 941–944. <https://doi.org/10.1016/j.elecom.2009.02.047>.
- Ben youcef, H., Alkan Gürsel, S., Buisson, A., et al, 2010. Influence of Radiation-Induced Grafting Process on Mechanical Properties of ETFE-Based Membranes for Fuel Cells. *Fuel Cells* 10, 401–410. <https://doi.org/10.1002/fuce.200900200>.
- Biancolli, A.L.G., Bsoul-Haj, S., Douglin, J.C., et al, 2022. High-performance radiation grafted anion-exchange membranes for fuel cell applications: Effects of irradiation conditions on ETFE-based membranes properties. *J. Membr. Sci.* 641, <https://doi.org/10.1016/j.memsci.2021.119879> 119879.
- Cai, Z., Liu, Y., Liu, S., et al, 2012b. High performance of lithium-ion polymer battery based on non-aqueous lithiated perfluorinated sulfonic ion-exchange membranes. *Energ. Environ. Sci.* 5, 5690–5693. <https://doi.org/10.1039/C1EE02708E>.
- Cai, G.-F., Tu, J.-P., Zhang, J., et al, 2012a. An efficient route to a porous NiO/reduced graphene oxide hybrid film with highly improved electrochromic properties. *Nanoscale* 4, 5724–5730. <https://doi.org/10.1039/C2NR31397A>.
- Cao, Y.-C., Wu, X., Scott, K., 2012. A quaternary ammonium grafted poly vinyl benzyl chloride membrane for alkaline anion

- exchange membrane water electrolyzers with no-noble-metal catalysts. *Int. J. Hydrog. Energy*. 37, 9524–9528. <https://doi.org/10.1016/j.ijhydene.2012.03.116>.
- Cardoso, D.S.P., Eugénio, S., Silva, T.M., et al, 2015. Hydrogen evolution on nanostructured Ni–Cu foams. *RSC Adv.* 5, 43456–43461. <https://doi.org/10.1039/C5RA06517H>.
- Carmo, M., Fritz, D.L., Mergel, J., et al, 2013. A comprehensive review on PEM water electrolysis. *Int. J. Hydrog. Energy*. 38, 4901–4934. <https://doi.org/10.1016/j.ijhydene.2013.01.151>.
- Chanda, D., Hnat, J., Paidar, M., et al, 2015. Synthesis and characterization of NiFe₂O₄ electrocatalyst for the hydrogen evolution reaction in alkaline water electrolysis using different polymer binders. *J. Power Sources* 285, 217–226. <https://doi.org/10.1016/j.jpowsour.2015.03.067>.
- Chang, J., Liang, L., Li, C., et al, 2016. Ultrathin cobalt phosphide nanosheets as efficient bifunctional catalysts for a water electrolysis cell and the origin for cell performance degradation. *Green Chem.* 18, 2287–2295. <https://doi.org/10.1039/c5gc02899j>.
- Changkhamchom, S., Kunanupatham, P., Phasukom, K., et al, 2021. Anion exchange membranes composed of quaternized polybenzimidazole and quaternized graphene oxide for glucose fuel cell. *Int. J. Hydrog. Energy*. 46, 5642–5652. <https://doi.org/10.1016/j.ijhydene.2020.11.043>.
- Chapiro, A., 1964. Radiation Chemistry of Polymers. *Radiat. Res. Suppl.* 4, 179–191. <https://doi.org/10.2307/3583578>.
- Chempath, S., Einsla, B.R., Pratt, L.R., et al, 2008. Mechanism of Tetraalkylammonium Headgroup Degradation in Alkaline Fuel Cell Membranes. *J. Phys. Chem. C* 112, 3179–3182. <https://doi.org/10.1021/jp7115577>.
- Chempath, S., Boncella, J.M., Pratt, L.R., et al, 2010. Density Functional Theory Study of Degradation of Tetraalkylammonium Hydroxides. *J. Phys. Chem. C* 114, 11977–11983. <https://doi.org/10.1021/jp9122198>.
- Chen, D., Hickner, M.A., 2012. Degradation of Imidazolium- and Quaternary Ammonium-Functionalized Poly(fluorenyl ether ketone sulfone) Anion Exchange Membranes. *ACS Appl. Mater. Interfaces* 4, 5775–5781. <https://doi.org/10.1021/am301557w>.
- Chen, D., Hickner, M.A., 2013. Ion Clustering in Quaternary Ammonium Functionalized Benzylmethyl Containing Poly(arylene ether ketone)s. *Macromolecules* 46, 9270–9278. <https://doi.org/10.1021/ma401620m>.
- Chen, W., Hu, M., Wang, H., et al, 2017. Dimensionally stable hexamethylenetetramine functionalized polysulfone anion exchange membranes. *J. Mater. Chem. A* 5, 15038–15047. <https://doi.org/10.1039/C7TA01218G>.
- Chen, P., Hu, X., 2020. High-Efficiency Anion Exchange Membrane Water Electrolysis Employing Non-Noble Metal Catalysts. *Adv. Energy Mater.* 10, 2002285. <https://doi.org/10.1002/aenm.202002285>.
- Chen, Y.-Z., Wang, C., Wu, Z.-Y., et al, 2015. From Bimetallic Metal–Organic Framework to Porous Carbon: High Surface Area and Multicomponent Active Dopants for Excellent Electrocatalysis. *Adv. Mater.* 27, 5010–5016. <https://doi.org/10.1002/adma.201502315>.
- Chen, N., Wang, H.H., Kim, S.P., et al, 2021. Poly(fluorenyl aryl piperidinium) membranes and ionomers for anion exchange membrane fuel cells. *Nat. Commun.* 12, 2367. <https://doi.org/10.1038/s41467-021-22612-3>.
- Cho, M.K., Park, H.-Y., Choe, S., et al, 2017. Factors in electrode fabrication for performance enhancement of anion exchange membrane water electrolysis. *J. Power Sources* 347, 283–290. <https://doi.org/10.1016/j.jpowsour.2017.02.058>.
- Cho, M.K., Park, H.-Y., Lee, H.J., et al, 2018. Alkaline anion exchange membrane water electrolysis: Effects of electrolyte feed method and electrode binder content. *J. Power Sources* 382, 22–29. <https://doi.org/10.1016/j.jpowsour.2018.02.025>.
- Choe, Y.-K., Fujimoto, C., Lee, K.-S., et al, 2014. Alkaline Stability of Benzyl Trimethyl Ammonium Functionalized Polyaromatics: A Computational and Experimental Study. *Chem. Mater.* 26, 5675–5682. <https://doi.org/10.1021/cm502422h>.
- Choi, W.-S., Jang, M.J., Park, Y.S., et al, 2018. Three-Dimensional Honeycomb-Like Cu_{0.81}Co_{2.19}O₄ Nanosheet Arrays Supported by Ni Foam and Their High Efficiency as Oxygen Evolution Electrodes. *ACS Applied Materials & Interfaces*. 10, 38663–38668. <https://doi.org/10.1021/acsami.8b12478>.
- Chu, X., Liu, L., Huang, Y., et al, 2019. Practical implementation of bis-six-membered N-cyclic quaternary ammonium cations in advanced anion exchange membranes for fuel cells: Synthesis and durability. *J. Membr. Sci.* 578, 239–250. <https://doi.org/10.1016/j.memsci.2019.02.051>.
- Chu, S., Majumdar, A., 2012. Opportunities and challenges for a sustainable energy future. *Nature* 488, 294–303. <https://doi.org/10.1038/nature11475>.
- Cope, A. C. and Trumbull, E. R. Olefins from Amines: The Hofmann Elimination Reaction and Amine Oxide Pyrolysis. *Organic Reactions*: 317–493.
- Cossar, E., Oyarce Barnett, A., Seland, F., et al, 2019. The Performance of Nickel and Nickel-Iron Catalysts Evaluated As Anodes in Anion Exchange Membrane Water Electrolysis. *Catalysts* 9, 814.
- Cossar, E., Barnett, A.O., Seland, F., et al, 2021. Ionomer content optimization in nickel-iron-based anodes with and without ceria for anion exchange membrane water electrolysis. *J. Power Sources* 514, <https://doi.org/10.1016/j.jpowsour.2021.230563> 230563.
- Dai, J., He, G., Ruan, X., et al, 2016. Constructing a rigid crosslinked structure for enhanced conductivity of imidazolium functionalized polysulfone hydroxide exchange membrane. *Int. J. Hydrog. Energy*. 41, 10923–10934. <https://doi.org/10.1016/j.ijhydene.2016.04.059>.
- Dang, H.-S., Jannasch, P., 2016. Alkali-stable and highly anion conducting poly(phenylene oxide)s carrying quaternary piperidinium cations. *J. Mater. Chem. A* 4, 11924–11938. <https://doi.org/10.1039/C6TA01905F>.
- Danks, T.N., Slade, R.C.T., Varcoe, J.R., 2003. Alkaline anion-exchange radiation-grafted membranes for possible electrochemical application in fuel cells. *J. Mater. Chem.* 13, 712–721. <https://doi.org/10.1039/B212164F>.
- Dawes, K., Glover, L.C., Vroom, D.A., 2007. The Effects of Electron Beam and g-Irradiation on Polymeric Materials. In: Mark, J.E. (Ed.), *Physical Properties of Polymers Handbook*. New York, NY, Springer, New, York, pp. 867–887.
- Di Vona, M.L., Narducci, R., Pasquini, L., et al, 2014. Anion-conducting ionomers: Study of type of functionalizing amine and macromolecular cross-linking. *Int. J. Hydrog. Energy*. 39, 14039–14049. <https://doi.org/10.1016/j.ijhydene.2014.06.166>.
- Dincer, I., Acar, C., 2015. Review and evaluation of hydrogen production methods for better sustainability. *Int. J. Hydrog. Energy*. 40, 11094–11111. <https://doi.org/10.1016/j.ijhydene.2014.12.035>.
- Dincer, I., Balta, M.T., 2011. Potential thermochemical and hybrid cycles for nuclear-based hydrogen production. *Int. J. Energy Res.* 35, 123–137. <https://doi.org/10.1002/er.1769>.
- Dincer, I., Zamfirescu, C., 2012. Sustainable hydrogen production options and the role of IAHE. *Int. J. Hydrog. Energy*. 37, 16266–16286. <https://doi.org/10.1016/j.ijhydene.2012.02.133>.
- Dong, X., Hou, S., Mao, H., et al, 2016. Novel hydrophilic-hydrophobic block copolymer based on cardo poly(arylene ether sulfone)s with bis-quaternary ammonium moieties for anion exchange membranes. *J. Membr. Sci.* 518, 31–39. <https://doi.org/10.1016/j.memsci.2016.06.036>.
- Dong, X., Xue, B., Qian, H., et al, 2017. Novel quaternary ammonium microblock poly (p-phenylene-co-aryl ether ketone)s as anion exchange membranes for alkaline fuel cells. *J. Power Sources* 342, 605–615. <https://doi.org/10.1016/j.jpowsour.2016.12.114>.
- Douglin, J.C., Singh, R.K., Haj-Bsoul, S., et al, 2021. A high-temperature anion-exchange membrane fuel cell with a critical raw

- material-free cathode. *Chemical Engineering Journal Advances*. 8., <https://doi.org/10.1016/j.ceja.2021.100153> 100153.
- Duan, Q., Ge, S., Wang, C.-Y., 2013. Water uptake, ionic conductivity and swelling properties of anion-exchange membrane. *J. Power Sources* 243, 773–778. <https://doi.org/10.1016/j.jpowsour.2013.06.095>.
- Esswein, A.J., McMurdo, M.J., Ross, P.N., et al, 2009. Size-Dependent Activity of Co_3O_4 Nanoparticle Anodes for Alkaline Water Electrolysis. *J. Phys. Chem. C* 113, 15068–15072. <https://doi.org/10.1021/jp904022e>.
- Fabbri, E., Nachtegaal, M., Binninger, T., et al, 2017. Dynamic surface self-reconstruction is the key of highly active perovskite nano-electrocatalysts for water splitting. *Nat. Mater.* 16, 925–931. <https://doi.org/10.1038/nmat4938>.
- Faid, A.Y., Barnett, A.O., Seland, F., et al, 2019. Optimized Nickel-Cobalt and Nickel-Iron Oxide Catalysts for the Hydrogen Evolution Reaction in Alkaline Water Electrolysis. *J. Electrochem. Soc.* 166, F519–F533. <https://doi.org/10.1149/2.0821908jes>.
- Faid, A.Y., Barnett, A.O., Seland, F., et al, 2021a. NiCu mixed metal oxide catalyst for alkaline hydrogen evolution in anion exchange membrane water electrolysis. *Electrochim. Acta* 371., <https://doi.org/10.1016/j.electacta.2021.137837> 137837.
- Faid, A.Y., Barnett, A.O., Seland, F., et al, 2021b. Tuning Ni-MoO₂ Catalyst-Ionomer and Electrolyte Interaction for Water Electrolyzers with Anion Exchange Membranes. *ACS Appl Energy Mater.* 4, 3327–3340. <https://doi.org/10.1021/acsaem.0c03072>.
- Faid, A., Oyarce Barnett, A., Seland, F., et al, 2018. Highly Active Nickel-Based Catalyst for Hydrogen Evolution in Anion Exchange Membrane Electrolysis. *Catalysts* 8. <https://doi.org/10.3390/catal8120614>.
- Fang, J., Lyu, M., Wang, X., et al, 2015. Synthesis and performance of novel anion exchange membranes based on imidazolium ionic liquids for alkaline fuel cell applications. *J. Power Sources* 284, 517–523. <https://doi.org/10.1016/j.jpowsour.2015.03.065>.
- Fang, J., Shen, P.K., 2006. Quaternized poly(phthalazinone ether sulfone ketone) membrane for anion exchange membrane fuel cells. *J. Membr. Sci.* 285, 317–322. <https://doi.org/10.1016/j.memsci.2006.08.037>.
- Fang, Z., Xu, C., Zhang, X., et al, 2022. MXene ($\text{Ti}_3\text{C}_2\text{T}_x$)-Supported Binary Co-, Zn-Doped Carbon as Oxygen Reduction Reaction Catalyst for Anion Exchange Membrane Fuel Cells. *Energy Technol.* 10, 2101168. <https://doi.org/10.1002/ente.202101168>.
- Fang, J., Yang, Y., Lu, X., et al, 2012. Cross-linked, ETFE-derived and radiation grafted membranes for anion exchange membrane fuel cell applications. *Int. J. Hydrog. Energy*. 37, 594–602. <https://doi.org/10.1016/j.ijhydene.2011.09.112>.
- Faraj, M., Elia, E., Boccia, M., et al, 2011. New anion conducting membranes based on functionalized styrene-butadiene-styrene triblock copolymer for fuel cells applications. *J. Polym. Sci. A Polym. Chem.* 49, 3437–3447. <https://doi.org/10.1002/pola.24781>.
- Faraj, M., Boccia, M., Miller, H., et al, 2012. New LDPE based anion-exchange membranes for alkaline solid polymeric electrolyte water electrolysis. *Int. J. Hydrog. Energy*. 37, 14992–15002. <https://doi.org/10.1016/j.ijhydene.2012.08.012>.
- Feng, S., Pang, J., Yu, X., et al, 2017. High-Performance Semicrystalline Poly(ether ketone)-Based Proton Exchange Membrane. *ACS Appl. Mater. Interfaces* 9, 24527–24537. <https://doi.org/10.1021/acsaami.7b03720>.
- Ferreira, A.C., Gonzalez, E.R., Ticianelli, E.A., et al, 1988. The effect of temperature on the water electrolysis reactions on nickel and nickel-based codeposits. *J. Appl. Electrochem.* 18, 894–898. <https://doi.org/10.1007/BF01016047>.
- Ferrero, D., Lanzini, A., Santarelli, M., et al, 2013. A comparative assessment on hydrogen production from low- and high-temperature electrolysis. *Int. J. Hydrog. Energy*. 38, 3523–3536. <https://doi.org/10.1016/j.ijhydene.2013.01.065>.
- Firouz Tadavani, K., Abdolmaleki, A., Molavian, M.R., et al, 2019. A mechanically robust multication double-network polymer as an anion-exchange membrane: High ion conductivity and excellent chemical stability. *Polymer* 178., <https://doi.org/10.1016/j.polymer.2019.121608> 121608.
- Fortin, P., Khoza, T., Cao, X., et al, 2020. High-performance alkaline water electrolysis using Aemion™ anion exchange membranes. *J. Power Sources* 451., <https://doi.org/10.1016/j.jpowsour.2020.227814> 227814.
- Frydendal, R., Paoli, E.A., Knudsen, B.P., et al, 2014. Benchmarking the Stability of Oxygen Evolution Reaction Catalysts: The Importance of Monitoring Mass Losses. *ChemElectroChem* 1, 2075–2081. <https://doi.org/10.1002/celc.201402262>.
- Fu, H.Q., Zhang, L., Wang, C.W., et al, 2018. 1D/1D Hierarchical Nickel Sulfide/Phosphide Nanostructures for Electrocatalytic Water Oxidation. *ACS Energy Lett.* 3, 2021–2029. <https://doi.org/10.1021/acsenergylett.8b00982>.
- E. Funk, J., 2001. Thermochemical hydrogen production: past and present. *Int. J. Hydrog. Energy*. 26, 185–190. [https://doi.org/10.1016/S0360-3199\(00\)00062-8](https://doi.org/10.1016/S0360-3199(00)00062-8).
- Ganesan, P., Sivanantham, A., Shanmugam, S., 2016. Inexpensive electrochemical synthesis of nickel iron sulphides on nickel foam: super active and ultra-durable electrocatalysts for alkaline electrolyte membrane water electrolysis. *J. Mater. Chem. A* 4, 16394–16402. <https://doi.org/10.1039/c6ta04499a>.
- Ganley, J.C., 2009. High temperature and pressure alkaline electrolysis. *Int. J. Hydrog. Energy*. 34, 3604–3611. <https://doi.org/10.1016/j.ijhydene.2009.02.083>.
- Gao, R., Yan, D., 2019. Recent Development of Ni/Fe-Based Micro/Nanostructures toward Photo/Electrochemical Water Oxidation. *Adv. Energy Mater.* 10. <https://doi.org/10.1002/aenm.201900954>.
- Gao, M.Y., Yang, C., Zhang, Q.B., et al, 2016. Electrochemical fabrication of porous Ni-Cu alloy nanosheets with high catalytic activity for hydrogen evolution. *Electrochim. Acta* 215, 609–616. <https://doi.org/10.1016/j.electacta.2016.08.145>.
- Gao, X., Yu, H., Jia, J., et al, 2017b. High performance anion exchange ionomer for anion exchange membrane fuel cells. *RSC Adv.* 7, 19153–19161. <https://doi.org/10.1039/C7RA01980G>.
- Gao, R., Zhang, H., Yan, D., 2017a. Iron diselenide nanoplatelets: Stable and efficient water-electrolysis catalysts. *Nano Energy* 31, 90–95. <https://doi.org/10.1016/j.nanoen.2016.11.021>.
- Gao, R., Zhu, J., Yan, D., 2021. Transition metal-based layered double hydroxides for photo(electro)chemical water splitting: a mini review. *Nanoscale* 13, 13593–13603. <https://doi.org/10.1039/d1nr03409j>.
- Goel, P., Mandal, B.E.P., et al, 2021. Di-quaternized graphene oxide based multi-cationic cross-linked monovalent selective anion exchange membrane for electro dialysis. *Sep. Purif. Technol.* 276., <https://doi.org/10.1016/j.seppur.2021.119361> 119361.
- Gonçalves Biancolli, A.L., Herranz, D., Wang, L., et al, 2018. ETFE-based anion-exchange membrane ionomer powders for alkaline membrane fuel cells: a first performance comparison of head-group chemistry. *J. Mater. Chem. A* 6, 24330–24341. <https://doi.org/10.1039/C8TA08309F>.
- Gong, M., Zhou, W., Kenney, M.J., et al, 2015. Blending Cr₂O₃ into a NiO–Ni Electro catalyst for Sustained Water Splitting. *Angew. Chem. Int. Ed.* 54, 11989–11993. <https://doi.org/10.1002/anie.201504815>.
- Gong, M., Wang, D.-Y., Chen, C.-C., et al, 2016. A mini review on nickel-based electrocatalysts for alkaline hydrogen evolution reaction. *Nano Res.* 9, 28–46. <https://doi.org/10.1007/s12274-015-0965-x>.
- Gong, X., Yan, X., Li, T., et al, 2017. Design of pendent imidazolium side chain with flexible ether-containing spacer for alkaline anion exchange membrane. *J. Membr. Sci.* 523, 216–224. <https://doi.org/10.1016/j.memsci.2016.09.050>.
- Gu, S., Cai, R., Luo, T., et al, 2009. A Soluble and Highly Conductive Ionomer for High-Performance Hydroxide Exchange Membrane

- Fuel Cells. *Angew. Chem. Int. Ed.* 48, 6499–6502. <https://doi.org/10.1002/anie.200806299>.
- Gu, S., Cai, R., Yan, Y., et al, 2011. Self-crosslinking for dimensionally stable and solvent-resistant quaternary phosphonium based hydroxide exchange membranes. *Chem. Commun.* 47, 2856–2858. <https://doi.org/10.1039/C0CC04335D>.
- Gu, F., Dong, H., Li, Y., et al, 2014. Highly Stable N3-Substituted Imidazolium-Based Alkaline Anion Exchange Membranes: Experimental Studies and Theoretical Calculations. *Macromolecules* 47, 208–216. <https://doi.org/10.1021/ma402334t>.
- Gu, S., Sheng, W., Cai, R., et al, 2013. An efficient Ag-ionomer interface for hydroxide exchange membrane fuel cells. *Chem. Commun.* 49, 131–133. <https://doi.org/10.1039/C2CC34862D>.
- Guan, Y., Li, N., Li, Y., et al, 2020. Two dimensional ZIF-derived ultra-thin Cu-N/C nanosheets as high performance oxygen reduction electrocatalysts for high-performance Zn-air batteries. *Nanoscale* 12, 14259–14266. <https://doi.org/10.1039/D0NR03495A>.
- Guo, M., Fang, J., Xu, H., et al, 2010. Synthesis and characterization of novel anion exchange membranes based on imidazolium-type ionic liquid for alkaline fuel cells. *J. Membr. Sci.* 362, 97–104. <https://doi.org/10.1016/j.memsci.2010.06.026>.
- Guo, W., Kim, J., Kim, H., et al, 2020. Direct electrodeposition of Ni-Co-S on carbon paper as an efficient cathode for anion exchange membrane water electrolyzers. *Int. J. Energy Res.* 45, 1918–1931. <https://doi.org/10.1002/er.5875>.
- Guo, D., Lai, A.N., Lin, C.X., et al, 2016. Imidazolium-Functionalized Poly(arylene ether sulfone) Anion-Exchange Membranes Densely Grafted with Flexible Side Chains for Fuel Cells. *ACS Appl. Mater. Interfaces* 8, 25279–25288. <https://doi.org/10.1021/acsami.6b07711>.
- Guo, D., Lin, C.X., Hu, E.N., et al, 2017. Clustered multi-imidazolium side chains functionalized alkaline anion exchange membranes for fuel cells. *J. Membr. Sci.* 541, 214–223. <https://doi.org/10.1016/j.memsci.2017.07.007>.
- Gürsel, S.A., youcef, H.B., Wokaun, A., et al, 2007. Influence of reaction parameters on grafting of styrene into poly(ethylene-alt-tetrafluoroethylene) films. *Nucl. Instrum. Methods Phys. Res., Sect. B* 265, 198–203. <https://doi.org/10.1016/j.nimb.2007.08.050>.
- Hadikhani, P., Hashemi, S.M.H., Schenk, S.A., et al, 2021. A membrane-less electrolyzer with porous walls for high throughput and pure hydrogen production. *Sustainable Energy Fuels* 5, 2419–2432. <https://doi.org/10.1039/D1SE00255D>.
- Hahn, S.-J., Won, M., Kim, T.-H., 2013. A morpholinium-functionalized poly(ether sulfone) as a novel anion exchange membrane for alkaline fuel cell. *Polym. Bull.* 70, 3373–3385. <https://doi.org/10.1007/s00289-013-1028-7>.
- He, Q., Li, Q., Khene, S., et al, 2013. High-Loading Cobalt Oxide Coupled with Nitrogen-Doped Graphene for Oxygen Reduction in Anion-Exchange-Membrane Alkaline Fuel Cells. *J. Phys. Chem. C* 117, 8697–8707. <https://doi.org/10.1021/jp401814f>.
- He, L., Liu, J., Liu, Y., et al, 2019b. Titanium dioxide encapsulated carbon-nitride nanosheets derived from MXene and melamine-cyanuric acid composite as a multifunctional electrocatalyst for hydrogen and oxygen evolution reaction and oxygen reduction reaction. *Appl Catal B* 248, 366–379. <https://doi.org/10.1016/j.apcatb.2019.02.033>.
- He, X.-D., Xu, F., Li, F., et al, 2017. Composition-performance relationship of NiCu nanoalloys as hydrogen evolution electrocatalyst. *J. Electroanal. Chem.* 799, 235–241. <https://doi.org/10.1016/j.jelechem.2017.05.050>.
- He, J., Zu, L., Liu, X., et al, 2019a. Porous NiCu alloy cathode with oriented pore structure for hydrogen evolution reaction by freeze casting. *J. Porous Mater.* 26, 1533–1539. <https://doi.org/10.1007/s10934-019-00751-9>.
- Henkensmeier, D., Kim, H.-J., Lee, H.-J., et al, 2011. Polybenzimidazolium-Based Solid Electrolytes. *Macromol. Mater. Eng.* 296, 899–908. <https://doi.org/10.1002/mame.201100100>.
- Henkensmeier, D., Cho, H., Brela, M., et al, 2014. Anion conducting polymers based on ether linked polybenzimidazole (PBI-OO). *Int. J. Hydrog. Energy.* 39, 2842–2853. <https://doi.org/10.1016/j.ijhydene.2013.07.091>.
- Henkensmeier, D., Najibah, M., Harms, C., et al, 2020. Overview: State-of-the Art Commercial Membranes for Anion Exchange Membrane Water Electrolysis. *J. Electrochem. Energy Convers. Storage* 18. <https://doi.org/10.1115/1.4047963>.
- Hibbs, M.R., Fujimoto, C.H., Cornelius, C.J., 2009. Synthesis and Characterization of Poly(phenylene)-Based Anion Exchange Membranes for Alkaline Fuel Cells. *Macromolecules* 42, 8316–8321. <https://doi.org/10.1021/ma901538c>.
- Hickner, M.A., Herring, A.M., Coughlin, E.B., 2013. Anion exchange membranes: Current status and moving forward. *J Polym Sci B* 51, 1727–1735. <https://doi.org/10.1002/polb.23395>.
- Hnát, J., Paidar, M., Schauer, J., et al, 2012. Polymer anion-selective membranes for electrolytic splitting of water. Part II: Enhancement of ionic conductivity and performance under conditions of alkaline water electrolysis. *J. Appl. Electrochem.* 42, 545–554. <https://doi.org/10.1007/s10800-012-0432-2>.
- Hnát, J., Paidar, M., Schauer, J., et al, 2014. Polymer anion-selective membrane for electrolytic water splitting: The impact of a liquid electrolyte composition on the process parameters and long-term stability. *Int. J. Hydrog. Energy.* 39, 4779–4787. <https://doi.org/10.1016/j.ijhydene.2014.01.086>.
- Hnát, J., Plevová, M., Žitka, J., et al, 2017. Anion-selective materials with 1,4-diazabicyclo[2.2.2]octane functional groups for advanced alkaline water electrolysis. *Electrochim. Acta* 248, 547–555. <https://doi.org/10.1016/j.electacta.2017.07.165>.
- Hong, Y.-R., Mhin, S., Kim, K.-M., et al, 2019. Electrochemically activated cobalt nickel sulfide for an efficient oxygen evolution reaction: partial amorphization and phase control. *J. Mater. Chem. A* 7, 3592–3602. <https://doi.org/10.1039/C8TA10142F>.
- Hossain, M.A., Jang, H., Lee, S., et al, 2015. Comparison of properties of anion conductive Parmax membranes containing imidazolium cation and quaternary ammonium. *Int. J. Hydrog. Energy.* 40, 1324–1332. <https://doi.org/10.1016/j.ijhydene.2014.09.145>.
- Hosseini, S.M., Koranian, P., Gholami, A., et al, 2013. Fabrication of mixed matrix heterogeneous ion exchange membrane by multi-walled carbon nanotubes: Electrochemical characterization and transport properties of mono and bivalent cations. *Desalination* 329, 62–67. <https://doi.org/10.1016/j.desal.2013.09.007>.
- Hou, H., Sun, G., He, R., et al, 2008. Alkali doped polybenzimidazole membrane for alkaline direct methanol fuel cell. *Int. J. Hydrog. Energy.* 33, 7172–7176. <https://doi.org/10.1016/j.ijhydene.2008.09.023>.
- Hou, H., Wang, S., Liu, H., et al, 2011. Synthesis and characterization of a new anion exchange membrane by a green and facile route. *Int. J. Hydrog. Energy.* 36, 11955–11960. <https://doi.org/10.1016/j.ijhydene.2011.06.054>.
- Hu, X., Huang, Y., Liu, L., et al, 2021. Piperidinium functionalized aryl ether-free polyaromatics as anion exchange membrane for water electrolyzers: Performance and durability. *J. Membr. Sci.* 621, <https://doi.org/10.1016/j.memsci.2020.118964> 118964.
- Hu, C., Park, J.H., Kim, H.M., et al, 2022. Elucidating the role of alkyl chain in poly(aryl piperidinium) copolymers for anion exchange membrane fuel cells. *J. Membr. Sci.* 647, <https://doi.org/10.1016/j.memsci.2022.120341> 120341.
- Hu, Q., Shang, Y., Wang, Y., et al, 2012. Preparation and characterization of fluorinated poly(aryl ether oxadiazole)s anion exchange membranes based on imidazolium salts. *Int. J. Hydrog. Energy.* 37, 12659–12665. <https://doi.org/10.1016/j.ijhydene.2012.05.077>.
- Hugar, K.M., Kostalik, H.A., Coates, G.W., 2015. Imidazolium Cations with Exceptional Alkaline Stability: A Systematic Study of Structure-Stability Relationships. *J. Am. Chem. Soc.* 137, 8730–8737. <https://doi.org/10.1021/jacs.5b02879>.

- Ito, H., Miyazaki, N., Sugiyama, S., et al, 2018. Investigations on electrode configurations for anion exchange membrane electrolysis. *J. Appl. Electrochem.* 48, 305–316. <https://doi.org/10.1007/s10800-018-1159-5>.
- Jakšić, M.M., 1987. Advances in electrocatalysis for hydrogen evolution in the light of the Brewer-Engel valence-bond theory. *Int. J. Hydrog. Energy.* 12, 727–752. [https://doi.org/10.1016/0360-3199\(87\)90090-5](https://doi.org/10.1016/0360-3199(87)90090-5).
- Jang, M.J., Yang, J., Lee, J., et al, 2020. Superior performance and stability of anion exchange membrane water electrolysis: pH-controlled copper cobalt oxide nanoparticles for the oxygen evolution reaction. *J. Mater. Chem. A* 8, 4290–4299. <https://doi.org/10.1039/C9TA13137J>.
- Jasti, A., Shahi, V.K., 2014. A facile synthesis of highly stable multiblock poly(arylene ether)s based alkaline membranes for fuel cells. *J. Power Sources* 267, 714–722. <https://doi.org/10.1016/j.jpowsour.2014.05.129>.
- Jervis, R., Mansor, N., Sobrido, A.J., et al, 2017. The Importance of Using Alkaline Ionomer Binders for Screening Electrocatalysts in Alkaline Electrolyte. *J. Electrochem. Soc.* 164, F1551–F1555. <https://doi.org/10.1149/2.044171jes>.
- Jheng, L.-C., Hsu, S.-L.-C., Lin, B.-Y., et al, 2014. Quaternized polybenzimidazoles with imidazolium cation moieties for anion exchange membrane fuel cells. *J. Membr. Sci.* 460, 160–170. <https://doi.org/10.1016/j.memsci.2014.02.043>.
- Jiang, J., Zhang, A., Li, L., et al, 2015. Nickel–cobalt layered double hydroxide nanosheets as high-performance electrocatalyst for oxygen evolution reaction. *J. Power Sources* 278, 445–451. <https://doi.org/10.1016/j.jpowsour.2014.12.085>.
- Jiang, J., Lu, S., Wang, W.-K., et al, 2018. Ultrahigh electrocatalytic oxygen evolution by iron-nickel sulfide nanosheets/reduced graphene oxide nanohybrids with an optimized autoxidation process. *Nano Energy* 43, 300–309. <https://doi.org/10.1016/j.nanoen.2017.11.049>.
- Jin, J., Li, L., Nie, X., et al, 2022. Electrochemically Fabricated Superhydrophilic/Superaerophobic Manganese Oxide Nanowires at Discontinuous Solid-Liquid Interfaces for Enhanced Oxygen Evolution Performances. *Adv. Mater. Interfaces* 9, 2101478. <https://doi.org/10.1002/admi.202101478>.
- Jović, B.M., Lačnjevac, U.Č., Krstajić, N.V., et al, 2013. Ni–Sn coatings as cathodes for hydrogen evolution in alkaline solutions. *Electrochim. Acta* 114, 813–818. <https://doi.org/10.1016/j.electacta.2013.06.024>.
- Jung, M.-S.-J., Arges, C.G., Ramani, V., 2011. A perfluorinated anion exchange membrane with a 1,4-dimethylpiperazinium cation. *J. Mater. Chem.* 21, 6158–6160. <https://doi.org/10.1039/C1JM10320B>.
- Kang, S.Y., Park, J.E., Jang, G.Y., et al, 2022. High-performance and durable water electrolysis using a highly conductive and stable anion-exchange membrane. *Int. J. Hydrog. Energy.* 47, 9115–9126. <https://doi.org/10.1016/j.ijhydene.2022.01.002>.
- Kiessling, A., Fornaciari, J.C., Anderson, G., et al, 2022. Influence of Supporting Electrolyte on Hydroxide Exchange Membrane Water Electrolysis Performance: Catholyte. *J. Electrochem. Soc.* 169, <https://doi.org/10.1149/1945-7111/ac4fed> 024510.
- Kim, H.-K., Bayarsaikhan, U., Na, S.-M., et al, 2019. Two newly recorded species of Tischeriidae (Lepidoptera: Tischerioidea) from Korea. *J. Asia-Pac. Biodivers.* 12, 273–277. <https://doi.org/10.1016/j.japb.2018.12.001>.
- Kim, D.S., Labouriau, A., Guiver, M.D., et al, 2011. Guanidinium-Functionalized Anion Exchange Polymer Electrolytes via Activated Fluorophenyl-Amine Reaction. *Chem. Mater.* 23, 3795–3797. <https://doi.org/10.1021/cm2016164>.
- Kim, J.-H., Lee, J.-N., Yoo, C.-Y., et al, 2015. Low-cost and energy-efficient asymmetric nickel electrode for alkaline water electrolysis. *Int. J. Hydrog. Energy.* 40, 10720–10725. <https://doi.org/10.1016/j.ijhydene.2015.07.025>.
- Kim, S., Yang, S., Kim, D., 2017. Poly(arylene ether ketone) with pendant pyridinium groups for alkaline fuel cell membranes. *Int. J. Hydrog. Energy.* 42, 12496–12506. <https://doi.org/10.1016/j.ijhydene.2017.03.187>.
- Kizewski, J.P., Mudri, N.H., Varcoe, J.R., 2013. An empirical study into the effect of long term storage ($-36 \pm 2^\circ\text{C}$) of electron-beamed ETFE on the properties of radiation-grafted alkaline anion-exchange membranes. *Radiat. Phys. Chem.* 89, 64–69. <https://doi.org/10.1016/j.radphyschem.2013.04.005>.
- Kjartansdóttir, C.K., Nielsen, L.P., Møller, P., 2013. Development of durable and efficient electrodes for large-scale alkaline water electrolysis. *Int. J. Hydrog. Energy.* 38, 8221–8231. <https://doi.org/10.1016/j.ijhydene.2013.04.101>.
- Konovalova, A., Kim, H., Kim, S., et al, 2018. Blend membranes of polybenzimidazole and an anion exchange ionomer (FAA3) for alkaline water electrolysis: Improved alkaline stability and conductivity. *J. Membr. Sci.* 564, 653–662. <https://doi.org/10.1016/j.memsci.2018.07.074>.
- Kostowskyj, M.A., Kirk, D.W., Thorpe, S.J., 2010. Ag and Ag–Mn nanowire catalysts for alkaline fuel cells. *Int. J. Hydrog. Energy.* 35, 5666–5672. <https://doi.org/10.1016/j.ijhydene.2010.02.125>.
- Kouchachvili, L., Yaïci, W., Entchev, E., 2018. Hybrid battery/supercapacitor energy storage system for the electric vehicles. *J. Power Sources* 374, 237–248. <https://doi.org/10.1016/j.jpowsour.2017.11.040>.
- Krol, J.J., Wessling, M., Strathmann, H., 1999. Concentration polarization with monopolar ion exchange membranes: current–voltage curves and water dissociation. *J. Membr. Sci.* 162, 145–154. [https://doi.org/10.1016/S0376-7388\(99\)00133-7](https://doi.org/10.1016/S0376-7388(99)00133-7).
- Kuai, C., Zhang, Y., Wu, D., et al, 2019. Fully Oxidized Ni–Fe Layered Double Hydroxide with 100% Exposed Active Sites for Catalyzing Oxygen Evolution Reaction. *ACS Catal.* 9, 6027–6032. <https://doi.org/10.1021/acscatal.9b01935>.
- Kuleshov, V.N., Kuleshov, N.V., Grigoriev, S.A., et al, 2016. Development and characterization of new nickel coatings for application in alkaline water electrolysis. *Int. J. Hydrog. Energy.* 41, 36–45. <https://doi.org/10.1016/j.ijhydene.2015.10.141>.
- Lai, Q., Zhu, J., Zhao, Y., et al, 2017. MOF-Based Metal-Doping-Induced Synthesis of Hierarchical Porous CuN/C Oxygen Reduction Electrocatalysts for Zn–Air Batteries. *Small* 13, 1700740. <https://doi.org/10.1002/smll.201700740>.
- Lappan, U., Geißler, U., Gohs, U., et al, 2010. Grafting of styrene into pre-irradiated fluoropolymer films: Influence of base material and irradiation temperature. *Radiat. Phys. Chem.* 79, 1067–1072. <https://doi.org/10.1016/j.radphyschem.2010.05.001>.
- Lee, H.-J., Choi, J., Han, J.Y., et al, 2013. Synthesis and characterization of poly(benzimidazolium) membranes for anion exchange membrane fuel cells. *Polym. Bull.* 70, 2619–2631. <https://doi.org/10.1007/s00289-013-0978-0>.
- Lee, N., Duong, D.T., Kim, D., 2018b. Cyclic ammonium grafted poly(arylene ether ketone) hydroxide ion exchange membranes for alkaline water electrolysis with high chemical stability and cell efficiency. *Electrochim. Acta* 271, 150–157. <https://doi.org/10.1016/j.electacta.2018.03.117>.
- Lee, J., Lee, H., Lim, B., 2018a. Chemical transformation of iron alkoxide nanosheets to FeOOH nanoparticles for highly active and stable oxygen evolution electrocatalysts. *J. Ind. Eng. Chem.* 58, 100–104. <https://doi.org/10.1016/j.jiec.2017.09.013>.
- Lee, J., Jung, H., Park, Y.S., et al, 2021a. Corrosion-engineered bimetallic oxide electrode as anode for high-efficiency anion exchange membrane water electrolyzer. *Chem. Eng. J.* 420, <https://doi.org/10.1016/j.cej.2020.127670> 127670.
- Lee, J., Jung, H., Park, Y.S., et al, 2021b. High-Efficiency Anion-Exchange Membrane Water Electrolyzer Enabled by Ternary Layered Double Hydroxide Anode. *Small* 17, 2100639. <https://doi.org/10.1002/smll.202100639>.
- Lee, W.-H., Kim, Y.S., Bae, C., 2015a. Robust Hydroxide Ion Conducting Poly(biphenyl alkylene)s for Alkaline Fuel Cell Membranes. *ACS Macro Lett.* 4, 814–818. <https://doi.org/10.1021/acsmacrolett.5b00375>.

- Lee, W.-H., Mohanty, A.D., Bae, C., 2015b. Fluorene-Based Hydroxide Ion Conducting Polymers for Chemically Stable Anion Exchange Membrane Fuel Cells. *ACS Macro Lett.* 4, 453–457. <https://doi.org/10.1021/acsmacrolett.5b00145>.
- Lee, W.-H., Park, E.J., Han, J., et al, 2017. Poly(terphenylene) Anion Exchange Membranes: The Effect of Backbone Structure on Morphology and Membrane Property. *ACS Macro Lett.* 6, 566–570. <https://doi.org/10.1021/acsmacrolett.7b00148>.
- Leng, Y., Chen, G., Mendoza, A.J., et al, 2012. Solid-State Water Electrolysis with an Alkaline Membrane. *J. Am. Chem. Soc.* 134, 9054–9057. <https://doi.org/10.1021/ja302439z>.
- Li, C., Baek, J.-B., 2021. The promise of hydrogen production from alkaline anion exchange membrane electrolyzers. *Nano Energy* 87. <https://doi.org/10.1016/j.nanoen.2021.106162> 106162.
- Li, B., Cao, H., Shao, J., et al, 2011a. Co₃O₄@graphene Composites as Anode Materials for High-Performance Lithium Ion Batteries. *Inorg. Chem.* 50, 1628–1632. <https://doi.org/10.1021/ic1023086>.
- Li, W., Fang, J., Lv, M., et al, 2011b. Novel anion exchange membranes based on polymerizable imidazolium salt for alkaline fuel cell applications. *J. Mater. Chem.* 21, 11340–11346. <https://doi.org/10.1039/C1JM11093D>.
- Li, N., Guiver, M.D., 2014. Ion Transport by Nanochannels in Ion-Containing Aromatic Copolymers. *Macromolecules* 47, 2175–2198. <https://doi.org/10.1021/ma402254h>.
- Li, N., Leng, Y., Hickner, M.A., et al, 2013. Highly Stable, Anion Conductive, Comb-Shaped Copolymers for Alkaline Fuel Cells. *J. Am. Chem. Soc.* 135, 10124–10133. <https://doi.org/10.1021/ja403671u>.
- Li, L., Lin, C.X., Wang, X.Q., et al, 2018a. Highly conductive anion exchange membranes with long flexible multication spacer. *J. Membr. Sci.* 553, 209–217. <https://doi.org/10.1016/j.memsci.2018.02.048>.
- Li, D., Park, E.J., Zhu, W., et al, 2020. Highly quaternized polystyrene ionomers for high performance anion exchange membrane water electrolyzers. *Nat. Energy* 5, 378–385. <https://doi.org/10.1038/s41560-020-0577-x>.
- Li, D., Motz, A.R., Bae, C., et al, 2021a. Durability of anion exchange membrane water electrolyzers. *Energ. Environ. Sci.* 14, 3393–3419. <https://doi.org/10.1039/D0EE04086J>.
- Li, Q., Peng, H., Wang, Y., et al, 2019a. The Comparability of Pt to Pt-Ru in Catalyzing the Hydrogen Oxidation Reaction for Alkaline Polymer Electrolyte Fuel Cells Operated at 80 °C. *Angew. Chem. Int. Ed.* 58, 1442–1446. <https://doi.org/10.1002/anie.201812662>.
- Li, X., Walsh, F.C., Pletcher, D., 2011c. Nickel based electrocatalysts for oxygen evolution in high current density, alkaline water electrolyzers. *PCCP* 13, 1162–1167. <https://doi.org/10.1039/C0CP00993H>.
- Li, L., Wang, Y., 2005. Quaternized polyethersulfone Cardo anion exchange membranes for direct methanol alkaline fuel cells. *J. Membr. Sci.* 262, 1–4. <https://doi.org/10.1016/j.memsci.2005.07.009>.
- Li, Y., Wang, H., Xie, L., et al, 2011d. MoS₂ Nanoparticles Grown on Graphene: An Advanced Catalyst for the Hydrogen Evolution Reaction. *J. Am. Chem. Soc.* 133, 7296–7299. <https://doi.org/10.1021/ja201269b>.
- Li, T., Wu, X., Chen, W., et al, 2018b. Poly(ether ether ketone) based imidazolium as anion exchange membranes for alkaline fuel cells. *Chin. J. Chem. Eng.* 26, 2130–2138. <https://doi.org/10.1016/j.cjche.2018.05.015>.
- Li, W., Xiong, D., Gao, X., et al, 2019b. The oxygen evolution reaction enabled by transition metal phosphide and chalcogenide pre-catalysts with dynamic changes. *Chem. Commun.* 55, 8744–8763. <https://doi.org/10.1039/C9CC02845E>.
- Li, N., Yan, T., Li, Z., et al, 2012a. Comb-shaped polymers to enhance hydroxide transport in anion exchange membranes. *Energ. Environ. Sci.* 5, 7888–7892. <https://doi.org/10.1039/C2EE22050D>.
- Li, Y., Zhang, L., Xiang, X., et al, 2014. Engineering of ZnCo-layered double hydroxide nanowalls toward high-efficiency electrochemical water oxidation. *J. Mater. Chem. A* 2. <https://doi.org/10.1039/c4ta01275e>.
- Li, Y., Yang, S., Li, H., et al, 2016. Electrodeposited ternary iron-cobalt-nickel catalyst on nickel foam for efficient water electrolysis at high current density. *Colloids Surf A Physicochem Eng Asp* 506, 694–702. <https://doi.org/10.1016/j.colsurfa.2016.07.047>.
- Li, Y., Yan, Y., He, Y., et al, 2022. Catalyst Electrodes with PtCu Nanowire Arrays In Situ Grown on Gas Diffusion Layers for Direct Formic Acid Fuel Cells. *ACS Appl Mater Interfaces.* 14, 11457–11464. <https://doi.org/10.1021/acscami.1c24010>.
- Li, N., Zhang, Q., Wang, C., et al, 2012b. Phenyltrimethylammonium Functionalized Polysulfone Anion Exchange Membranes. *Macromolecules* 45, 2411–2419. <https://doi.org/10.1021/ma202681z>.
- Li, P., Zhang, T., Mushtaq, M.A., et al, 2021b. Research Progress in Organic Synthesis by Means of Photoelectrocatalysis. *Chem Rec.* 21, 841–857. <https://doi.org/10.1002/tcr.202000186>.
- Li, Y.S., Zhao, T.S., Liang, Z.X., 2009. Performance of alkaline electrolyte-membrane-based direct ethanol fuel cells. *J. Power Sources* 187, 387–392. <https://doi.org/10.1016/j.jpowsour.2008.10.132>.
- Liang, Z.X., Zhao, T.S., Xu, J.B., et al, 2009. Mechanism study of the ethanol oxidation reaction on palladium in alkaline media. *Electrochim. Acta* 54, 2203–2208. <https://doi.org/10.1016/j.electacta.2008.10.034>.
- Liao, G.-M., Yang, C.-C., Hu, C.-C., et al, 2015. Novel quaternized polyvinyl alcohol/quaternized chitosan nano-composite as an effective hydroxide-conducting electrolyte. *J. Membr. Sci.* 485, 17–29. <https://doi.org/10.1016/j.memsci.2015.02.043>.
- Lim, A., Kim, H.-J., Henkensmeier, D., et al, 2019. A study on electrode fabrication and operation variables affecting the performance of anion exchange membrane water electrolysis. *J. Ind. Eng. Chem.* 76, 410–418. <https://doi.org/10.1016/j.jiec.2019.04.007>.
- Lin, B., Qiu, L., Lu, J., et al, 2010. Cross-Linked Alkaline Ionic Liquid-Based Polymer Electrolytes for Alkaline Fuel Cell Applications. *Chem. Mater.* 22, 6718–6725. <https://doi.org/10.1021/cm102957g>.
- Lin, B., Qiu, L., Qiu, B., et al, 2011. A Soluble and Conductive Polyfluorene Ionomer with Pendant Imidazolium Groups for Alkaline Fuel Cell Applications. *Macromolecules* 44, 9642–9649. <https://doi.org/10.1021/ma202159d>.
- Lin, B., Dong, H., Li, Y., et al, 2013a. Alkaline Stable C2-Substituted Imidazolium-Based Anion-Exchange Membranes. *Chem. Mater.* 25, 1858–1867. <https://doi.org/10.1021/cm400468u>.
- Lin, X., Liu, Y., Poynton, S.D., et al, 2013b. Cross-linked anion exchange membranes for alkaline fuel cells synthesized using a solvent free strategy. *J. Power Sources* 233, 259–268. <https://doi.org/10.1016/j.jpowsour.2013.01.059>.
- Lin, X., Varcoe, J.R., Poynton, S.D., et al, 2013c. Alkaline polymer electrolytes containing pendant dimethylimidazolium groups for alkaline membrane fuel cells. *J. Mater. Chem. A* 1, 7262–7269. <https://doi.org/10.1039/C3TA10308K>.
- Lin, C.X., Zhuo, Y.Z., Lai, A.N., et al, 2016. Side-chain-type anion exchange membranes bearing pendent imidazolium-functionalized poly(phenylene oxide) for fuel cells. *J. Membr. Sci.* 513, 206–216. <https://doi.org/10.1016/j.memsci.2016.04.054>.
- Lin, C.X., Zhuo, Y.Z., Hu, E.N., et al, 2017. Crosslinked side-chain-type anion exchange membranes with enhanced conductivity and dimensional stability. *J. Membr. Sci.* 539, 24–33. <https://doi.org/10.1016/j.memsci.2017.05.063>.
- Lindquist, G.A., Xu, Q., Oener, S.Z., et al, 2020. Membrane Electrolyzers for Impure-Water Splitting. *Joule* 4, 2549–2561. <https://doi.org/10.1016/j.joule.2020.09.020>.
- Liu, X., Gao, H., Chen, X., et al, 2016b. Synthesis of perfluorinated ionomers and their anion exchange membranes. *J. Membr. Sci.* 515, 268–276. <https://doi.org/10.1016/j.memsci.2016.05.062>.
- Liu, Z., Sajjad, S.D., Gao, Y., et al, 2017a. An Alkaline Water Electrolyzer with Sustainion™ Membranes: 1 A/cm² at 1.9V with

- Base Metal Catalysts. *ECS Trans.* 77, 71–73. <https://doi.org/10.1149/07709.0071ecst>.
- Liu, Z., Sajjad, S.D., Gao, Y., et al, 2017b. The effect of membrane on an alkaline water electrolyzer. *Int. J. Hydrog. Energy.* 42, 29661–29665. <https://doi.org/10.1016/j.ijhydene.2017.10.050>.
- Liu, L., Tong, C., He, Y., et al, 2015. Enhanced properties of quaternized graphenes reinforced polysulfone based composite anion exchange membranes for alkaline fuel cell. *J. Membr. Sci.* 487, 99–108. <https://doi.org/10.1016/j.memsci.2015.03.077>.
- Liu, M., Wang, Z., Mei, J., et al, 2016a. A facile functionalized routine for the synthesis of imidazolium-based anion-exchange membrane with excellent alkaline stability. *J. Membr. Sci.* 505, 138–147. <https://doi.org/10.1016/j.memsci.2016.01.036>.
- López-Fernández, E., Gil-Rostra, J., Espinós, J.P., et al, 2019. $\text{Cu}_x\text{Co}_{3-x}\text{O}_4$ ultra-thin film as efficient anodic catalysts for anion exchange membrane water electrolyzers. *J. Power Sources* 415, 136–144. <https://doi.org/10.1016/j.jpowsour.2019.01.056>.
- López-Fernández, E., Gil-Rostra, J., Escudero, C., et al, 2021. Active sites and optimization of mixed copper-cobalt oxide anodes for anion exchange membrane water electrolysis. *J. Power Sources* 485. <https://doi.org/10.1016/j.jpowsour.2020.229217>.
- Lu, S., Pan, J., Huang, A., et al, 2008. Alkaline polymer electrolyte fuel cells completely free from noble metal catalysts. *Proc. Natl. Acad. Sci.* 105, 20611–20614. <https://doi.org/10.1073/pnas.0810041106>.
- Lu, D., Li, D., Wen, L., et al, 2017. Effects of non-planar hydrophobic cyclohexylidene moiety on the structure and stability of poly(arylene ether sulfone)s based anion exchange membranes. *J. Membr. Sci.* 533, 210–219. <https://doi.org/10.1016/j.memsci.2017.03.011>.
- Lu, L.-N., Luo, Y.-L., Liu, H.-J., et al, 2022. Multivalent CoSx coupled with N-doped CNTs/Ni as an advanced oxygen electrocatalyst for zinc-air batteries. *Chem. Eng. J.* 427. <https://doi.org/10.1016/j.cej.2021.132041> 132041.
- Lu, X., Zhao, C., 2015. Electrodeposition of hierarchically structured three-dimensional nickel-iron electrodes for efficient oxygen evolution at high current densities. *Nat. Commun.* 6, 6616. <https://doi.org/10.1038/ncomms7616>.
- Luo, Y., Guo, J., Wang, C., et al, 2010. Quaternized poly(methyl methacrylate-co-butyl acrylate-co-vinylbenzyl chloride) membrane for alkaline fuel cells. *J. Power Sources* 195, 3765–3771. <https://doi.org/10.1016/j.jpowsour.2009.12.106>.
- Luo, Y., Guo, J., Liu, Y., et al, 2012. Copolymerization of methyl methacrylate and vinylbenzyl chloride towards alkaline anion exchange membrane for fuel cell applications. *J. Membr. Sci.* 423–424, 209–214. <https://doi.org/10.1016/j.memsci.2012.08.016>.
- Lv, B., Zeng, S., Yang, W., et al, 2019. In-situ embedding zeolitic imidazolate framework derived Co–N–C bifunctional catalysts in carbon nanotube networks for flexible Zn–air batteries. *Journal of Energy Chemistry.* 38, 170–176. <https://doi.org/10.1016/j.jechem.2019.04.005>.
- Mahmoud, A.M.A., Elsaghier, A.M.M., Otsuji, K., et al, 2017. High Hydroxide Ion Conductivity with Enhanced Alkaline Stability of Partially Fluorinated and Quaternized Aromatic Copolymers as Anion Exchange Membranes. *Macromolecules* 50, 4256–4266. <https://doi.org/10.1021/acs.macromol.7b00401>.
- Mamlouk, M., Horsfall, J.A., Williams, C., et al, 2012. Radiation grafted membranes for superior anion exchange polymer membrane fuel cells performance. *Int. J. Hydrog. Energy.* 37, 11912–11920. <https://doi.org/10.1016/j.ijhydene.2012.05.117>.
- Manabe, A., Kashiwase, M., Hashimoto, T., et al, 2013. Basic study of alkaline water electrolysis. *Electrochim. Acta* 100, 249–256. <https://doi.org/10.1016/j.electacta.2012.12.105>.
- Mandal, M., Huang, G., Hassan, N.U., et al, 2019. The Importance of Water Transport in High Conductivity and High-Power Alkaline Fuel Cells. *J. Electrochem. Soc.* 167. <https://doi.org/10.1149/2.0022005jes> 054501.
- Manjula, N., Balaji, R., Ramya, K., et al, 2020. Hydrogen production by electrochemical methanol reformation using alkaline anion exchange membrane based cell. *Int. J. Hydrog. Energy.* 45, 10304–10312. <https://doi.org/10.1016/j.ijhydene.2019.08.202>.
- Marceta Kaninski, M.P., Miulovic, S.M., Tasic, G.S., et al, 2011. A study on the Co–W activated Ni electrodes for the hydrogen production from alkaline water electrolysis – Energy saving. *Int. J. Hydrog. Energy.* 36, 5227–5235. <https://doi.org/10.1016/j.ijhydene.2011.02.046>.
- Marini, S., Salvi, P., Nelli, P., et al, 2012. Advanced alkaline water electrolysis. *Electrochim. Acta* 82, 384–391. <https://doi.org/10.1016/j.electacta.2012.05.011>.
- Marinkas, A., Strużyńska-Piron, I., Lee, Y., et al, 2018. Anion-conductive membranes based on 2-mesityl-benzimidazolium functionalised poly(2,6-dimethyl-1,4-phenylene oxide) and their use in alkaline water electrolysis. *Polymer* 145, 242–251. <https://doi.org/10.1016/j.polymer.2018.05.008>.
- Marino, M.G., Kreuer, K.D., 2015. Alkaline Stability of Quaternary Ammonium Cations for Alkaline Fuel Cell Membranes and Ionic Liquids. *ChemSusChem* 8, 513–523. <https://doi.org/10.1002/cssc.201403022>.
- Matsui, K., Tobita, E., Sugimoto, K., et al, 1986. Novel anion exchange membranes having fluorocarbon backbone: Preparation and stability. *J. Appl. Polym. Sci.* 32, 4137–4143. <https://doi.org/10.1002/app.1986.070320327>.
- Maurya, S., Noh, S., Matanovic, I., et al, 2018. Rational design of polyaromatic ionomers for alkaline membrane fuel cells with $> 1 \text{ W cm}^{-2}$ power density. *Energ. Environ. Sci.* 11, 3283–3291. <https://doi.org/10.1039/C8EE02192A>.
- Meek, K.M., Antunes, C.M., Strasser, D., et al, 2019. High-Throughput Anion Exchange Membrane Characterization at NREL. *ECS Trans.* 92, 723–731. <https://doi.org/10.1149/09208.0723ecst>.
- Merle, G., Wessling, M., Nijmeijer, K., 2011. Anion exchange membranes for alkaline fuel cells: A review. *J. Membr. Sci.* 377, 1–35. <https://doi.org/10.1016/j.memsci.2011.04.043>.
- Millet, P., Grigoriev, S., 2013. Chapter 2 - Water Electrolysis Technologies. In: Gandia, L.M., Arzamendi, G., Diéguez, P.M. (Eds.), *Renewable Hydrogen Technologies*. Elsevier, Amsterdam, pp. 19–41.
- Millet, P., Ngameni, R., Grigoriev, S.A., et al, 2010. PEM water electrolyzers: From electrocatalysis to stack development. *Int. J. Hydrog. Energy.* 35, 5043–5052. <https://doi.org/10.1016/j.ijhydene.2009.09.015>.
- Millet, P., Mbemba, N., Grigoriev, S.A., et al, 2011. Electrochemical performances of PEM water electrolysis cells and perspectives. *Int. J. Hydrog. Energy.* 36, 4134–4142. <https://doi.org/10.1016/j.ijhydene.2010.06.105>.
- Mohanty, A.D., Bae, C., 2014. Mechanistic analysis of ammonium cation stability for alkaline exchange membrane fuel cells. *J. Mater. Chem. A* 2, 17314–17320. <https://doi.org/10.1039/C4TA03300K>.
- Mohanty, A.D., Lee, Y.-B., Zhu, L., et al, 2014. Anion Exchange Fuel Cell Membranes Prepared from C–H Borylation and Suzuki Coupling Reactions. *Macromolecules* 47, 1973–1980. <https://doi.org/10.1021/ma500125t>.
- Mohanty, A.D., Ryu, C.Y., Kim, Y.S., et al, 2015. Stable Elastomeric Anion Exchange Membranes Based on Quaternary Ammonium-Tethered Polystyrene-*b*-poly(ethylene-co-butylene)-*b*-polystyrene Triblock Copolymers. *Macromolecules* 48, 7085–7095. <https://doi.org/10.1021/acs.macromol.5b01382>.
- Mustain, W.E., Chatenet, M., Page, M., et al, 2020. Durability challenges of anion exchange membrane fuel cells. *Energ. Environ. Sci.* 13, 2805–2838. <https://doi.org/10.1039/D0EE01133A>.
- Najam, T., Ahmad Shah, S.S., Ali, H., et al, 2020. A metal free electrocatalyst for high-performance zinc-air battery applications with good resistance towards poisoning species. *Carbon* 164, 12–18. <https://doi.org/10.1016/j.carbon.2020.03.036>.

- Nasef, M.M., 2014. Radiation-Grafted Membranes for Polymer Electrolyte Fuel Cells: Current Trends and Future Directions. *Chem. Rev.* 114, 12278–12329. <https://doi.org/10.1021/cr4005499>.
- Nasef, M.M., Hegazy, E.-S.-A., 2004. Preparation and applications of ion exchange membranes by radiation-induced graft copolymerization of polar monomers onto non-polar films. *Prog. Polym. Sci.* 29, 499–561. <https://doi.org/10.1016/j.progpolymsci.2004.01.003>.
- Nasef, M.M., Saidi, H., Dahlan, K.Z.M., 2003. Electron beam irradiation effects on ethylene-tetrafluoroethylene copolymer films. *Radiat. Phys. Chem.* 68, 875–883. [https://doi.org/10.1016/S0969-806X\(03\)00209-3](https://doi.org/10.1016/S0969-806X(03)00209-3).
- Nasef, M.M., Gürsel, S.A., Karabelli, D., et al, 2016. Radiation-grafted materials for energy conversion and energy storage applications. *Prog. Polym. Sci.* 63, 1–41. <https://doi.org/10.1016/j.progpolymsci.2016.05.002>.
- Noonan, K.J.T., Hugar, K.M., Kostalik, H.A., et al, 2012. Phosphonium-Functionalized Polyethylene: A New Class of Base-Stable Alkaline Anion Exchange Membranes. *J. Am. Chem. Soc.* 134, 18161–18164. <https://doi.org/10.1021/ja307466s>.
- Oh, J.H., Han, G.H., Kim, H., et al, 2021. Activity and stability of Ir-based gas diffusion electrode for proton exchange membrane water electrolyzer. *Chem. Eng. J.* 420,. <https://doi.org/10.1016/j.cej.2020.127696> 127696.
- Omasta, T.J., Wang, L., Peng, X., et al, 2018. Importance of balancing membrane and electrode water in anion exchange membrane fuel cells. *J. Power Sources* 375, 205–213. <https://doi.org/10.1016/j.jpowsour.2017.05.006>.
- Oshchepkov, A.G., Simonov, P.A., Cherstiouk, O.V., et al, 2015. On the Effect of Cu on the Activity of Carbon Supported Ni Nanoparticles for Hydrogen Electrode Reactions in Alkaline Medium. *Top. Catal.* 58, 1181–1192. <https://doi.org/10.1007/s11244-015-0487-5>.
- Pan, Z.F., An, L., Zhao, T.S., et al, 2018. Advances and challenges in alkaline anion exchange membrane fuel cells. *Prog. Energy Combust. Sci.* 66, 141–175. <https://doi.org/10.1016/j.pecs.2018.01.001>.
- Pan, J., Lu, S., Li, Y., et al, 2010. High-Performance Alkaline Polymer Electrolyte for Fuel Cell Applications. *Adv. Funct. Mater.* 20, 312–319. <https://doi.org/10.1002/adfm.200901314>.
- Pandiarajan, T., John Berchmans, L., Ravichandran, S., 2015. Fabrication of spinel ferrite based alkaline anion exchange membrane water electrolyzers for hydrogen production. *RSC Adv.* 5, 34100–34108. <https://doi.org/10.1039/c5ra01123j>.
- Paoli, E.A., Masini, F., Frydendal, R., et al, 2015. Oxygen evolution on well-characterized mass-selected Ru and RuO₂ nanoparticles. *Chem. Sci.* 6, 190–196. <https://doi.org/10.1039/C4SC02685C>.
- Paraknowitsch, J.P., Thomas, A., 2013. Doping carbons beyond nitrogen: an overview of advanced heteroatom doped carbons with boron, sulphur and phosphorus for energy applications. *Energ. Environ. Sci.* 6, 2839–2855. <https://doi.org/10.1039/C3EE41444B>.
- Park, E.J., Capuano, C.B., Ayers, K.E., et al, 2018. Chemically durable polymer electrolytes for solid-state alkaline water electrolysis. *J. Power Sources* 375, 367–372. <https://doi.org/10.1016/j.jpowsour.2017.07.090>.
- Park, H., Lee, Y., Noh, B. et al., 2008. Design of an event system adopting ontology-based event model for ubiquitous environment. Proceedings of the 5th international conference on Soft computing as transdisciplinary science and technology. Cergy-Pontoise, France, Association for Computing Machinery 620–626.
- Park, Y.S., Lee, J.H., Jang, M.J., et al, 2020a. Co₃S₄ nanosheets on Ni foam via electrodeposition with sulfurization as highly active electrocatalysts for anion exchange membrane electrolyzer. *Int. J. Hydrog. Energy.* 45, 36–45. <https://doi.org/10.1016/j.ijhydene.2019.10.169>.
- Park, Y.S., Jeong, J., Noh, Y., et al, 2021. Commercial anion exchange membrane water electrolyzer stack through non-precious metal electrocatalysts. *Appl Catal B* 292,. <https://doi.org/10.1016/j.apcatb.2021.120170> 120170.
- Park, J.E., Kang, S.Y., Oh, S.-H., et al, 2019b. High-performance anion-exchange membrane water electrolysis. *Electrochim. Acta* 295, 99–106. <https://doi.org/10.1016/j.electacta.2018.10.143>.
- Park, E.J., Maurya, S., Lee, A.S., et al, 2019a. How does a small structural change of anode ionomer make a big difference in alkaline membrane fuel cell performance? *J. Mater. Chem. A* 7, 25040–25046. <https://doi.org/10.1039/C9TA10157H>.
- Park, J.-S., Park, S.-H., Yim, S.-D., et al, 2008b. Performance of solid alkaline fuel cells employing anion-exchange membranes. *J. Power Sources* 178, 620–626. <https://doi.org/10.1016/j.jpowsour.2007.08.043>.
- Park, Y.S., Yang, J., Lee, J., et al, 2020b. Superior performance of anion exchange membrane water electrolyzer: Ensemble of producing oxygen vacancies and controlling mass transfer resistance. *Appl Catal B* 278,. <https://doi.org/10.1016/j.apcatb.2020.119276> 119276.
- Parrondo, J., Arges, C.G., Niedzwiecki, M., et al, 2014. Degradation of anion exchange membranes used for hydrogen production by ultrapure water electrolysis. *RSC Adv.* 4. <https://doi.org/10.1039/c3ra46630b>.
- Pavel, C.C., Cecconi, F., Emiliani, C., et al, 2014. Highly Efficient Platinum Group Metal Free Based Membrane-Electrode Assembly for Anion Exchange Membrane Water Electrolysis. *Angew. Chem. Int. Ed.* 53, 1378–1381. <https://doi.org/10.1002/anie.201308099>.
- Peng, X., Kulkarni, D., Huang, Y., et al, 2020b. Using operando techniques to understand and design high performance and stable alkaline membrane fuel cells. *Nat. Commun.* 11, 3561. <https://doi.org/10.1038/s41467-020-17370-7>.
- Peng, H., Li, Q., Hu, M., et al, 2018. Alkaline polymer electrolyte fuel cells stably working at 80 °C. *J. Power Sources* 390, 165–167. <https://doi.org/10.1016/j.jpowsour.2018.04.047>.
- Peng, W., Luo, M., Xu, X., et al, 2020a. Spontaneous Atomic Ruthenium Doping in Mo₂CTx MXene Defects Enhances Electrocatalytic Activity for the Nitrogen Reduction Reaction. *Adv. Energy Mater.* 10, 2001364. <https://doi.org/10.1002/aenm.202001364>.
- Pérez-Alonso, F.J., Adán, C., Rojas, S., et al, 2015. Ni–Co electrodes prepared by electroless-plating deposition. A study of their electrocatalytic activity for the hydrogen and oxygen evolution reactions. *Int. J. Hydrog. Energy.* 40, 51–61. <https://doi.org/10.1016/j.ijhydene.2014.11.015>.
- Pham, T.H., Olsson, J.S., Jannasch, P., 2017. N-Spirocyclic Quaternary Ammonium Ionenes for Anion-Exchange Membranes. *J. Am. Chem. Soc.* 139, 2888–2891. <https://doi.org/10.1021/jacs.6b12944>.
- Pham, T.H., Olsson, J.S., Jannasch, P., 2018. Poly(arylene alkylene)s with pendant N-spirocyclic quaternary ammonium cations for anion exchange membranes. *J. Mater. Chem. A* 6, 16537–16547. <https://doi.org/10.1039/C8TA04699A>.
- Piana, M., Catanorchi, S., Gasteiger, H.A., 2008. Kinetics of Non-Platinum Group Metal Catalysts for the Oxygen Reduction Reaction in Alkaline Medium. *ECS Trans.* 16, 2045–2055. <https://doi.org/10.1149/1.2982044>.
- Piana, M., Boccia, M., Filpi, A., et al, 2010. H₂/air alkaline membrane fuel cell performance and durability, using novel ionomer and non-platinum group metal cathode catalyst. *J. Power Sources* 195, 5875–5881. <https://doi.org/10.1016/j.jpowsour.2009.12.085>.
- Pierozynski, B., Mikołajczyk, T., Kowalski, I.M., 2014. Hydrogen evolution at catalytically-modified nickel foam in alkaline solution. *J. Power Sources* 271, 231–238. <https://doi.org/10.1016/j.jpowsour.2014.07.188>.
- Pletcher, D., Li, X., 2011. Prospects for alkaline zero gap water electrolyzers for hydrogen production. *Int. J. Hydrog. Energy.* 36, 15089–15104. <https://doi.org/10.1016/j.ijhydene.2011.08.080>.
- Pletcher, D., Li, X., Wang, S., 2012. A comparison of cathodes for zero gap alkaline water electrolyzers for hydrogen production. *Int. J. Hydrog. Energy.* 37, 7429–7435. <https://doi.org/10.1016/j.ijhydene.2012.02.013>.

- Poynton, S.D., Kizewski, J.P., Slade, R.C.T., et al, 2010. Novel electrolyte membranes and non-Pt catalysts for low temperature fuel cells. *Solid State Ion.* 181, 219–222. <https://doi.org/10.1016/j.ssi.2009.01.019>.
- Poynton, S.D., Slade, R.C.T., Omasta, T.J., et al, 2014. Preparation of radiation-grafted powders for use as anion exchange ionomers in alkaline polymer electrolyte fuel cells. *J. Mater. Chem. A* 2, 5124–5130. <https://doi.org/10.1039/C4TA00558A>.
- Praats, R., Käärik, M., Kikas, A., et al, 2020. Electrocatalytic oxygen reduction reaction on iron phthalocyanine-modified carbide-derived carbon/carbon nanotube composite electrocatalysts. *Electrochim. Acta* 334, <https://doi.org/10.1016/j.electacta.2019.135575>.
- Price, S.C., Ren, X., Jackson, A.C., et al, 2013. Bicontinuous Alkaline Fuel Cell Membranes from Strongly Self-Segregating Block Copolymers. *Macromolecules* 46, 7332–7340. <https://doi.org/10.1021/ma400995n>.
- Pushkareva, I.V., Pushkarev, A.S., Grigoriev, S.A., et al, 2020. Comparative study of anion exchange membranes for low-cost water electrolysis. *Int. J. Hydrog. Energy.* 45, 26070–26079. <https://doi.org/10.1016/j.ijhydene.2019.11.011>.
- Qiu, B., Lin, B., Qiu, L., et al, 2012. Alkaline imidazolium- and quaternary ammonium-functionalized anion exchange membranes for alkaline fuel cell applications. *J. Mater. Chem.* 22, 1040–1045. <https://doi.org/10.1039/C1JM14331J>.
- Ramaswamy, N., Mukerjee, S., 2019. Alkaline Anion-Exchange Membrane Fuel Cells: Challenges in Electrocatalysis and Interfacial Charge Transfer. *Chem. Rev.* 119, 11945–11979. <https://doi.org/10.1021/acs.chemrev.9b00157>.
- Ran, J., Wu, L., Lin, X., et al, 2012a. Synthesis of soluble copolymers bearing ionic graft for alkaline anion exchange membrane. *RSC Adv.* 2, 4250–4257. <https://doi.org/10.1039/C2RA20336G>.
- Ran, J., Wu, L., Varcoe, J.R., et al, 2012b. Development of imidazolium-type alkaline anion exchange membranes for fuel cell application. *J. Membr. Sci.* 415–416, 242–249. <https://doi.org/10.1016/j.memsci.2012.05.006>.
- Ran, J., Wu, L., Xu, T., 2013. Enhancement of hydroxide conduction by self-assembly in anion conductive comb-shaped copolymers. *Polym. Chem.* 4, 4612–4620. <https://doi.org/10.1039/C3PY00421J>.
- Rao, A.H.N., Kim, H.-J., Nam, S., et al, 2013. Cardo poly(arylene ether sulfone) block copolymers with pendant imidazolium side chains as novel anion exchange membranes for direct methanol alkaline fuel cell. *Polymer* 54, 6918–6928. <https://doi.org/10.1016/j.polymer.2013.10.052>.
- Rashid, M., Al Mesfer, M.K., Naseem, H., et al, 2015. Hydrogen production by water electrolysis: a review of alkaline water electrolysis, PEM water electrolysis and high temperature water electrolysis. *International Journal of Engineering and Advanced Technology.*
- Ren, X., Price, S.C., Jackson, A.C., et al, 2014. Highly Conductive Anion Exchange Membrane for High Power Density Fuel-Cell Performance. *ACS Appl. Mater. Interfaces* 6, 13330–13333. <https://doi.org/10.1021/am503870g>.
- Roche, I., Chainet, E., Chatenet, M., et al, 2007. Carbon-Supported Manganese Oxide Nanoparticles as Electrocatalysts for the Oxygen Reduction Reaction (ORR) in Alkaline Medium: Physical Characterizations and ORR Mechanism. *J. Phys. Chem. C* 111, 1434–1443. <https://doi.org/10.1021/jp0647986>.
- Rossmesl, J., Qu, Z.W., Zhu, H., et al, 2007. Electrolysis of water on oxide surfaces. *J. Electroanal. Chem.* 607, 83–89. <https://doi.org/10.1016/j.jelechem.2006.11.008>.
- Sajjad, S.D., Liu, D., Wei, Z., et al, 2015. Guanidinium based blend anion exchange membranes for direct methanol alkaline fuel cells (DMAFCs). *J. Power Sources* 300, 95–103. <https://doi.org/10.1016/j.jpowsour.2015.08.002>.
- Sanchez, J., Hellstern, T.R., King, L.A., et al, 2019. Surface Engineering of 3D Gas Diffusion Electrodes for High-Performance H₂ Production with Nonprecious Metal Catalysts. *Adv. Energy Mater.* 9, 1901824. <https://doi.org/10.1002/aenm.201901824>.
- Schauer, J., Hnát, J., Brožová, L., et al, 2015. Anionic catalyst binders based on trimethylamine-quaternized poly(2,6-dimethyl-1,4-phenylene oxide) for alkaline electrolyzers. *J. Membr. Sci.* 473, 267–273. <https://doi.org/10.1016/j.memsci.2014.09.011>.
- Schmidt, O., Gambhir, A., Staffell, I., et al, 2017. Future cost and performance of water electrolysis: An expert elicitation study. *Int. J. Hydrog. Energy.* 42, 30470–30492. <https://doi.org/10.1016/j.ijhydene.2017.10.045>.
- Schniepp, H.C., Li, J.-L., McAllister, M.J., et al, 2006. Functionalized Single Graphene Sheets Derived from Splitting Graphite Oxide. *J. Phys. Chem. B* 110, 8535–8539. <https://doi.org/10.1021/jp060936f>.
- Seetharaman, S., Balaji, R., Ramya, K., et al, 2013. Graphene oxide modified non-noble metal electrode for alkaline anion exchange membrane water electrolyzers. *Int. J. Hydrog. Energy.* 38, 14934–14942. <https://doi.org/10.1016/j.ijhydene.2013.09.033>.
- Senfite, F.E., Grant, J.R., Senfite, F.P., 2010. Low-voltage DC/AC electrolysis of water using porous graphite electrodes. *Electrochim. Acta* 55, 5148–5153. <https://doi.org/10.1016/j.electacta.2010.04.022>.
- Shen, K., Zhang, Z., Zhang, H., et al, 2015. Poly(arylene ether ketone) carrying hyperquaternized pendants: Preparation, stability and conductivity. *J. Power Sources* 287, 439–447. <https://doi.org/10.1016/j.jpowsour.2015.04.017>.
- Sherazi, T.A., Zahoor, S., Raza, R., et al, 2015. Guanidine functionalized radiation induced grafted anion-exchange membranes for solid alkaline fuel cells. *Int. J. Hydrog. Energy.* 40, 786–796. <https://doi.org/10.1016/j.ijhydene.2014.08.086>.
- Shin, M.-S., Lim, S., Park, J.-H., et al, 2020. Thermally crosslinked and quaternized polybenzimidazole ionomer binders for solid alkaline fuel cells. *Int. J. Hydrog. Energy.* 45, 11773–11783. <https://doi.org/10.1016/j.ijhydene.2020.02.081>.
- Shiva Kumar, S., Himabindu, V., 2019. Hydrogen production by PEM water electrolysis – A review. *Materials Science for Energy Technologies.* 2, 442–454. <https://doi.org/10.1016/j.mset.2019.03.002>.
- Solmaz, R., Döner, A., Kardaş, G., 2009. The stability of hydrogen evolution activity and corrosion behavior of NiCu coatings with long-term electrolysis in alkaline solution. *Int. J. Hydrog. Energy.* 34, 2089–2094. <https://doi.org/10.1016/j.ijhydene.2009.01.007>.
- Song, Y., Liu, C., Zhao, J., et al, 2016. Imidazolium-functionalized anion exchange polymer containing fluorine group for fuel cell application. *Int. J. Hydrog. Energy.* 41, 10446–10457. <https://doi.org/10.1016/j.ijhydene.2016.01.177>.
- Spendelov, J.S., Goodpaster, J.D., Kenis, P.J.A., et al, 2006. Mechanism of CO Oxidation on Pt(111) in Alkaline Media. *J. Phys. Chem. B* 110, 9545–9555. <https://doi.org/10.1021/jp060100c>.
- Sproll, V., Nagy, G., Gasser, U., et al, 2016. Radiation Grafted Ion-Conducting Membranes: The Influence of Variations in Base Film Nanostructure. *Macromolecules* 49, 4253–4264. <https://doi.org/10.1021/acs.macromol.6b00180>.
- Steinfeld, A., 2005. Solar thermochemical production of hydrogen—a review. *Sol. Energy* 78, 603–615. <https://doi.org/10.1016/j.solener.2003.12.012>.
- Strasser, D.J., Graziano, B.J., Knauss, D.M., 2017. Base stable poly(diallylpiperidinium hydroxide) multiblock copolymers for anion exchange membranes. *J. Mater. Chem. A* 5, 9627–9640. <https://doi.org/10.1039/C7TA00905D>.
- Sun, L., Guo, J., Zhou, J., et al, 2012. Novel nanostructured high-performance anion exchange ionomers for anion exchange membrane fuel cells. *J. Power Sources* 202, 70–77. <https://doi.org/10.1016/j.jpowsour.2011.11.023>.
- Tang, D., Pan, J., Lu, S., et al, 2010. Alkaline polymer electrolyte fuel cells: Principle, challenges, and recent progress. *Sci. China Chem.* 53, 357–364. <https://doi.org/10.1007/s11426-010-0080-5>.

- Tang, H., Peikang, S., Jiang, S.P., et al, 2007. A degradation study of Nafion proton exchange membrane of PEM fuel cells. *J. Power Sources* 170, 85–92. <https://doi.org/10.1016/j.jpowsour.2007.03.061>.
- Tang, X., Xiao, L., Yang, C., et al, 2014. Noble fabrication of Ni–Mo cathode for alkaline water electrolysis and alkaline polymer electrolyte water electrolysis. *Int. J. Hydrog. Energy*. 39, 3055–3060. <https://doi.org/10.1016/j.ijhydene.2013.12.053>.
- Tasić, G.S., Lačnjevac, U., Tasić, M.M., et al, 2013. Influence of electrodeposition parameters of Ni–W on Ni cathode for alkaline water electrolyser. *Int. J. Hydrog. Energy*. 38, 4291–4297. <https://doi.org/10.1016/j.ijhydene.2013.01.193>.
- Tham, D.D., Kim, D., 2019. C2 and N3 substituted imidazolium functionalized poly(arylene ether ketone) anion exchange membrane for water electrolysis with improved chemical stability. *J. Membr. Sci.* 581, 139–149. <https://doi.org/10.1016/j.memsci.2019.03.060>.
- Thangavel, P., Ha, M., Kumaraguru, S., et al, 2020. Graphene-nanoplatelets-supported NiFe-MOF: high-efficiency and ultra-stable oxygen electrodes for sustained alkaline anion exchange membrane water electrolysis. *Energ. Environ. Sci.* 13, 3447–3458. <https://doi.org/10.1039/D0EE00877J>.
- Thomas, J., Francis, B., Thomas, S., et al, 2021. Dependable polysulfone based anion exchange membranes incorporating triazatriangulenium cations. *Solid State Ion.* 370, <https://doi.org/10.1016/j.ssi.2021.115731> 115731.
- Thomas, O.D., Soo, K.J.W.Y., Peckham, T.J., et al, 2011. Anion conducting poly(dialkyl benzimidazolium) salts. *Polym. Chem.* 2, 1641–1643. <https://doi.org/10.1039/C1PY00142F>.
- Truong, V.M., Wang, C.-L., Yang, M., et al, 2018. Effect of tunable hydrophobic level in the gas diffusion substrate and microporous layer on anion exchange membrane fuel cells. *J. Power Sources* 402, 301–310. <https://doi.org/10.1016/j.jpowsour.2018.09.053>.
- Tuan, C.M., Kim, D., 2016. Anion-exchange membranes based on poly(arylene ether ketone) with pendant quaternary ammonium groups for alkaline fuel cell application. *J. Membr. Sci.* 511, 143–150. <https://doi.org/10.1016/j.memsci.2016.03.059>.
- Tuckerman, M.E., Marx, D., Parrinello, M., 2002. The nature and transport mechanism of hydrated hydroxide ions in aqueous solution. *Nature* 417, 925–929. <https://doi.org/10.1038/nature00797>.
- Tufa, R.A., Rugiero, E., Chanda, D., et al, 2016. Salinity gradient power-reverse electro dialysis and alkaline polymer electrolyte water electrolysis for hydrogen production. *J. Membr. Sci.* 514, 155–164. <https://doi.org/10.1016/j.memsci.2016.04.067>.
- Ul Hassan, N., Mandal, M., Huang, G., et al, 2020. Achieving High-Performance and 2000 h Stability in Anion Exchange Membrane Fuel Cells by Manipulating Ionomer Properties and Electrode Optimization. *Adv. Energy Mater.* 10, 2001986. <https://doi.org/10.1002/aenm.202001986>.
- Valdes, T.I., Ciridon, W., Ratner, B.D., et al, 2008. Surface modification of a perfluorinated ionomer using a glow discharge deposition method to control protein adsorption. *Biomaterials* 29, 1356–1366. <https://doi.org/10.1016/j.biomaterials.2007.11.035>.
- Varcoe, J.R., Slade, R.C.T., Wright, G.L., et al, 2006. Steady-State dc and Impedance Investigations of H₂/O₂ Alkaline Membrane Fuel Cells with Commercial Pt/C, Ag/C, and Au/C Cathodes. *J. Phys. Chem. B* 110, 21041–21049. <https://doi.org/10.1021/jp064898b>.
- Varcoe, J.R., Atanassov, P., Dekel, D.R., et al, 2014. Anion-exchange membranes in electrochemical energy systems. *Energ. Environ. Sci.* 7, 3135–3191. <https://doi.org/10.1039/C4EE01303D>.
- Vincent, I., 2018. Hydrogen Production by water Electrolysis with an Ultrathin Anion-exchange membrane (AEM). *Int. J. Electrochem. Sci.*
- Vincent, I., Bessarabov, D., 2018. Low cost hydrogen production by anion exchange membrane electrolysis: A review. *Renew. Sustain. Energy Rev.* 81, 1690–1704. <https://doi.org/10.1016/j.rser.2017.05.258>.
- Vincent, I., Kruger, A., Bessarabov, D., 2017. Development of efficient membrane electrode assembly for low cost hydrogen production by anion exchange membrane electrolysis. *Int. J. Hydrog. Energy*. 42, 10752–10761. <https://doi.org/10.1016/j.ijhydene.2017.03.069>.
- Vincent, I., Lee, E.-C., Kim, H.-M., 2021. Comprehensive impedance investigation of low-cost anion exchange membrane electrolysis for large-scale hydrogen production. *Sci. Rep.* 11, 293. <https://doi.org/10.1038/s41598-020-80683-6>.
- Wan, L., Xu, Z., Wang, P., et al, 2022. Dual regulation both intrinsic activity and mass transport for self-supported electrodes using in anion exchange membrane water electrolysis. *Chem. Eng. J.* 431, <https://doi.org/10.1016/j.cej.2021.133942> 133942.
- Wang, W.-T., Batoool, N., Zhang, T.-H., et al, 2021c. When MOFs meet MXenes: superior ORR performance in both alkaline and acidic solutions. *J. Mater. Chem. A* 9, 3952–3960. <https://doi.org/10.1039/D0TA10811A>.
- Wang, L., Bellini, M., Miller, H.A., et al, 2018b. A high conductivity ultrathin anion-exchange membrane with 500+ h alkali stability for use in alkaline membrane fuel cells that can achieve 2 W cm⁻² at 80 °C. *J. Mater. Chem. A* 6, 15404–15412. <https://doi.org/10.1039/C8TA04783A>.
- Wang, J., Chen, H., Ma, Y., et al, 2020. Grafting high content of imidazolium polymer brushes on graphene oxide for nanocomposite membranes with enhanced anion transport. *React. Funct. Polym.* 146, <https://doi.org/10.1016/j.reactfunctpolym.2019.104447> 104447.
- Wang, H., Du, X., Zhang, H., et al, 2021b. Synthesis and characterization of long-side-chain type quaternary ammonium-functionalized poly(ether ether ketone) anion exchange membranes. *Int. J. Hydrog. Energy*. 46, 8156–8166. <https://doi.org/10.1016/j.ijhydene.2020.11.281>.
- Wang, J., Gu, S., Kaspar, R.B., et al, 2013. Stabilizing the Imidazolium Cation in Hydroxide-Exchange Membranes for Fuel Cells. *ChemSusChem* 6, 2079–2082. <https://doi.org/10.1002/cssc.201300285>.
- Wang, W., Jia, Q., Mukerjee, S., et al, 2019e. Recent Insights into the Oxygen-Reduction Electrocatalysis of Fe/N/C Materials. *ACS Catal.* 9, 10126–10141. <https://doi.org/10.1021/acscatal.9b02583>.
- Wang, J., Li, S., Zhang, S., 2010. Novel Hydroxide-Conducting Polyelectrolyte Composed of an Poly(arylene ether sulfone) Containing Pendant Quaternary Guanidinium Groups for Alkaline Fuel Cell Applications. *Macromolecules* 43, 3890–3896. <https://doi.org/10.1021/ma100260a>.
- Wang, C., Liao, J., Li, J., et al, 2021a. Alkaline enrichment via electro dialysis with alkaline stable side-chain-type polysulfone-based anion exchange membranes. *Sep. Purif. Technol.* 275, <https://doi.org/10.1016/j.seppur.2021.119075> 119075.
- Wang, A.-Q., Lin, Y.-L., Xu, B., et al, 2017a. Kinetics and modeling of iodoform degradation during UV/chlorine advanced oxidation process. *Chem. Eng. J.* 323, 312–319. <https://doi.org/10.1016/j.cej.2017.04.061>.
- Wang, X.Q., Lin, C.X., Zhang, Q.G., et al, 2017d. Anion exchange membranes from hydroxyl-bearing poly(ether sulfone)s with flexible spacers via ring-opening grafting for fuel cells. *Int. J. Hydrog. Energy*. 42, 19044–19055. <https://doi.org/10.1016/j.ijhydene.2017.06.186>.
- Wang, L., Magliocca, E., Cunningham, E.L., et al, 2017c. An optimised synthesis of high performance radiation-grafted anion-exchange membranes. *Green Chem.* 19, 831–843. <https://doi.org/10.1039/C6GC02526A>.
- Wang, L., Peng, X., Mustain, W.E., et al, 2019b. Radiation-grafted anion-exchange membranes: the switch from low- to high-density polyethylene leads to remarkably enhanced fuel cell performance. *Energ. Environ. Sci.* 12, 1575–1579. <https://doi.org/10.1039/C9EE00331B>.
- Wang, L., Saveleva, V.A., Eslamibidgoli, M.J., et al, 2022. Deciphering the Exceptional Performance of NiFe Hydroxide for the

- Oxygen Evolution Reaction in an Anion Exchange Membrane Electrolyzer. *ACS Applied Energy Materials*. 5, 2221–2230. <https://doi.org/10.1021/acsaem.1c03761>.
- Wang, C., Shen, B., Xu, C., et al, 2015. Side-chain-type poly(arylene ether sulfone)s containing multiple quaternary ammonium groups as anion exchange membranes. *J. Membr. Sci.* 492, 281–288. <https://doi.org/10.1016/j.memsci.2015.05.060>.
- Wang, T., Shi, L., Wang, J., et al, 2019d. High-Performance Hydroxide Exchange Membrane Fuel Cells through Optimization of Relative Humidity, Backpressure and Catalyst Selection. *J. Electrochem. Soc.* 166, F3305–F3310. <https://doi.org/10.1149/2.0361907jes>.
- Wang, B., Sun, W., Bu, F., et al, 2016. Comparison of alkaline stability of benzyltrimethylammonium, benzylmethylimidazolium and benzyldimethylimidazolium functionalized poly(arylene ether ketone) anion exchange membranes. *Int. J. Hydrog. Energy*. 41, 3102–3112. <https://doi.org/10.1016/j.ijhydene.2015.12.123>.
- Wang, L., Weissbach, T., Reissner, R., et al, 2019c. High Performance Anion Exchange Membrane Electrolysis Using Plasma-Sprayed, Non-Precious-Metal Electrodes. *ACS Applied Energy Materials*. 2, 7903–7912. <https://doi.org/10.1021/acsaem.9b01392>.
- Wang, G., Weng, Y., Chu, D., et al, 2009a. Preparation of alkaline anion exchange membranes based on functional poly(ether-imide) polymers for potential fuel cell applications. *J. Membr. Sci.* 326, 4–8. <https://doi.org/10.1016/j.memsci.2008.09.037>.
- Wang, K., Xia, M., Xiao, T., et al, 2017b. Metallurgically prepared NiCu alloys as cathode materials for hydrogen evolution reaction. *Mater. Chem. Phys.* 186, 61–66. <https://doi.org/10.1016/j.matchemphys.2016.10.029>.
- Wang, J., Zhao, Z., Gong, F., et al, 2009b. Synthesis of Soluble Poly(arylene ether sulfone) Ionomers with Pendant Quaternary Ammonium Groups for Anion Exchange Membranes. *Macromolecules* 42, 8711–8717. <https://doi.org/10.1021/ma901606z>.
- Wang, J., Zhang, Z.-G., Ding, Z.-Y., et al, 2018a. IDH1 mutation correlates with a beneficial prognosis and suppresses tumor growth in IHCC. *J. Surg. Res.* 231, 116–125. <https://doi.org/10.1016/j.jss.2018.04.056>.
- Wang, J., Zhao, Y., Setzler, B.P., et al, 2019a. Poly(aryl piperidinium) membranes and ionomers for hydroxide exchange membrane fuel cells. *Nat. Energy* 4, 392–398. <https://doi.org/10.1038/s41560-019-0372-8>.
- Wei, J., Hu, Y., Liang, Y., et al, 2017. Graphene oxide/core-shell structured metal-organic framework nano-sandwiches and their derived cobalt/N-doped carbon nanosheets for oxygen reduction reactions. *J. Mater. Chem. A* 5, 10182–10189. <https://doi.org/10.1039/C7TA00276A>.
- Wei, Z.D., Ji, M.B., Chen, S.G., et al, 2007. Water electrolysis on carbon electrodes enhanced by surfactant. *Electrochim. Acta* 52, 3323–3329. <https://doi.org/10.1016/j.electacta.2006.10.011>.
- Weiber, E.A., Jannasch, P., 2015. Polysulfones with highly localized imidazolium groups for anion exchange membranes. *J. Membr. Sci.* 481, 164–171. <https://doi.org/10.1016/j.memsci.2015.02.002>.
- Wendt, H., Hofmann, H., 1989. Ceramic diaphragms for advanced alkaline water electrolysis. *J. Appl. Electrochem.* 19, 605–610. <https://doi.org/10.1007/BF01022121>.
- Wright, A.G., Fan, J., Britton, B., et al, 2016. Hexamethyl-*p*-terphenyl poly(benzimidazolium): a universal hydroxide-conducting polymer for energy conversion devices. *Energy. Environ. Sci.* 9, 2130–2142. <https://doi.org/10.1039/C6EE00656F>.
- Wu, X., Scott, K., 2011b. $Cu_xCo_3-xO_4$ ($0 \leq x < 1$) nanoparticles for oxygen evolution in high performance alkaline exchange membrane water electrolyzers. *J. Mater. Chem.* 21. <https://doi.org/10.1039/c1jm11312g>.
- Wu, X., Scott, K., 2012a. A non-precious metal bifunctional oxygen electrode for alkaline anion exchange membrane cells. *J. Power Sources* 206, 14–19. <https://doi.org/10.1016/j.jpowsour.2011.12.052>.
- Wu, X., Scott, K., 2012b. A polymethacrylate-based quaternary ammonium OH⁻ ionomer binder for non-precious metal alkaline anion exchange membrane water electrolyzers. *J. Power Sources* 214, 124–129. <https://doi.org/10.1016/j.jpowsour.2012.03.069>.
- Wu, X., Scott, K., 2013. A Li-doped Co_3O_4 oxygen evolution catalyst for non-precious metal alkaline anion exchange membrane water electrolyzers. *Int. J. Hydrog. Energy*. 38, 3123–3129. <https://doi.org/10.1016/j.ijhydene.2012.12.087>.
- Wu, X., Chen, W., Yan, X., et al, 2014. Enhancement of hydroxide conductivity by the di-quaternization strategy for poly(ether ether ketone) based anion exchange membranes. *J. Mater. Chem. A* 2, 12222–12231. <https://doi.org/10.1039/C4TA01397B>.
- Wu, M., Fan, L., Ma, R., et al, 2016. NiO and CrO₃ double surface-decorate Ni nanofibers for hydrogen evolution reduction. *Mater. Lett.* 182, 15–18. <https://doi.org/10.1016/j.matlet.2016.06.060>.
- Wu, X.-T., Peng, L.-J., Xiao, K., et al, 2021. Rational design and synthesis of hollow Fe-N/C electrocatalysts for enhanced oxygen reduction reaction. *Chem. Commun.* 57, 5258–5261. <https://doi.org/10.1039/D1CC00460C>.
- Wu, X., Scott, K., 2011a. $Cu_xCo_3-xO_4$ ($0 \leq x < 1$) nanoparticles for oxygen evolution in high performance alkaline exchange membrane water electrolyzers. *J. Mater. Chem.* 21, 12344–12351. <https://doi.org/10.1039/C1JM11312G>.
- Wu, L., Zhou, G., Liu, X., et al, 2011. Environmentally friendly synthesis of alkaline anion exchange membrane for fuel cells via a solvent-free strategy. *J. Membr. Sci.* 371, 155–162. <https://doi.org/10.1016/j.memsci.2011.01.036>.
- Xia, Z., Yuan, S., Jiang, G., et al, 2012. Polybenzimidazoles with pendant quaternary ammonium groups as potential anion exchange membranes for fuel cells. *J. Membr. Sci.* 390–391, 152–159. <https://doi.org/10.1016/j.memsci.2011.11.032>.
- Xiao, Y., Guo, B., Zhang, J., et al, 2020. A bimetallic MOF@-graphene oxide composite as an efficient bifunctional oxygen electrocatalyst for rechargeable Zn-air batteries. *Dalton Trans.* 49, 5730–5735. <https://doi.org/10.1039/D0DT00976H>.
- Xiao, Z., Wang, Y., Huang, Y.-C., et al, 2017. Filling the oxygen vacancies in Co_3O_4 with phosphorus: an ultra-efficient electrocatalyst for overall water splitting. *Energy. Environ. Sci.* 10, 2563–2569. <https://doi.org/10.1039/C7EE01917C>.
- Xiao, L., Wu, S.-Y., Li, Y.-R., 2012a. Advances in solar hydrogen production via two-step water-splitting thermochemical cycles based on metal redox reactions. *Renew. Energy* 41, 1–12. <https://doi.org/10.1016/j.renene.2011.11.023>.
- Xiao, L., Zhang, S., Pan, J., et al, 2012b. First implementation of alkaline polymer electrolyte water electrolysis working only with pure water. *Energy. Environ. Sci.* 5, 7869–7871. <https://doi.org/10.1039/C2EE22146B>.
- Xie, Y., Wang, X., Tang, K., et al, 2018. Blending Fe_3O_4 into a Ni/NiO composite for efficient and stable bifunctional electrocatalyst. *Electrochim. Acta* 264, 225–232. <https://doi.org/10.1016/j.electacta.2018.01.136>.
- Xiong, Y., Liu, Q.-L., Zeng, Q.H., 2009. Quaternized cardo polyetherketone anion exchange membrane for direct methanol alkaline fuel cells. *J. Power Sources* 193, 541–546. <https://doi.org/10.1016/j.jpowsour.2009.04.043>.
- Xu, H., Cao, J., Shan, C., et al, 2018a. MOF-Derived Hollow CoS Decorated with CeOx Nanoparticles for Boosting Oxygen Evolution Reaction Electrocatalysis. *Angew. Chem. Int. Ed.* 57, 8654–8658. <https://doi.org/10.1002/anie.201804673>.
- Xu, W., Lyu, F., Bai, Y., et al, 2018b. Porous cobalt oxide nanoplates enriched with oxygen vacancies for oxygen evolution reaction. *Nano Energy* 43, 110–116. <https://doi.org/10.1016/j.nanoen.2017.11.022>.
- Xu, W., Scott, K., 2010. The effects of ionomer content on PEM water electrolyser membrane electrode assembly performance. *Int. J. Hydrog. Energy*. 35, 12029–12037. <https://doi.org/10.1016/j.ijhydene.2010.08.055>.

- Xu, D., Stevens, M.B., Cosby, M.R., et al, 2019. Earth-Abundant Oxygen Electrocatalysts for Alkaline Anion-Exchange-Membrane Water Electrolysis: Effects of Catalyst Conductivity and Comparison with Performance in Three-Electrode Cells. *ACS Catal.* 9, 7–15. <https://doi.org/10.1021/acscatal.8b04001>.
- Xu, S., Zhang, G., Zhang, Y., et al, 2012. Cross-linked hydroxide conductive membranes with side chains for direct methanol fuel cell applications. *J. Mater. Chem.* 22, 13295–13302. <https://doi.org/10.1039/C2JM16593G>.
- Xu, P.Y., Zhou, K., Han, G.L., et al, 2014. Effect of Fluorene Groups on the Properties of Multiblock Poly(arylene ether sulfone) s-Based Anion-Exchange Membranes. *ACS Appl. Mater. Interfaces* 6, 6776–6785. <https://doi.org/10.1021/am5017599>.
- Xue, B., Dong, X., Li, Y., et al, 2017. Synthesis of novel guanidinium-based anion-exchange membranes with controlled microblock structures. *J. Membr. Sci.* 537, 151–159. <https://doi.org/10.1016/j.memsci.2017.05.030>.
- Xue, X., Yang, H., Yang, T., et al, 2019. N, P-coordinated fullerene-like carbon nanostructures with dual active centers toward highly-efficient multi-functional electrocatalysis for CO₂RR, ORR and Zn-air battery. *J. Mater. Chem. A* 7, 15271–15277. <https://doi.org/10.1039/C9TA03828K>.
- Xu, C., Shen, P.K., Liu, Y., 2007. Ethanol electrooxidation on Pt/C and Pd/C catalysts promoted with oxide. *J. Power Sources* 164, 527–531. <https://doi.org/10.1016/j.jpowsour.2006.10.071>.
- Yan, X., He, G., Gu, S., et al, 2011. Quaternized poly(ether ether ketone) hydroxide exchange membranes for fuel cells. *J. Membr. Sci.* 375, 204–211. <https://doi.org/10.1016/j.memsci.2011.03.046>.
- Yan, X., He, G., Gu, S., et al, 2012. Imidazolium-functionalized polysulfone hydroxide exchange membranes for potential applications in alkaline membrane direct alcohol fuel cells. *Int. J. Hydrog. Energy.* 37, 5216–5224. <https://doi.org/10.1016/j.ijhydene.2011.12.069>.
- Yan, X., Gu, S., He, G., et al, 2014. Imidazolium-functionalized poly(ether ether ketone) as membrane and electrode ionomer for low-temperature alkaline membrane direct methanol fuel cell. *J. Power Sources* 250, 90–97. <https://doi.org/10.1016/j.jpowsour.2013.10.140>.
- Yan, J., Hickner, M.A., 2010. Anion Exchange Membranes by Bromination of Benzylmethyl-Containing Poly(sulfone)s. *Macromolecules* 43, 2349–2356. <https://doi.org/10.1021/ma902430y>.
- Yan, X., Tian, L., Chen, X., 2015. Crystalline/amorphous Ni/NiO core/shell nanosheets as highly active electrocatalysts for hydrogen evolution reaction. *J. Power Sources* 300, 336–343. <https://doi.org/10.1016/j.jpowsour.2015.09.089>.
- Yan, X., Yang, X., Su, X., et al, 2020. Twisted ether-free polymer based alkaline membrane for high-performance water electrolysis. *J. Power Sources* 480,. <https://doi.org/10.1016/j.jpowsour.2020.228805>
- Yanagi, H., Fukuta, K., 2008. Anion Exchange Membrane and Ionomer for Alkaline Membrane Fuel Cells (AMFCs). *ECS Trans.* 16, 257–262. <https://doi.org/10.1149/1.2981860>.
- Yang, Y., Wang, J., Zheng, J., et al, 2014b. A stable anion exchange membrane based on imidazolium salt for alkaline fuel cell. *J. Membr. Sci.* 467, 48–55. <https://doi.org/10.1016/j.memsci.2014.05.017>.
- Yang, Y., Dang, L., Shearer, M.J., et al, 2018. Highly Active Trimetallic NiFeCr Layered Double Hydroxide Electrocatalysts for Oxygen Evolution Reaction. *Adv. Energy Mater.* 8, 1703189. <https://doi.org/10.1002/aenm.201703189>.
- Yang, K., Li, X., Guo, J., et al, 2020. Preparation and properties of anion exchange membranes with exceptional alkaline stable polymer backbone and cation groups. *J. Membr. Sci.* 596,. <https://doi.org/10.1016/j.memsci.2019.117720>
- Yang, J., Liu, C., Hao, Y., et al, 2016. Preparation and investigation of various imidazolium-functionalized poly(2,6-dimethyl-1,4-phenylene oxide) anion exchange membranes. *Electrochim. Acta* 207, 112–119. <https://doi.org/10.1016/j.electacta.2016.04.176>.
- Yang, C., Wang, S., Jiang, L., et al, 2015a. 1,2-Dimethylimidazolium-functionalized cross-linked alkaline anion exchange membranes for alkaline direct methanol fuel cells. *Int. J. Hydrog. Energy.* 40, 2363–2370. <https://doi.org/10.1016/j.ijhydene.2014.12.050>.
- Yang, C., Wang, S., Ma, W., et al, 2015b. Comparison of alkaline stability of quaternary ammonium- and 1,2-methylimidazolium-based alkaline anion exchange membranes. *J. Membr. Sci.* 487, 12–18. <https://doi.org/10.1016/j.memsci.2015.03.067>.
- Yang, C., Wang, S., Ma, W., et al, 2015c. Highly alkaline stable N1-alkyl substituted 2-methylimidazolium functionalized alkaline anion exchange membranes. *J. Mater. Chem. A* 3, 8559–8565. <https://doi.org/10.1039/C5TA00562K>.
- Yang, D., Yu, H., Li, G., et al, 2014a. Effect of gas diffusion electrode parameters on anion exchange membrane fuel cell performance. *Chin. J. Catal.* 35, 1091–1097. [https://doi.org/10.1016/S1872-2067\(14\)60050-4](https://doi.org/10.1016/S1872-2067(14)60050-4).
- Yao, L., Zhang, N., Wang, Y., et al, 2018. Facile formation of 2D Co₂P@Co₃O₄ microspheres through in-situ topotactic conversion and surface corrosion: Bifunctional electrocatalysts towards overall water splitting. *J. Power Sources* 374, 142–148. <https://doi.org/10.1016/j.jpowsour.2017.11.028>.
- Ye, Y., Elabd, Y.A., 2011. Relative Chemical Stability of Imidazolium-Based Alkaline Anion Exchange Polymerized Ionic Liquids. *Macromolecules* 44, 8494–8503. <https://doi.org/10.1021/ma201864u>.
- Ye, Y.-S., Tseng, C.-Y., Shen, W.-C., et al, 2011. A new graphene-modified protic ionic liquid-based composite membrane for solid polymer electrolytes. *J. Mater. Chem.* 21, 10448–10453. <https://doi.org/10.1039/C1JM11152C>.
- Yoo, E., Okata, T., Akita, T., et al, 2009. Enhanced Electrocatalytic Activity of Pt Subnanoclusters on Graphene Nanosheet Surface. *Nano Lett.* 9, 2255–2259. <https://doi.org/10.1021/nl900397t>.
- Yu, F., Zhou, H., Huang, Y., et al, 2018a. High-performance bifunctional porous non-noble metal phosphide catalyst for overall water splitting. *Nat. Commun.* 9, 2551. <https://doi.org/10.1038/s41467-018-04746-z>.
- Yu, M., Zhou, S., Wang, Z., et al, 2018b. Boosting electrocatalytic oxygen evolution by synergistically coupling layered double hydroxide with MXene. *Nano Energy* 44, 181–190. <https://doi.org/10.1016/j.nanoen.2017.12.003>.
- Yuan, T.-C., Li, R.-D., Zhou, K.-C., 2007. Electrocatalytic properties of Ni-S-Co coating electrode for hydrogen evolution in alkaline medium. *Trans. Nonferrous Met. Soc. Chin.* 17, 762–765. [https://doi.org/10.1016/S1003-6326\(07\)60170-8](https://doi.org/10.1016/S1003-6326(07)60170-8).
- Zakaria, Z., Kamarudin, S.K., 2020. Evaluation of Quaternized polyvinyl alcohol/graphene oxide-based membrane towards improving the performance of air-breathing passive direct methanol fuel cells. *Int. J. Energy Res.* 44, 8988–9000. <https://doi.org/10.1002/er.5607>.
- Zarrin, H., Wu, J., Fowler, M., et al, 2012. High durable PEK-based anion exchange membrane for elevated temperature alkaline fuel cells. *J. Membr. Sci.* 394–395, 193–201. <https://doi.org/10.1016/j.memsci.2011.12.041>.
- Zeng, Q.H., Liu, Q.L., Broadwell, I., et al, 2010. Anion exchange membranes based on quaternized polystyrene-block-poly(ethylene-ran-butylene)-block-polystyrene for direct methanol alkaline fuel cells. *J. Membr. Sci.* 349, 237–243. <https://doi.org/10.1016/j.memsci.2009.11.051>.
- Zeng, K., Zhang, D., 2010. Recent progress in alkaline water electrolysis for hydrogen production and applications. *Prog. Energy Combust. Sci.* 36, 307–326. <https://doi.org/10.1016/j.peccs.2009.11.002>.
- Zeng, L., Zhao, T.S., 2015. Integrated inorganic membrane electrode assembly with layered double hydroxides as ionic conductors for anion exchange membrane water electrolysis. *Nano Energy* 11, 110–118. <https://doi.org/10.1016/j.nanoen.2014.10.019>.
- Zeng, L., Zhao, T.S., Zhang, R.H., et al, 2018. NiCo₂O₄ nanowires@MnOx nanoflakes supported on stainless steel mesh with

- superior electrocatalytic performance for anion exchange membrane water splitting. *Electrochem. Commun.* 87, 66–70. <https://doi.org/10.1016/j.elecom.2018.01.002>.
- Zha, Y., Disabb-Miller, M.L., Johnson, Z.D., et al, 2012. Metal-Cation-Based Anion Exchange Membranes. *J. Am. Chem. Soc.* 134, 4493–4496. <https://doi.org/10.1021/ja211365r>.
- Zhang, C., Anasori, B., Seral-Ascaso, A., et al, 2017. Transparent, Flexible, and Conductive 2D Titanium Carbide (MXene) Films with High Volumetric Capacitance. *Adv. Mater.* 29, 1702678. <https://doi.org/10.1002/adma.201702678>.
- Zhang, Z., Gao, C., Wu, Z., et al, 2016. Toward efficient photoelectrochemical water-splitting by using screw-like SnO₂ nanostructures as photoanode after being decorated with CdS quantum dots. *Nano Energy* 19, 318–327. <https://doi.org/10.1016/j.nanoen.2015.11.011>.
- Zhang, B., Gu, S., Wang, J., et al, 2012. Tertiary sulfonium as a cationic functional group for hydroxide exchange membranes. *RSC Adv.* 2, 12683–12685. <https://doi.org/10.1039/C2RA21402D>.
- Zhang, Q., Li, S., Zhang, S., 2010. A novel guanidinium grafted poly (aryl ether sulfone) for high-performance hydroxide exchange membranes. *Chem. Commun.* 46, 7495–7497. <https://doi.org/10.1039/C0CC01834A>.
- Zhang, K., McDonald, M.B., Genina, I.E.A., et al, 2018a. A Highly Conductive and Mechanically Robust OH⁻ Conducting Membrane for Alkaline Water Electrolysis. *Chem. Mater.* 30, 6420–6430. <https://doi.org/10.1021/acs.chemmater.8b02709>.
- Zhang, L., Xiong, K., Chen, S., et al, 2015. In situ growth of ruthenium oxide-nickel oxide nanorod arrays on nickel foam as a binder-free integrated cathode for hydrogen evolution. *J. Power Sources* 274, 114–120. <https://doi.org/10.1016/j.jpowsour.2014.10.038>.
- Zhang, F., Zhang, H., Qu, C., 2011. Imidazolium functionalized polysulfone anion exchange membrane for fuel cell application. *J. Mater. Chem.* 21, 12744–12752. <https://doi.org/10.1039/C1JM10656B>.
- Zhang, S., Zhu, X., Jin, C., et al, 2018b. Cyclodextrin edge functionalized graphene oxide modified poly(phthalazinone ether ketone) composite membrane with enhanced properties for anion exchange membrane. *Solid State Ion.* 320, 360–368. <https://doi.org/10.1016/j.ssi.2018.03.024>.
- Zhang, S., Zhu, X., Jin, C., 2019. Development of a high-performance anion exchange membrane using poly(isatin biphenylene) with flexible heterocyclic quaternary ammonium cations for alkaline fuel cells. *J. Mater. Chem. A* 7, 6883–6893. <https://doi.org/10.1039/C8TA11291F>.
- Zhao, S., Tsen, W.-C., Gong, C., 2021. 3D nanoflower-like layered double hydroxide modified quaternized chitosan/polyvinyl alcohol composite anion conductive membranes for fuel cells. *Carbohydr. Polym.* 256, <https://doi.org/10.1016/j.carbpol.2020.117439> 117439.
- Zhiani, M., Jalili, F., Kamali, S., 2017. In situ cathode polarization measurement in alkaline anion exchange membrane water electrolyzer equipped with a PdNiFeCo/C-Ceria hydrogen evolution electrocatalyst. *Int. J. Hydrog. Energy.* 42, 26563–26574. <https://doi.org/10.1016/j.ijhydene.2017.09.038>.
- Zhou, Q., Chen, Y., Zhao, G., et al, 2018. Active-Site-Enriched Iron-Doped Nickel/Cobalt Hydroxide Nanosheets for Enhanced Oxygen Evolution Reaction. *ACS Catal.* 8, 5382–5390. <https://doi.org/10.1021/acscatal.8b01332>.
- Zhou, J., Unlu, M., Vega, J.A., et al, 2009. Anionic polysulfone ionomers and membranes containing fluorenyl groups for anionic fuel cells. *J. Power Sources* 190, 285–292. <https://doi.org/10.1016/j.jpowsour.2008.12.127>.
- Zhu, M., Zhang, M., Chen, Q. et al., 2017. Synthesis of midblock-quaternized triblock copolystyrenes as highly conductive and alkaline-stable anion-exchange membranes. Electronic supplementary information (ESI) available. See DOI: 10.1039/c6py02213h. *Polymer Chemistry.* 8, 2074–2086. <https://doi.org/10.1039/c6py02213h>.
- Zhu, L., Pan, J., Christensen, C.M., et al, 2016. Functionalization of Poly(2,6-dimethyl-1,4-phenylene oxide)s with Hindered Fluorene Side Chains for Anion Exchange Membranes. *Macromolecules* 49, 3300–3309. <https://doi.org/10.1021/acs.macromol.6b00578>.
- Zhu, L.D., Zhao, T.S., Xu, J.B., et al, 2009. Preparation and characterization of carbon-supported sub-monolayer palladium decorated gold nanoparticles for the electro-oxidation of ethanol in alkaline media. *J. Power Sources* 187, 80–84. <https://doi.org/10.1016/j.jpowsour.2008.10.089>.